GRAĐEVINSKI
MATERIJALI I KONSTRUKCIJE

Volume 68
March 2025
ISSN 2217-8139 (Print)
ISSN 2335-0229 (Online)
UDK: 06.055.2:62-03+620.1+624.001.5(497.1)=861

BUILDING
MATERIALS AND STRUCTURES

1

Society for Materials and Structures Testing of Serbia
University of Belgrade Faculty of Civil Engineering
Association of Structural Engineers of Serbia

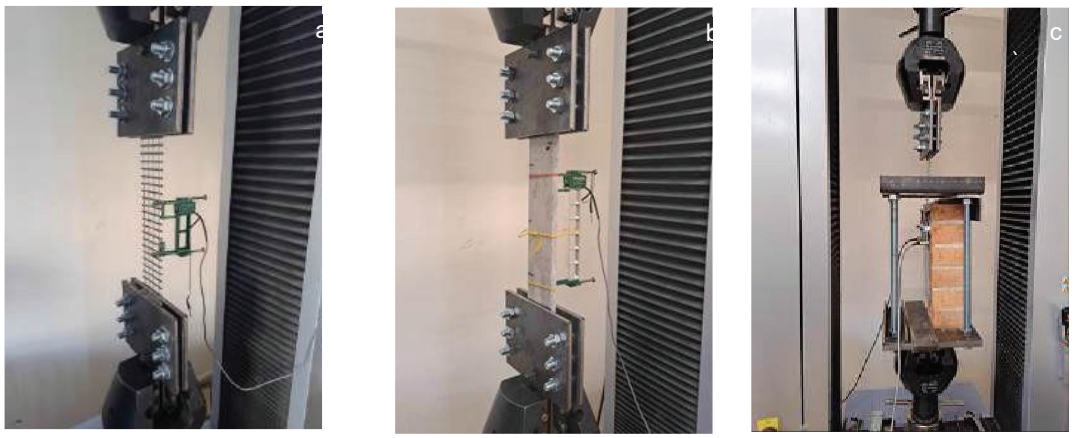

GRAĐEVINSKI MATERIJALI I KONSTRUKCIJE

BUILDING MATERIALS AND STRUCTURES

ISSN 2217-8139 (PRINT)
ISSN 2335-0229 (Online)

VOLUME 68(1)
March 2025

CONTENTS

GRAĐEVINSKI MATERIJALI I KONSTRUKCIJE

BUILDING MATERIALS AND STRUCTURES

ISSN 2217-8139 (PRINT)
ISSN 2335-0229 (Online)

VOLUME 68(1)
March 2025

EDITORIAL BOARD

Aims and scope

Building Materials and Structures aims at providing an international forum for communication and dissemination of innovative research and application in the field of building materials and structures. Journal publishes papers on the characterization of building materials properties, their technologies and modeling. In the area of structural engineering Journal publishes papers dealing with new developments in application of structural mechanics principles and digital technologies for the analysis and design of structures, as well as on the application and skillful use of novel building materials and technologies.

The scope of Building Materials and Structures encompasses, but is not restricted to, the following areas: conventional and non-conventional building materials, recycled materials, smart materials such as nanomaterials and bio-inspired materials, infrastructure engineering, earthquake engineering, wind engineering, fire engineering, blast engineering, structural reliability and integrity, life cycle assessment, structural optimization, structural health monitoring, digital design methods, data-driven analysis methods, experimental methods, performance-based design, innovative construction technologies, and value engineering.

Publishers Society for Materials and Structures Testing of Serbia, Belgrade, Serbia, veb sajt: www.dimk.rs
University of Belgrade Faculty of Civil Engineering, Belgrade, Serbia, www.grf.bg.ac.rs
Association of Structural Engineers of Serbia, Belgrade, Serbia, dgks.grf.bg.ac.rs

Print Razvojno istraživački centar grafičkog inženjerstva, Belgrade, Serbia

Edition quarterly

Peer reviewed journal

Journal homepage www.dimk.rs

Cover Specimens during the testing a) represent of group I, b) represent of group II, c) represent of group III, from *Methods of testing systems for strengthening masonry structures based on cement composites reinforced with glass fiber mesh* by Milica Petrović, Marko Popović, Marina Škondrić, Aleksandar Savić, and Dimitrije Zakić

Financial support Ministry of Education, Science and Technological Development of Republic of Serbia
University of Belgrade Faculty of Civil Engineering
Institute for testing of materials-IMS Institute, Belgrade
Faculty of Technical Sciences, University of Novi Sad, Department of Civil Engineering
Serbian Chamber of Engineers

CIP - Каталогизација у публикацији
Народна библиотека Србије, Београд

620.1

GRAĐEVINSKI materijali i konstrukcije = Building materials and structures / editor-in-chief Snežana Marinković
. - God. 54, br. 3 (2011)- . - Belgrade : Society for Materials and Structures Testing of Serbia : University of Belgrade, Faculty of Civil Engineering : Association of Structural Engineers of Serbia, 2011- (Belgrade : Razvojno istraživački centar grafičkog inženjerstva). - 30 cm

Tromesečno. - Je nastavak: Materijali i konstrukcije = ISSN 0543-0798. - Drugo izdanje na drugom medijumu: Građevinski materijali i konstrukcije (Online) = ISSN 2335-0229
ISSN 2217-8139 = Građevinski materijali i konstrukcije
COBISS.SR-ID 188695820

Građevinski materijali i konstrukcije
Building Materials and Structures
journal homepage: www.dimk.rs

https://doi.org/10.5937/GRMK2400013G UDK: 624.971:620.1
627.235.6:620.1

Original scientific paper

Application of the polynomial chaos expansion method for forecasting structural response of two full-scale case studies

Viktor Georgijev[1)], Simona Bogoevska[*2)]

[1)] *Matrics engineering GmbH, Nyphenburger Str. 20a, D-80335, Munich, Germany*
[2)] *University of Ss. Cyril and Methodius, Faculty of Civil Engineering, Blvd. Partizanski Odredi 24, 1000 Skopje, North Macedonia*

Article history
Received: 25 October 2024
Received in revised form:
16 December 2024
Accepted: 25 December 2024
Available online: 05 February 2025

Keywords
structural health monitoring,
polynomial chaos expansion,
data-driven models,
engineering structures,
sensitivity,
uncertainty,
forecasting

ABSTRACT

Predicting the behavior of engineering structures with high accuracy remains a challenging task as a result of their continuous interaction with the immediate environment and varying operating conditions. In that context, forecasting tools are primarily focused on the creation of a model of a so-called baseline system. This established model serves as a foundation for identifying changes when new outputs deviate from the predictions made by the model. Physics-based numerical models, like the finite element method, often carry significant uncertainty stemming from assumptions regarding structural characteristics, environmental influences, and various loads affecting the system under study. Consequently, identifying the source of any existing discrepancies between obtained model results and measured data is difficult. This paper demonstrates a straightforward implementation of the polynomial chaos expansion method for the formulation of prognostic data-driven models targeted at tracking changes in continuously measured structural response. The method's effectiveness and positive features are showcased via practical application onto two full-scale engineering structures: a concrete arch dam and an industrial steel chimney. The models utilize environmental as well as response data collected over two years and two months of monitoring of these structures, respectively. The obtained results reveal the models' considerable potential as a long-term monitoring tool for autonomous assessment of structural behavior.

1 Introduction

As a four-dimensional concept, Structural Health Monitoring (SHM) enables real-time as well as spatial assessment of monitored systems [1-3]. It targets diagnosis of the current condition of structures, however also, based on recorded full data history, learning about load and response mechanisms, prognosis of evolution of damages, estimation of fatigue and residual life of structures [4]. SHM frameworks are commonly based on approaches which utilize either physics-based, data-driven or hybrid models [5]. In [6] the SHM paradigm is concisely described as continuous system identification of a physical or parametric model of the structure using time-dependent data.

The term "model" can be best summarized as a collection of numerical or analytical processes employed to mimic the behavior and response of a real-world system to various changing factors [7]. However, all mathematical models inherently include uncertainties [8]. These are related to: i) modeling errors caused by oversimplified assumptions for the modeled process, ii) numerical errors due to insufficient resolution of applied numerical methods, and iii) data errors linked to limited knowledge and availability of input data, the inherent variability of the system being studied [9]. Various uncertainty quantification tools deal with systems affected by stochastic variations in system parameters (data errors) by taking into account the evolution of the probability distribution of random inputs [10]. In contrast to traditional collocation methods used for uncertainty quantification, spectral methods are based on a fundamentally different concept. Rather than conducting multiple simulations on an established mathematical model, non-sampling approaches aim to construct a functional relationship between a model's output quantity and a random input [11]. While these Fourier-like series representations impose certain requirements on both the output and input parameters, they offer a much lower computational cost compared to the widely used Monte Carlo method and other sampling techniques, which encompass a more "local" nature and asymptotic convergence rates [11-12].

This paper is focused on one representative of the spectral methods class, the Polynomial Chaos Expansion (PCE). The PCE method enables the generation of data-driven models as an approximation of input–output relationship by casting the model response onto orthogonal polynomials, with relatively simple mathematical formulation

* Corresponding author:
E-mail address: simona.bogoevska@gf.ukim.edu.mk

and efficiently spent computer time [13]. Additionally, the PCE method provides a suitable mathematical formulation for analyzing the sensitivity of the measured response of the structure to a large number of input variables describing the influence of the environment and operating conditions [14-15]. In this context, the possibility for assessing response statistics via direct and mathematically simple post-processing of the expansion coefficients makes the PCE model a desirable tool for real-life applications [16].

PCE is a commonly employed method in uncertainty quantification, where it is often used to substitute a computationally intensive model, which is affected by random inputs, with a more cost-efficient polynomial function. In recent years it has been successfully applied to a number of civil engineering problems dealing with construction of metamodels [17-23]. In [17] PC expansion is used to represent the stochastic system output responses of three numerical modeled systems of civil bridge structures. The results obtained are compared with those from the widely used MCS and FOSM methods. The obtained PC coefficients are directly used for calculating the global sensitivity indices, which verifies the accuracy and significantly reduced computational demand of the presented method compared to the MCS-based calculation. In [18] the application of PCE for meta-modeling of dam engineering problems is explored. The response prognosis of four numerical case studies with different complexities is investigated with uncertainties propagated in material properties and modeling. The method is found as an effective technique to deal with uncertainty quantification in concrete dams. Ghanem et al. [19] focused on an embankment dam using stochastic finite element analysis involving the PCE method, where material's elastic and shear moduli are modelled as stochastic processes. The work in [20] presents a metamodeling approach designed to handle uncertainties in simulating nonlinear, dynamically evolving engineering systems. The authors utilized nonlinear autoregressive with exogenous input (NARX) models, where random parameters are used to represent uncertainty propagation within the numerical model. The random NARX parameters are expanded into a polynomial chaos. The resulting PC-NARX metamodel significantly reduces computational time while maintaining adequate accuracy. Guo et al. [21] also investigated the stability of an embankment dam using sparse PCE, assuming three soil properties—dry density, cohesion, and friction angle—as random variables. They applied both the finite difference and limit equilibrium methods to assess the dam's safety factor, presenting failure probability distributions for normal operating conditions and seismic loading. DeFalco et al. [22] introduced a method for calibrating model parameters in a Bayesian framework. This approach replaces the original model with a proxy model obtained through generalized PCE, reducing computational load while providing a global model error estimate. The method is tested on a case study of one Italian concrete gravity dam, where recorded displacements have been used to estimate model parameters values which provide a model response with minimal error. Exploring the problems of finite element model updating and structural damage identification for a small-scaled laboratory dam, the research in [23] proposed a sparse PCE method for substituting the computationally expensive FE model, enabling a low-cost and high predictive accuracy.

The application of the PCE tool for the purpose of purely data-driven diagnostics and prognosis of monitored structures was explored in [14,24]. Spiridonakos and Chatzi [24] introduced the PCE method together with the independent component analysis (ICA) tool in a long-term scale, delivering a robust performance indicator. The PCE -ICA scheme was successfully verified on damage detection for the benchmark SHM project of the Z24 bridge. Related to tower-like structures, in [14] the authors combined the PCE method with the parametric smoothness priors time varying autoregressive moving average (SP-TARMA) method. The proposed PCE-SPTARMA approach delivers a holistic model for long-term tracking of the structural behavior of two full-scale operational wind turbine structures, demonstrating the high potential of the proposed method for automated condition assessment of large real-world structures, operating in a wide range of conditions.

In recent years, significant advancements in the automation of structural monitoring systems have facilitated the collection of vast amounts of data. This has, in turn, accelerated the adoption of data-driven techniques for structural safety monitoring [25-28]. Given the limited availability of accessible monitoring data from full-scale operational engineering structures for research purposes, this study makes a key contribution by offering valuable insights into the practical implementation of a selected prognostic tool, applied to data gathered from real-world engineering structures. While previously reported studies focus on meta-modelling or multi-componential utilization of the PCE tool, herein we are testing a rather straightforward application of the PCE method, exploring direct employment of uncorrelated input set of measured environmental data and not extensively preprocessed measured response quantity, serving directly as a model output variable. The examination of the limitations and advantages of this basic methodology enhances the understanding of its limitations for practical implementation.

To this end, the applicability of the PCE method is herein tested on two distinct full-scale structures: a concrete arch dam and a steel chimney. The constructed models for both structures extrapolate on a selected single measured response variable (displacement for the dam structure and acceleration for the chimney structure), representing the model's output parameter, by incorporating the variability of measured environmental conditions (water level and ambient temperature for the dam structure and wind velocity, direction and ambient temperature for the chimney structure), serving as model inputs. The analysis of the first example of the arch dam demonstrates the effect of incomplete training set on the accuracy of the model prediction, while the second case study underlines the aspect of data condensation via the effective sensitivity analysis via the PCE-based obtained Sobol indices. The obtained results showcase the potential of the method for its efficient utilization in prognostic and diagnostic tasks within holistic and autonomous SHM frameworks.

2 Polynomial chaos expansion- theoretical background

The field of uncertainty quantification deals with systems affected by stochastic variations in system parameters, i.e. data errors which rise from limited knowledge and availability of input data, or operating (inherent) variability of the studied system. To this end, uncertainty quantification models take into account the evolution of the probability distribution of the random input. The term of "Homogeneous Chaos" was initially introduced by Wiener [29] for the purpose of modeling stochastic processes involving Gaussian random variables through the use of Hermite polynomials. To extend this approach to different types of random variables, Xiu et al.

proposed the "generalized polynomial chaos" framework [30], which adapts the method to both discrete and continuous random variables by employing orthogonal polynomials from the so-called Askey scheme [31]. In recent decades, polynomial chaos expansion has found increasing popularization in various research fields, with key developments shown in Fig. 2.1.

More specifically, if we assume the system $Y = S(X)$ is comprised of M random input parameters represented by independent random variables, e.g. measured water level, wind velocities and temperature values, gathered in the random vector X of prescribed joint Probability Density Function (PDF), and the output variable is of finite variance, the PCE model assumes the form [14]:

$$Y = S(X) = \sum_{\alpha \in N^M} y_\alpha \psi_\alpha(X) \tag{1}$$

where $\psi_\alpha(X)$ are polynomials dependent on multiple variables, orthonormal with respect to the probability density function f_X, $\alpha \in N^M$ is a vector of multi-indices of the multivariate polynomial basis identifying the components of the polynomials ψ_α and $y_\alpha \in R$ are the corresponding unknown deterministic coefficients of projection.

In practical applications, the sum in expression (1) is truncated to a finite sum, which is typically achieved by limiting the total maximum degree p of the polynomials in the polynomial basis to:

$$|\alpha_i| = \sum_{m=1}^{M} \alpha_{i,m} \leq p \; \forall \; i \tag{2}$$

This constraint ensures that the total number of terms in the polynomial basis will be:

$$\mathrm{P} = \frac{(M+p)!}{M!\,p!} \tag{3}$$

where M designates the number of random variables and p denotes maximum basis degree.

Polynomials dependent on multiple variables $\psi_\alpha(X)$ are obtained through the tensor product of corresponding one-dimensional orthonormal polynomials, selected based on the probability density function of the random input variables and the known Askey scheme for orthonormal polynomials [31]. Finally, the truncated PCE model to the first P terms yields a finite parameter vector y_α which may be estimated by solving Eq. (1) in a least squares sense. The least squares approach is based on minimization of the cost function R, estimated as sum of the squared residuals between true (observed) and modeled (predicted) system outputs.

An approach for global sensitivity analysis of PC output variables, based on computationally inexpensive post-processing of estimated PC coefficients, was proposed in the work of Sudret [16]. Exploiting the orthonormality of the PC basis and their subsequent convenient properties, the approach utilizes a variance-based sensitivity analysis tool, namely the Sobol' decomposition. Its final goal is estimation of Sobol' sensitivity indices, which represent the fraction of the total variance of the model output that can be attributed to each input variable or combinations of variables [16].

Sobol' indices are obtained as a sum of squares of the PC coefficients and represent the fraction of the total variance D of the model output that can be attributed to each input variable or combinations of variables. More precisely, the index for a single input variable X_i is called the first-order Sobol index and represents the effect of X_i alone, Eq. 4. Indices for the influence of multiple variables, such as $S_{ij}, i \neq j$, are known as higher-order Sobol indices and represent interaction effects between X_i and X_j that cannot be attributed to the individual contributions of each variable separately.

$$S_i = \sum_{\cdot \in A_i} y_\alpha^2 / D, \tag{4}$$

$$A_i = \{\cdot \in A : \cdot_i > 0, \cdot_{j \neq i} = 0\}$$

3 Case study I: Concrete arch dam

The first presented case study herein is a concrete arch dam, located southwest (30 km aerial distance) of Skopje, RN Macedonia. The structure represents a thin concrete shell with double curvature, with a structural height of 64 meters. The dam is unreinforced, except for the upper third, which potentially would handle intensified oscillations in the event of an earthquake. The crest level is located at 364 meters above sea level (asl), while the lowest point at the bottom is at 300 m asl. The thickness of the crest is 2.0 m, gradually increasing to 10 m at the bottom. The structure was built over the period of six years (2006-2012), utilizing 27362 m^3 concrete for the dam body. The hydroelectric plant began operating on August 1, 2012, with an output capacity of 36.4 megawatts.

Since its construction the structure is equipped with a comprehensive monitoring system measuring: reservoir water level, underground water levels, ambient temperature and temperatures of concrete and water, rainfall, displacements at the crest and dam body, strains, rotations, accelerations during triggered earthquake events, contact stresses, etc. All aforementioned parameters are mainly

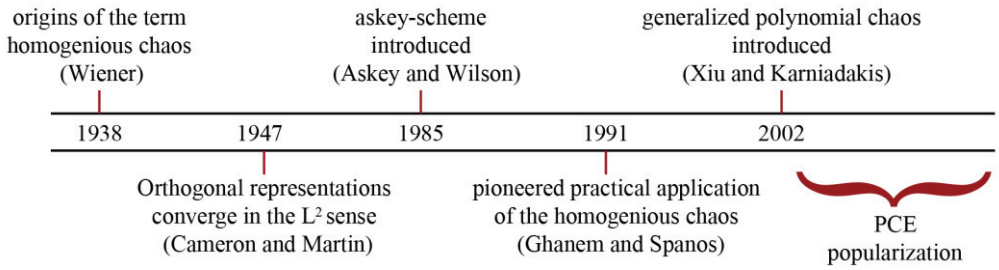

Figure 2.1. Developmental milestones for the PCE method (adopted from [4])

recorded once in six hours. The sensor distribution is based on results obtained from static and seismic analyses of a FE mathematical model, taking into account variations in the characteristics of the rock mass. This resulted in a nearly symmetrical layout of the instruments. The instruments are placed at five levels: +305.00; +320.00; +335.00, and +357.00 meters above sea level. These levels mainly correspond to points determined by the computational model at locations where the calculated values are of particular importance for the behavior of the dam. A more detailed overview of the complete acquisition system can be found in [32].

3.1 PCE application

Within this section the formulation and application of the PCE model is tested on data obtained from a two-year long monitoring period (years 2013 and 2014) for the dam structure, for a selected number of sensors, Fig.3.1.

The sampling frequency of the selected measured variables is once per six hours, which for the analyzed period of two years (excluding spurious data or missing records) provided in total of 2268 data sets, distributed as in Fig. 3.2. In order to select the appropriate physical quantities representing the influence of the environment on the structure (model input matrix), a correlation matrix has been computed as a first step. The selection of uncorrelated (or weakly correlated) input variables is a theoretical prerequisite of the PCE model [4]. Whereas various mathematical approaches do exist in transforming correlated data into uncorrelated variables [33], an advantage of the direct employment of uncorrelated (weakly correlated) input parameters is the possibility of straightforward calculation of the PCE-based Sobol' indices, demonstrated in Section 4.

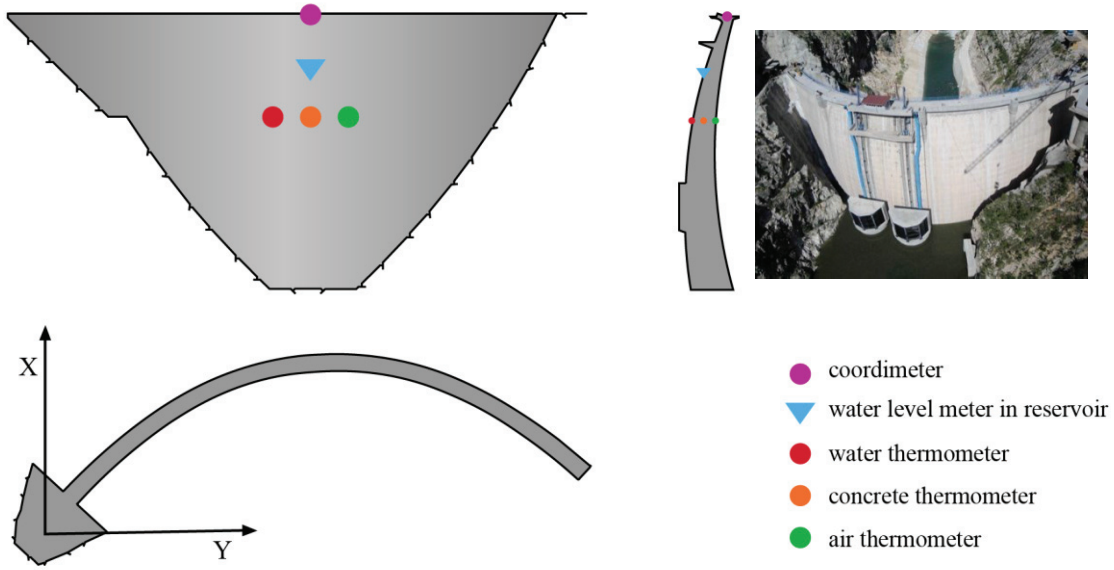

Figure 3.1. The concrete arch dam and a schematic overview of employed sensors from the installed monitoring system

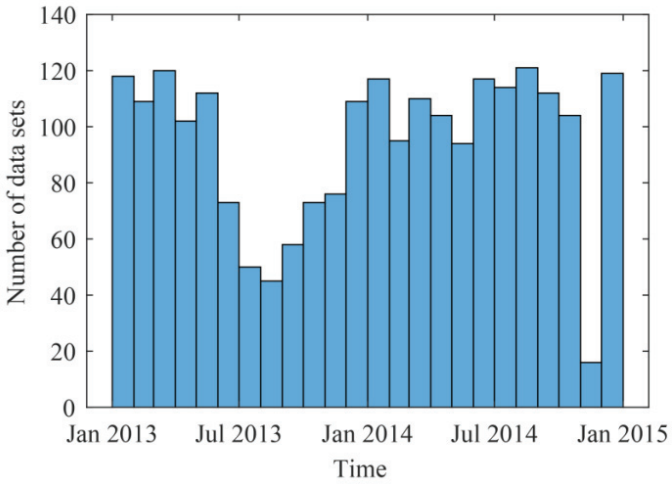

Figure 3.2. Available data sets over the two-year long period

In Fig. 3.3 the correlation plots for each pair of available input variables are presented. Due to the high correlation among the three measured temperatures, Pearson Correlation Coefficient (PCC) is 0.968 and 0.683, a single temperature-related variable, namely the ambient temperature (as most correlated to the measured displacement) was selected as an input quantity. In addition, the ambient temperature is correlated to the measured reservoir water level with the lowest PCC equal to 0.078. This enables the utilization of both quantities as PCE inputs.

On the other hand, the recorded crest displacement in X direction is selected as representing structural behavior, or as the PCE output parameter. The input/output variables are recorded at a frequency of one measurement every 6 hours, time history plots presented in Fig. 3.4.

An additional important criterion, particularly in the case of handling of a large database, is computational efficiency. In this context, the selection of the PC order, which affects the modeling precision, can also directly influence the total number of unknown PC coefficients and as a result computational time. For the assessed case study, the number of unknown PC coefficients in correlation to selected maximal PC order and the Leave One Out (LOO) error for the training and validation set of the actual case study is demonstrated in Fig. 3.5.

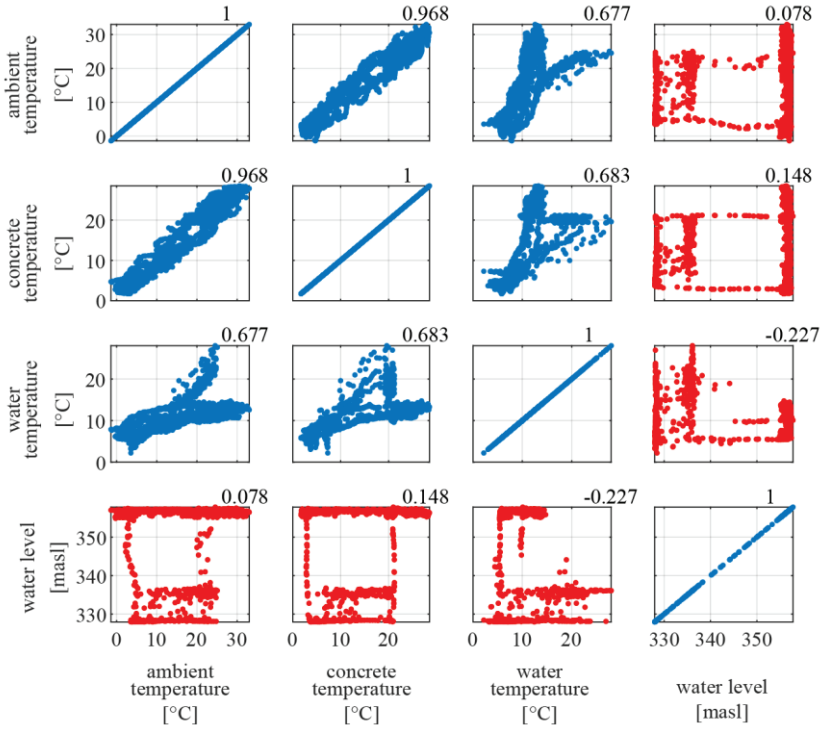

Figure 3.3. Correlation plots for the PCE input variables

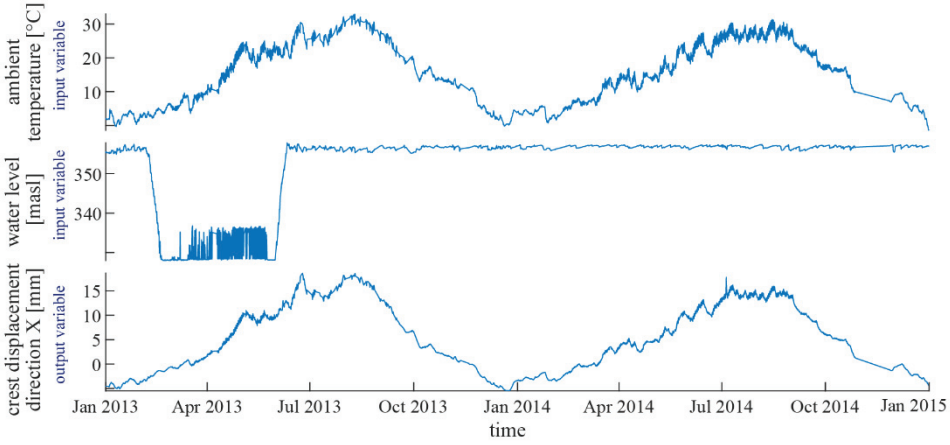

Figure 3.4. Time history plots for the selected PCE input and output quantities

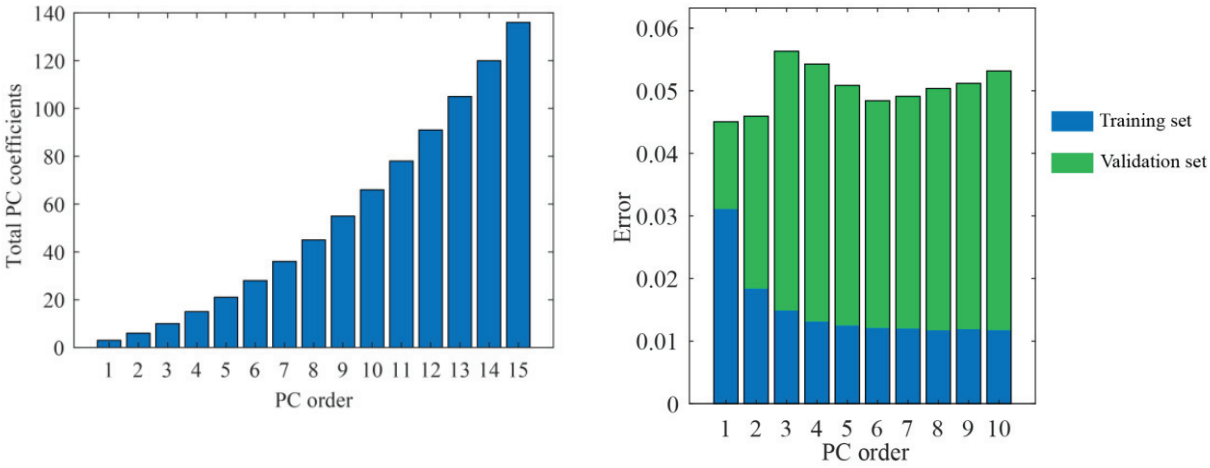

Figure 3.5. (Left) Number of unknown PC coefficients in correlation to selected maximal PC order; (Right) LOO error in correlation to PC model order for the dam case study

As a last step, the model output variable and the PDFs of the measured operational input data are fed into the PCE framework. In accordance with the PDFs of the input data, the Hermite polynomials are selected as the PC functional basis and the maximal polynomial order is selected as p=2.

In Fig. 3.6, the performance of the model with the selected output variable is demonstrated. The graphs demonstrate good alignment between the computed displacement (using the PCE model) and the actual measured displacement. The vertical dashed line marks the time interval used for training the PCE model (applied 70% of data). In the portion of the time interval (right of the vertical line) corresponding to the validation period, after training is completed, the model generates the displacement of the structure using “new” input data. From the results presented, it is evident that the model exhibits good capability in predicting the displacement of the structure in the considered direction.

The water level in the reservoir of the analyzed dam is maintained almost constant over time because, among other things, the dam is used for electricity production. To demonstrate the workings of the model to unknown data two additional analyses were performed by training the PCE model on an altered timeline, producing two different training scenarios.

In the first case (Scenario A), the training set includes data from the trial filling and emptying of the reservoir, while in the second case (Scenario B) this data is excluded. On the other hand, both scenarios include this data in the validation set. Both cases are graphically presented in Fig. 3.7, and the results of the analysis are shown in Figs. 3.8 – 3.9.

When the filling/emptying of the reservoir is not included in the training period of the model (Scenario B), the PCE validation set values drastically deviate from the monitored data. Having this in mind, in a potential autonomous SHM framework development such a deviation from "normal" expected ranges (usually $\pm 3std$) would trigger an alarm, which in this case would be a false positive (since it stems from changes in environmental conditions, not actual structural changes). This highlights the importance of using a holistic dataset during the model’s training phase, which captures the complete operational spectrum of the structure.

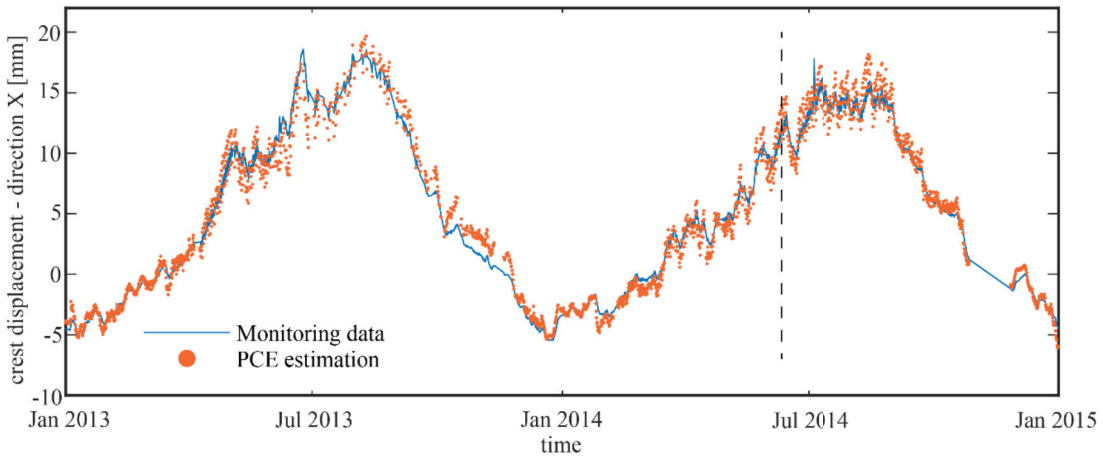

Figure 3.6. The output variable and the capability of the PCE model to predict it

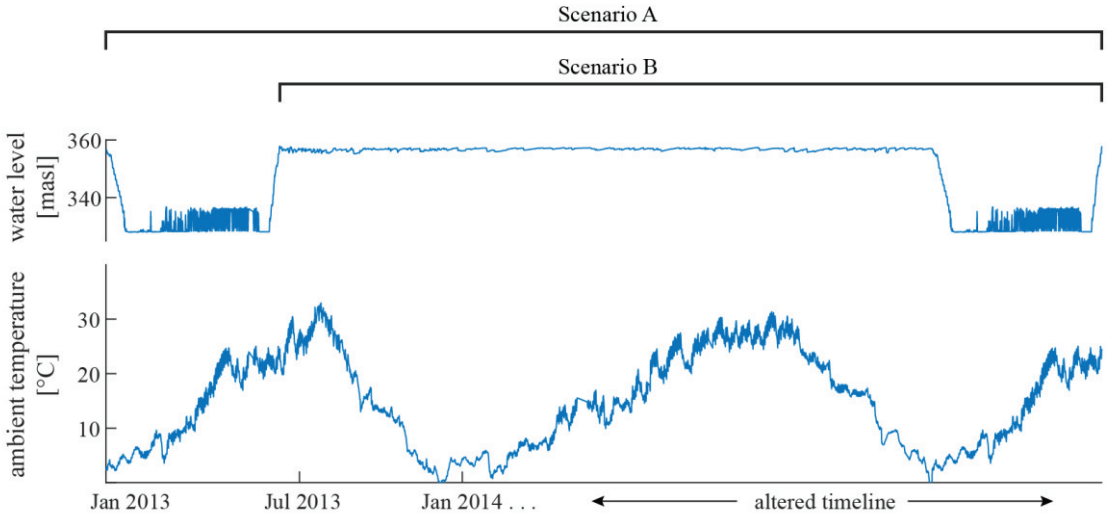

Figure 3.7. Input variables included for training for Scenario A and Scenario B

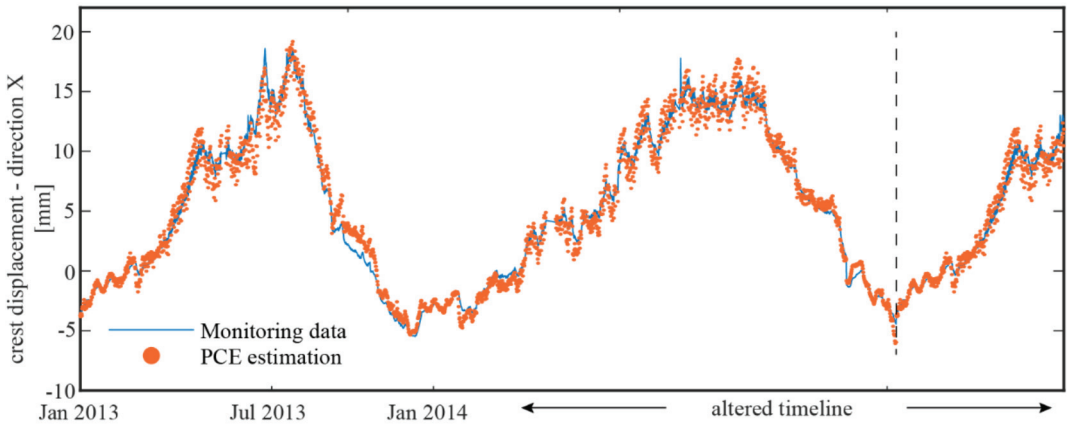

Figure 3.8. PCE model estimates for Scenario A

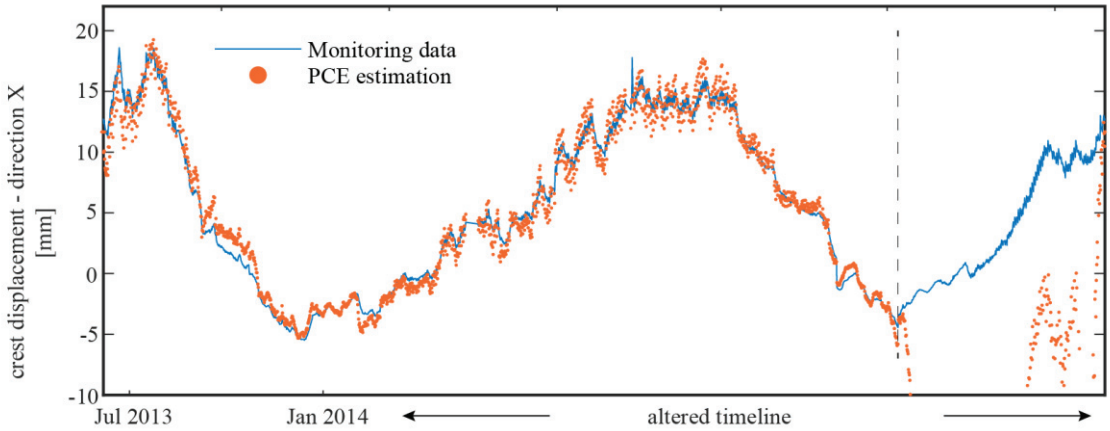

Figure 3.9. PCE model estimates for Scenario B

4 Case study II : Industrial steel chimney

The second testing case study is an industrial out of use steel chimney located at the Ohis factory in Skopje, RN Macedonia. A SHM campaign was undertaken in the period 14/12/2013 to 14/02/2014. An installed monitoring system for the complete timeframe of two months continuously measured: structural vibration responses (accelerations), environmental parameters (wind velocity and ambient temperature), as well as ground vibrations nearby the structure (Fig. 4.1).

Acceleration time histories were recorded by five tri-axial accelerometers for ambient vibration placed along the structure's height, with the sampling frequency of 200 Hz. Details on the placement and positioning of the sensors, as well as structural identification results are presented in a previous work in [34]. The authors successfully applied operational modal analysis for two identified loading scenarios: i) recurring train induced vibrations from a nearby railway, and ii) wind induced vibrations for a time frame corresponding to the maximal value of recorded wind velocity within the two months period of monitoring. The identified natural frequencies of the structure were verified with a FEM of the structure.

4.1 PCE application

In this case study, due to detected spurious trends in collected data, a three-week time frame was selected as a testbed for simplified showcasing the PC-based sensitivity analysis potential. The collected data was averaged to a sampling frequency of one record per minute, or for the analyzed period of 22 days in total 30407 data sets were used. The PCE output variable utilized to describe the behavior of the structure is the one-minute standard deviation of the measured acceleration at the top of the chimney in horizontal direction. The measured ambient temperature, wind velocity and direction were employed as PCE input variables, describing the environmental effects. The time histories and correlation plot of the selected variables are plotted in Fig. 4.2 and Fig.4.3.

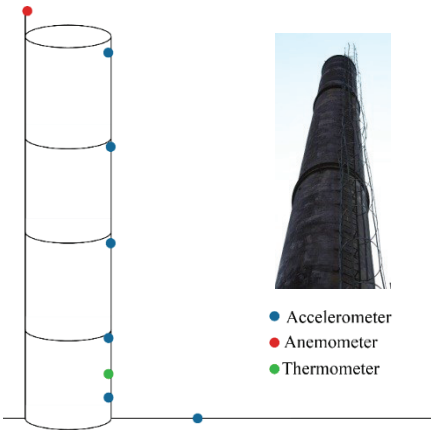

Height: 40 m
Diameter: 1.9 m
Thickness: 6-10 mm
Material: Steel S235
Construction year: 1970

Figure 4.1. Installed monitoring system and information for the structure under study

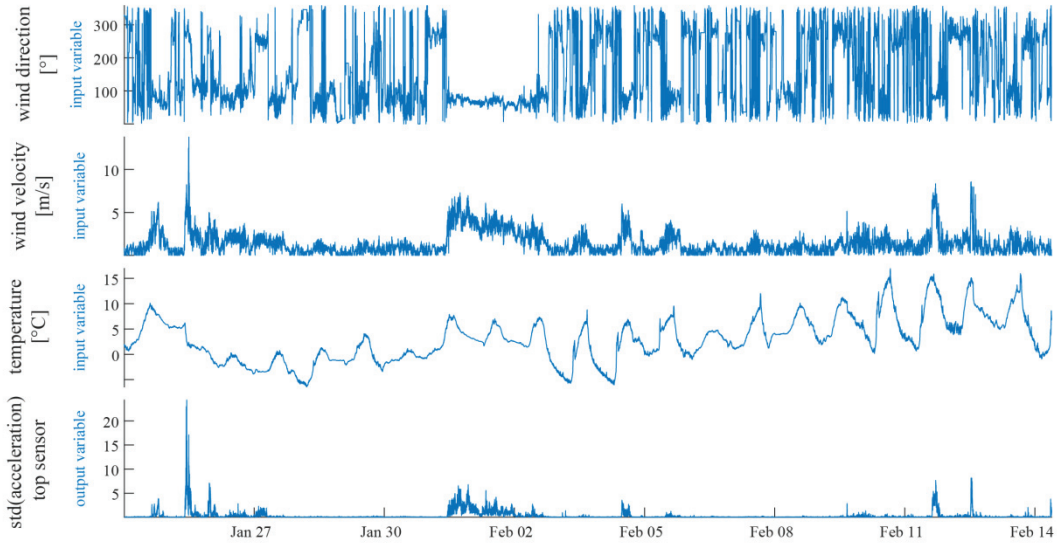

Figure 4.2. Time history plots for the selected PCE input and output quantities

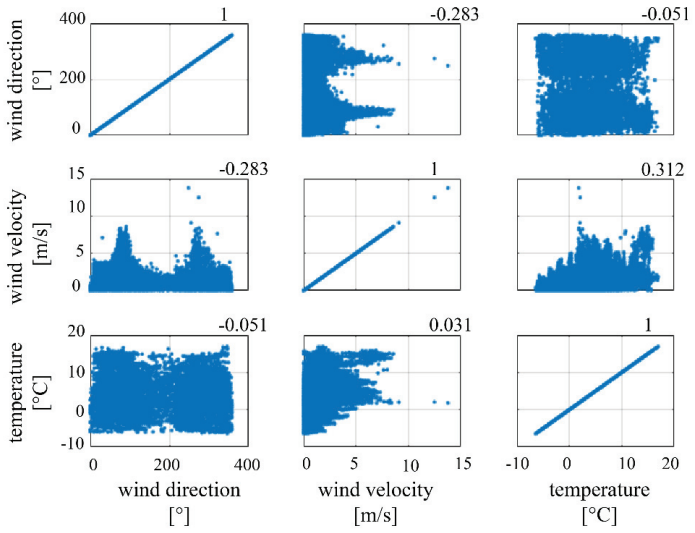

Figure 4.3. Correlation plots for the PCE input variables

In order to analyze how the variability of each individual input variable affects the chimney measured vibration, Sobol indices were calculated. The indices of first, second, and third order, along with total indices, were computed using coefficients obtained from a developed PCE data model (selected maximum PC order 4; adopted PC basis in accordance with the individual pdf of the three input variables), Fig. 4.4.

The analysis of the Sobol indices demonstrates that the variability of temperature has the least influence on the selected output representing the behavior of the structure (standard deviation of the measured acceleration) compared to the other two input variables. Therefore, a model with a reduced number of input variables is constructed, specifically with the input variables (1) wind direction angle and (2) wind velocity, Fig. 4.5. The results demonstrate that the difference between the models' LOO errors is negligibly small, specifically 6%, indicating that Model 2 (the model with a reduced number of input variables) has a slightly lower average error. This confirms the advantage of the Sobol indices analysis, as they potentially can reduce the dimensionality of the problem and enable a balance between computational efficiency and modeling precision.

In addition to Fig. 4.5., a look at the comparison of the PCE estimated values for the validation set for the both models in Fig. 4.6 (b) shows that model 2 in general produced higher values of the amplitudes of the modeled output parameter in comparison with model 1, which serves well for the estimated higher peaks of the std of the acceleration. Both models, however, perform similar for the training sets Fig. 4.6 (a).

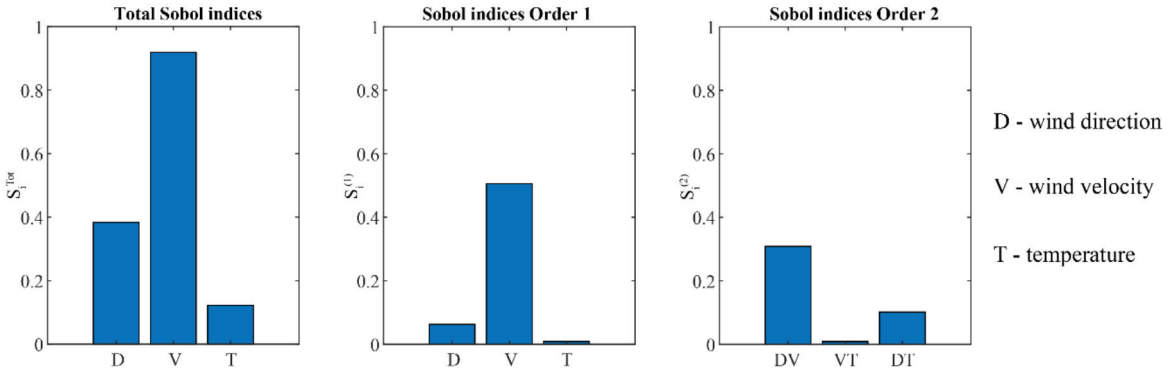

Figure 4.4. Calculated PCE-based Sobol indices

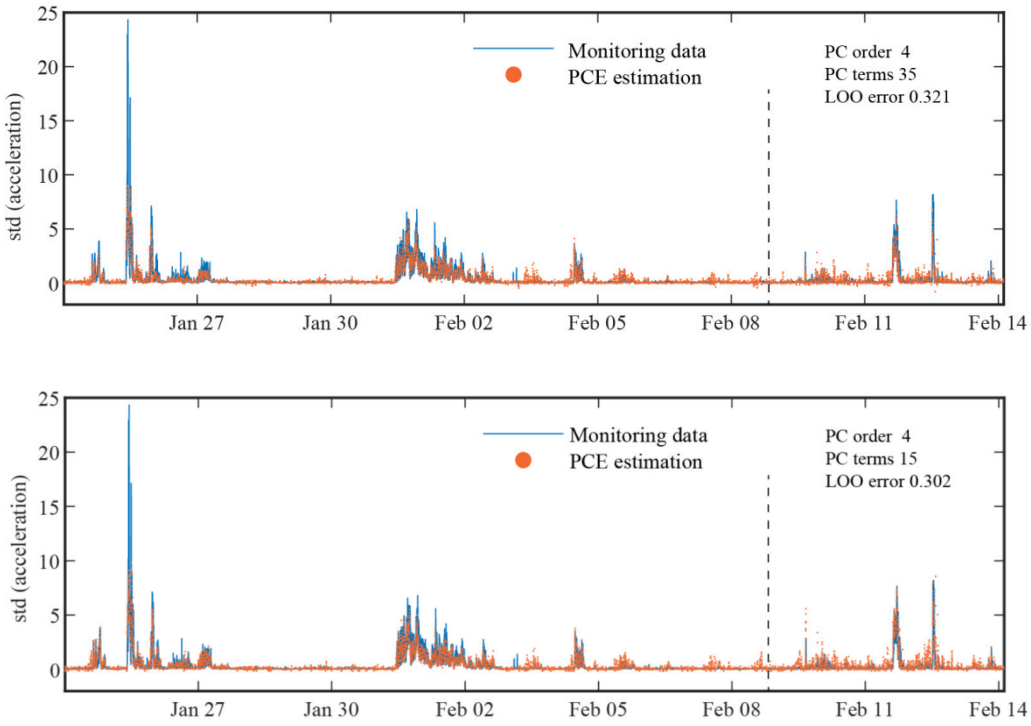

Figure 4.5. (Top) PCE model estimates for three input variables; (Bottom) PCE model estimates for two input variables;

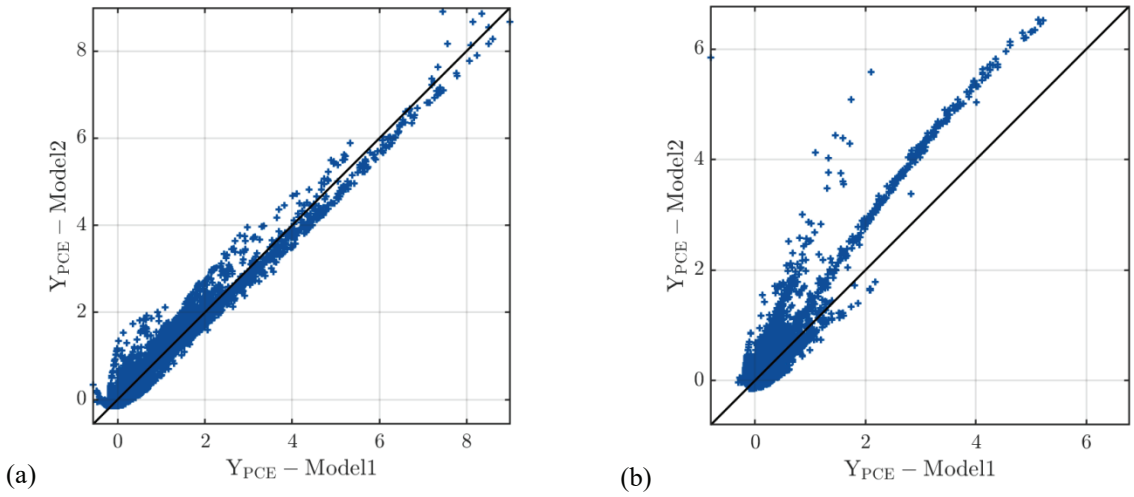

Figure 4.6. (a) PCE model 1 estimates versus PCE model 2 estimates - training data; (b) PCE model 1 estimates versus PCE model 2 estimates - validation data;

5 Conclusions

The research study presented herein focused on the construction and implementation of two separate data models using the polynomial chaos expansion method. Both models were successfully applied on two different full-scale case studies, namely a concrete arch dam and an industrial steel chimney, demonstrating the significant potential of the method to be used as a tool for long-term monitoring of engineering structures. In effort to present the workings of the method a rather straightforward utilization of the models was tested, i.e. featuring uncorrelated input sets and crude application of measured output parameters.

The obtained results demonstrated that the method represents an efficient tool for constructing data-driven models, characterized with simplicity of construction and little parameter tuning required. Specifically, after selecting the appropriate type and maximum degree of the polynomials in the basis, the coefficients are obtained through simple matrix algebra. Additionally, the obtained results with PC-based estimated Sobol's indices have accentuated the convenience of the tool for sensitivity analysis and as a result reducing the dimensionality of the studied problems.

Future research efforts are extended towards incorporating mutually dependent input variables aided by additional mathematical tools which will ensure preservation of the physical meaning of the transformed variables, as well as practicing the PCE tool with an accompanying diagnostic SHM tool which will allow for improved tracking of changes in structural responses.

CRediT authorship contribution statement

Viktor Georgijev: Writing- original draft, Formal Analysis, Resources, Visualization.

Simona Bogoevska: Writing-review & editing, Conceptualization, Methodology, Resources, Visualization, Validation, Supervision.

Declaration of competing interest

The authors declare that they have no known competing financial interests or personal relationships that could have appeared to influence the work reported in this paper.

Acknowledgments

The authors wish to extend their gratitude to the relevant authorities for providing the data for research purposes.

References

[1] Mishra, M., Lourenço, P.B. and Ramana, G.V., 2022. Structural health monitoring of civil engineering structures by using the internet of things: A review. *Journal of Building Engineering*, *48*, p.103954.

[2] Wang, G. and Ke, J., 2024. Literature Review on the Structural Health Monitoring (SHM) of Sustainable Civil Infrastructure: An Analysis of Influencing Factors in the Implementation. *Buildings*, *14*(2), p.402.

[3] Malekloo, A., Ozer, E., AlHamaydeh, M. and Girolami, M., 2022. Machine learning and structural health monitoring overview with emerging technology and high-dimensional data source highlights. *Structural Health Monitoring*, *21*(4), pp.1906-1955.

[4] Bogoevska, S., 2020. *A holistic framework for data-driven diagnostics of operational wind turbines* (Doctoral dissertation, Ruhr University Bochum).

[5] Barthorpe, R.J., 2010. *On model-and data-based approaches to structural health monitoring* (Doctoral dissertation, University of Sheffield).

[6] Brownjohn, J.M., 2007. Structural health monitoring of civil infrastructure. *Philosophical Transactions of the Royal Society A: Mathematical, Physical and Engineering Sciences*, *365*(1851), pp.589-622.

[7] Shahab Araghinejad. 2013. Data-driven modeling using MATLAB in water resources and environmental engineering. Springer.

[8] Chen, W., Kesidis, G., Morrison, T., Oden, J.T., Panchal, J.H., Paredis, C., Pennock, M., Atamturktur, S., Terejanu, G. and Yukish, M., 2017. Uncertainty in modeling and simulation. *Research Challenges in Modeling and Simulation for Engineering Complex Systems*, pp.75-86.

[9] Le Maître, O. and Knio, O.M., 2010. *Spectral methods for uncertainty quantification: with applications to computational fluid dynamics*. Springer Science & Business Media.

[10] Reis, J.F., Gori, G., Congedo, P.M. and Maître, O.L., 2021. Introduction to Spectral Methods for Uncertainty Quantification. *Optimization Under Uncertainty with Applications to Aerospace Engineering*, pp.1-34.

[11] Schick, M., 2012. *Uncertainty quantification for stochastic dynamical systems: Spectral methods using generalized polynomial chaos* (Doctoral dissertation, Karlsruhe, Karlsruher Institut für Technologie (KIT), Diss., 2011).

[12] Van Mai, C., 2016. *Polynomial Chaos Expansions for Uncertain Dynamical Systems-Applications in Earthquake Engineering* (Doctoral dissertation, ETH Zürich).

[13] Torre, E., Marelli, S., Embrechts, P. and Sudret, B., 2019. Data-driven polynomial chaos expansion for machine learning regression. *Journal of Computational Physics*, *388*, pp.601-623.

[14] Bogoevska, S., Spiridonakos, M., Chatzi, E., Dumova-Jovanoska, E. and Höffer, R., 2017. A data-driven diagnostic framework for wind turbine structures: A holistic approach. *Sensors*, *17*(4), p.720.

[15] Spiridonakos, M.D., Chatzi, E.N. and Sudret, B., 2016. Polynomial chaos expansion models for the monitoring of structures under operational variability. *ASCE-ASME Journal of Risk and Uncertainty in Engineering Systems, Part A: Civil Engineering*, *2*(3), p.B4016003.

[16] Sudret, B., 2008. Global sensitivity analysis using polynomial chaos expansions. *Reliability engineering & system safety*, *93*(7), pp.964-979.

[17] Ni, P., Xia, Y., Li, J. and Hao, H., 2019. Using polynomial chaos expansion for uncertainty and sensitivity analysis of bridge structures. *Mechanical Systems and Signal Processing*, *119*, pp.293-311.

[18] Hariri-Ardebili, M.A. and Sudret, B., 2020. Polynomial chaos expansion for uncertainty quantification of dam engineering problems. *Engineering Structures*, *203*, p.109631.

[19] Ghanem, R., Saad, G. and Doostan, A., 2007. Efficient solution of stochastic systems: application to the embankment dam problem. *Structural safety*, *29*(3), pp.238-251.

[20] Spiridonakos, M.D. and Chatzi, E.N., 2015. Metamodeling of dynamic nonlinear structural systems through polynomial chaos NARX models. *Computers & Structures*, *157*, pp.99-113.

[21] Guo, X., Dias, D., Carvajal, C., Peyras, L. and Breul, P., 2018. Reliability analysis of embankment dam sliding stability using the sparse polynomial chaos expansion. *Engineering Structures*, *174*, pp.295-307.

[22] De Falco, A., Mori, M. and Sevieri, G., 2018. Bayesian updating of existing concrete gravity dams model parameters using static measurements. In *6th European conference on computational mechanics & 7th European conference on computational fluid dynamics, ECCM-ECFD* (Vol. 1, pp. 2245-2256).

[23] YiFei, L., Minh, H.L., Khatir, S., Sang-To, T., Cuong-Le, T., MaoSen, C. and Wahab, M.A., 2023. Structure damage identification in dams using sparse polynomial chaos expansion combined with hybrid K-means clustering optimizer and genetic algorithm. *Engineering Structures*, *283*, p.115891.

[24] Spiridonakos, M. and Chatzi E., 2014. Polynomial chaos expansion models for SHM under environmental variability. In Proceedings of the 9th International Conference on Structural Dynamics (EURODYN), Porto, Portugal.

[25] International Commission on Large Dams (2012) Dam surveil lance guide. Tech. Rep. B-158, ICOLD

[26] He, Z., Li, W., Salehi, H., Zhang, H., Zhou, H. and Jiao, P., 2022. Integrated structural health monitoring in bridge engineering. *Automation in construction*, *136*, p.104168.

[27] Salazar, F., Morán, R., Toledo, M.Á. and Oñate, E., 2017. Data-based models for the prediction of dam behaviour: a review and some methodological considerations. *Archives of computational methods in engineering*, *24*, pp.1-21.

[28] Liu, Y., Zhang, J.M., Min, Y.T., Yu, Y., Lin, C. and Hu, Z.Z., 2023. A digital twin-based framework for simulation and monitoring analysis of floating wind turbine structures. *Ocean Engineering*, *283*, p.115009.

[29] Wiener, N., 1938. The homogeneous chaos. *American Journal of Mathematics*, *60*(4), pp.897-936.

[30] Xiu, D. and Karniadakis, G.E., 2002. The Wiener--Askey polynomial chaos for stochastic differential equations. *SIAM journal on scientific computing*, *24*(2), pp.619-644.

[31] Askey, R. and Wilson, J.A., 1985. *Some basic hypergeometric orthogonal polynomials that generalize Jacobi polynomials* (Vol. 319). American Mathematical Soc..

[32] Nikolovski Z., Jovanovski A., Mantev V. and Bejatovic D., 2013. Monitoring of Dam St. Petka. In Proceedings of the Third Dam Congress, Struga, North Macedonia.

[33] Bogoevska, S., Spiridonakos, M., Chatzi, E., Jovanoska, E.D. and Höffer, R., 2016. A data-driven framework for comprehensive identification of operational wind turbines under uncertainty. In Proceedings of the 5th International Conference on Uncertainty in Structural Dynamics (USD), Leuven, Belgium.

[34] Bogoevska, S., Dumova-Jovanoska, E. and Höffer, R., 2016. Response based modal identification of a real steel chimney. *Scientific Journal of Civil Engineering, 5(1), pp.27-31.*

Građevinski materijali i konstrukcije
Building Materials and Structures
journal homepage: www.dimk.rs

https://doi.org/10.5937/GRMK2400016P UDK: 624.012:625.815.5

Original scientific paper

Methods of testing systems for strengthening masonry structures based on cement composites reinforced with glass fiber mesh

Milica Petrović[1)], Marko Popović[2)], Marina Škondrić[*2)], Aleksandar Savić[2)], Dimitrije Zakić[2)]

[1)] *DB Inženjering d.o.o, Golsvordijeva 36, 11000, Belgrade, Serbia*
[2)] *University of Belgrade, Faculty of Civil Engineering, Bulevar kralja Aleksandra 73, 11000, Belgrade, Serbia*

Article history
Received: 21 November 2024
Received in revised form: 29 December 2024
Accepted: 26 January 2025
Available online: 25 February 2025

Keywords
rehabilitation of masonry structures,
FRCM systems,
glass-fibre grid,
testing methods

ABSTRACT

The paper presents the testing methods used for the contemporary masonry strengthening system, FRCM (fibre-reinforced cementitious matrix), which consists of glass fabric and mortar matrix. The FRCM system is suitable for strengthening masonry structures since it doesn't significantly change their mass and stiffness but increases the capacity for certain loads, especially ones induced by earthquakes. Following the recommendations, the mechanical properties of component materials and three groups (fibers, fibers in mortar, and masonry system) of specimens were tested. The main parameters necessary for calculating this system were defined and compared with the results found in the literature. It was shown that the chosen geometry for the mechanical test was appropriate for comparing the results within different groups. The importance of the type of fixtures used for the specimens (clevis- or clamping-grip) was more pronounced in the second group of specimens. Results of the first and the third group of specimens were in accordance with the literature, with the ultimate tensile stress of the dry fabric reaching 742,2 MPa, and the ultimate tensile strain of the dry fabric reaching 1.53%.The conventional strain obtained from the third group of specimens was 1.28%.

1 Introduction

Masonry structures represent a considerable percentage of the human-built heritage. After intense urbanization and the use of natural materials on large scales, contemporary society strives to apply principles of sustainable development in all areas of civil engineering. Therefore, one of the development directions in the building sector is strengthening and preserving existing structures and prolonging their service life [1].

Although masonry structures are very durable, theyare vulnerable to seismic forces [2]. Masonry walls are the most sensitive part of the system, and under seismic loads perpendicular to the wall, they can lose stability very quickly. The damage level and type of the structure determine the rehabilitation methods for masonry structures damaged by seismic loads.

Traditional strengthening methods, such as: injecting, shotcreting, reticulating, or overlaying the walls with cement-based mortars, are still widely used [3]. These techniques can sometimes be complicated for application; they usually increase the structure's mass and often influence the building's appearance [4].

The development of a fiber-reinforced cementitious matrix (FRCM) system primarily targeted masonry walls It is considered a substitute for the system with mortar and steel reinforcement since it is corrosion-resistant. The FRCM system fixes some problems with the fiber-reinforced polymer (FRP) system, like the fact that it is easily damaged by fire, does not work with masonry substrates, and cannot be used on damp walls [5] It consists of cement-based composites reinforced with fibre-based grids that can be of different origins: basalt, carbon, steel, or glass, usually overlaid with the inorganic matrix. Carbon fibers possess the highest tensile strength, elasticity, and durability. In contrast, glass and basalt fibers have lower tensile strength and modulus of elasticity and require additional alkali-resistant protective layers, but they are more economical [6]. Furthermore, glass and basalt fibers are better suited for masonry structures, known for their low modulus of elasticity.

To enable the application of the FRCM systems, it was necessary to develop testing methods for determination of the most important properties of the system, used in the calculations. Since it is a complex system, testing all component materials individually and then the system as a whole was obligatory. A group of researchers within the RILEM Technical Committee 250-CSM formed a document titled "Test Method for Textile Reinforced Mortar to Substrate Bond Characterization" [7], and published results from the Round Robin test performed within this RILEM committee [8].Similarly, European Assessment Document – EAD 340275-00-0104 was developed for composite systems with

* Corresponding author:
E-mail address: amarina@imk.grf.bg.ac.rs

inorganic matrixes to strengthen concrete and masonry structures externally [9]. The National Research Council of Italy, Advisory Committee on Technical Recommendations for Construction, has published CNR-DT 215/2018: Guideline for designing and constructing externally bonded fibre-reinforced *inorganic matrix systems for strengthening existing structures* [10]. This document presents the main points in the calculation and placement of FRCM systems. The document is optional, but it contains recommendations to help engineers apply these systems.. Based on this document, testing methods for the system have been described in the document titled: *„Linea Guida per la identificazione, la qualificazione ed il controllo di accettazione di compositi fibrorinforzati a matrice inorganica (FRCM) da utilizzarsi per il consolidamento strutturale di costruzioni esistenti"* [11].

2 Methodology

The paper presents the results of mechanical testing the FRCM system. The testing was divided into three groups:

1. testing the dry fabric in tension,
2. testing the composite specimen consisting of two mortar layers, with a glass-fibre grid placed between them,
3. testing the specimens with joint configuration (the wall strengthened with FRCM).

When the second group of specimens is concerned, the behaviour of the composite can be divided into three stages, according to the results. In stage A, the cement mortar matrix does not show any damage or cracks; the stress at the moment of the formation of the crack should be approximately equal to the tensile strength of the mortar [12]. Nevertheless, the differences in the production and curing of the specimens can lead to different measured stresses at the end of stage A. In stage B, which begins with the formation of the first crack, new cracks are expected to appear in the mortar matrix. The appearance of each new crack is visible in the stress-strain diagram as a sharp drop of stress. This phase ends when stress and strain again reach a linear relation. In the final stage (stage C), the existing cracks in the matrix start to widen, and the fabric becomes visible. The complete tensile strength is entrusted to the fabric in this phase. Stage C ends with the fracture of the specimen. For some of the composites, especially ones with glass fibre grid, the second stage is not visible in the diagram, and their behaviour is usually described as bilinear [12].

Apart from the behaviour of the system composed of cement-based mortar and fabric, it is important to test the relation between this system and the substrate. Therefore, the third group of specimens is usually tested by putting the ends of the fabric through a tensile test while the masonry substrate is restrained (push-pull method).

Different fracture types can be expected in this group of specimens,. As observed in the literature, for mortar matrix with glass fiber fabric, the tensile failure of the fabric is the most common. [8].

According to the Italian document CNR-DT 215/2018 [10] for the calculation of the strengthening system the following parameters need to be measured:

1) first group of specimens:
   - ultimate tensile stress of the dry fabric, $\sigma_{u,f}$,
   - elastic modulus of the dry fabric (E_f),
   - ultimate tensile strain of the dry fabric $\varepsilon_{u,f} = \sigma_{u,f}/E_f$,
2) second group of specimens:
   - tensile stiffness of the specimens in the stage A, if detectable (E_1),
   - ultimate tensile stress σ_u and ultimate tensile strain ε_u of the FRCM composite that are calculated based on the maximum force (at failure),
3) third group of specimens:
   - conventional stress $\sigma_{lim,conv}$ and conventional strain $\varepsilon_{lim,conv} = \sigma_{lim,conv}/E_f$.

The main property of the matrix (mortar) that needs to be determined is its compressive strength $f_{c,mat.}$The compressive strength of masonry ($f_{m,d}$) and the elastic modulus of masonry (E_m) are important parameters for the substrate.

Stresses are, within all tests, referred to the cross-sectional area of the dry fabric, regardless of the presence of the matrix/mortar.The conventional stress limit, which is evaluated through the bond test (third group of specimens), represents the bond strength of the specific FRCM system.It depends both on the type of substrate and on the properties of the system. The conventional strain limit is calculated based on the conventional stress limit and elastic modulus of dry fabric. It is then commonly used in the design of the strengthening interventions [9].

In the large-scale Round Robin test organised by the RILEM Technical Committee 250-CSM [8], 19 research centres were involved in defining the basic mechanical properties of the 30 FRCM, SRG (steel-reinforced grout) and other strengthening systems present in the market. All three groups of specimens were produced and tested. The testing was performed using the clamping-grip method [8].

The main differences in the results obtained on similar FRCM systems are a consequence of two possible methods for the seizing of the specimens in the tensile machine, known as clamping- and clevis-grip, as shown in Figure 1.

According to Arboleda et al. [12], it can be expected that specimens tested using the clamping-grip method reach higher values of strength when compared to the specimens tested using the clevis-grip method. It is assumed that this is a consequence of additional lateral pressures that are developed when the clamping-grip method is applied. In conclusion, the authors state that the clevis-grip method presents a more realistic behaviour of the composite and, therefore, a more realistic stress-strain diagram, but the final tensile strength values are more realistic for the clamping grip method.

The presented research's objective was to test the FRCM strengthening system with a cement-mortar matrix and a glass-fibre grid. Based on the testing of the three groups of specimens, the main parameters necessary for calculating this system were defined. Also, the benefits and flaws of the applied testing methods for each group of specimens were analyzed.

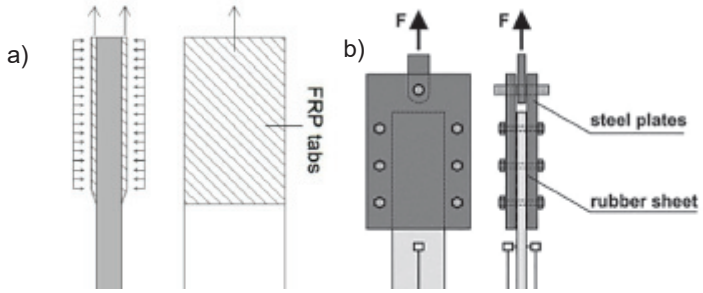

Figure 1. Presentation of the two gripping methods: a)clamping-grip[12], b)clevis-grip [13]

3 Experimental procedures

3.1 Materials

The present paper investigates the FRCM system comprised of glass-fibre mesh embedded within the cementitious mortar matrix.

The fabric used in this experiment is a bi-directional glass fibre mesh equipped with an alkali-resistant coating. The fabric is packed in rolls, where one roll has a width of 1m and a length of 50 m. Glass fibre yarns are oriented in the warp (longitudinal) and weft (transversal) directions. Warp direction is assumed as the direction of the main resistance. The average mesh size between warp fibre yarns is 18.2 mm, while weft fibre yarns have an axial distance of 14.2 mm. Mesh openings for warp and weft fibre yarns are 16 mm and 10.7 mm, respectively. The declared dry fibre density is 2.6 g/cm^3. According to the producer, its tensile strength is approximately equal in both directions and equals 77 kN/m. Cross section area of one glass fibre yarn is one of the main variables influencing fabric mechanical properties in the direction that is dominantly exposed to tension. This value is not defined in the official product datasheet but should be calculated according to the procedure given in EAD 340275-00-0104[9]. The cross-section area should always be calculated for a single yarn. To calculate the total grid specimen cross-section area, a value of one yarn area should be multiplied by the number of yarns that make a grid specimen. The calculation of the cross-section area of one glass fibre yarn should be done based on the following formula:

$$A_f = \frac{p_{yarn}}{\rho * l_{yarn}} * 1000 \quad (1)$$

where:

- p_{yarn} is mass of one yarn [g], measured based on instrument resolution of at least 0.01 g,
- l_{yarn} islength of one yarn [mm],
- ρ isfibredensity [g/cm^3].

Four specimens, each 1000 mm long and made of a single yarn, underwent mass measurements.The average mass measurement was equal to 2.446 g, which determined the value of cross sectional area equal to 0.941 mm^2.The cross-sectional area of one yarn determined above is used in the following stress calculations.

As a mortar matrix,pre-mix fiber-reinforced cementitious mortar, Sika MonoTop-722 Mur, with a maximum grain size of 1.4 mm was used. This mortar is delivered as dry-mix of cement, aggregate, fibers, and different mineral and chemical admixtures. During production, it was mixed with water, where mass of water to mass of dry-mix was 1:4.

Mortar prisms were prepared for testing mechanical characteristics of the hardened mortar; 15 prisms (40 x 40 x 160 mm) were prepared using a dry mix and an additional 20% of water. Specimens were cured in standard laboratory atmospheric conditions (temperature 23±2˚C, relative humidity 50±5%). Flexural and compressive strength testing (Figure 2) were executed per EN 1015-11. Average values calculated out of three specimens for flexural strength and six specimens for compressive strength are given in Table 1. According to the results, $f_{c,mat}$ of 26.8 MPa was obtained at the age of 28 days.

Table 1. Mechanical properties of the tested mortar

Age [days]	Flexural strength [MPa]	Compressive strength [MPa]
1	1.9	5.0
7	4.6	19.5
14	5.1	22.5
28	6.8	26.8

Besides mechanical properties, the water absorption coefficient due to capillary action was determined on prisms (40 x 40 x 80 mm) per EN 1015-18 (Table 2). After adequately preparing the specimens, they were placed into the water at a 5-10 mm depth. Their mass was measured 10 and 90 minutes after the first contact with water. The water absorption coefficient due to capillary action was determined based on the following formula:

$$C = 0{,}1\,(M_3 - M_0) \quad (2)$$

where:

- M_0 mass of dry prism [g],
- M_3 mass of prism after finalization of the test [g].

Table 2. Water absorption coefficient due to capillary action

Age [days]	Prism	Water absorption coefficient [kg/(m^2·min^{0,5})]
28	1	0.219
	2	0.220
	3	0.214
	average	0.218

Figure 2.Testing of the mortar specimen

3.2 Specimen preparation

Three groups of specimens were prepared to investigate the characteristics of the FRCM composite:

Group I) Dry fabric

Group II) FRCM coupons (fabric embedded in mortar matrix)

Group III) FRCM system applied on masonry element with dry fabric overhang

Specimens were prepared following previously mentioned and available guides, technical documentation, manuals, papers, and studies [7, 8 ,9, 11].In these documents minimal requirements for the width, length, and number of yarns of one specimen are defined. Nevertheless, it is up to the researchers to define the optimum specimen dimensions for the tests in question. To approximate realistic conditions, the specimens were as wide as possible, preserving the recomended ratio between the width and the length of the specimens.

The first group of specimens (I) consists of dry fibre fabric specimens that are 75 mm wide (4 warp yarns) and 500 mm long. Those specimens were cut out of a roll using scissors. At the end of fabric specimens steel tabs (75 x 100 x 3 mm) were bonded using epoxy resin. Three specimens were prepared in this manner.

The second group of specimens (II) consists of FRCM coupons made of two mortar layers (5 mm thick) with glass fibre fabric embedded between them. Specimens were prepared by the lay-up procedure in a few steps, using timber moulds (Figure 3.a), ensuring the proper dimension of each coupon (75 x 500 x 10 mm). In the first step, moldes are made of longitudinal and transversal timber battens with a thickness of 5 mm. After the 1st layer of mortar was applied, the moulds were exposed to vibration on the vibro-table for 5-10 s. In the next step, dry fabric pre-cut with 75 x 500 mm dimensions is slightly embedded in the first mortar layer (Figure 3.b). The control of fabric alignment in the middle of coupon thickness is crucial in such a procedure. In the last step (Figure 3.c), the additional timber battens with a thickness of 5 mm are mounted on the existing mouldes, ensuring a total mould thickness of 10 mm. The top layer of mortar was then applied and flattened using a finishing trowel. It is essential to complete the lay-up procedure within the pot life of the mortar. Prepared specimens were cured in mouldes for 7 days in standard laboratory atmospheric conditions and then cured in water for the next 21 days.

Since the geometry of specimens in the second group is specific due to their length-to-thickness ratio, EAD 340275-00-0104 [9] requires testing at least 20 specimens to determine appropriate insight into the characteristics of the coupons.

In the third group of specimens (III), the FRCM system is applied on masonry element. Before applying the FRCM system, it was necessary to investigate the mechanical properties of bricks and mortar joints, properly prepare the substrate that the system will be applied on, and investigate the substrate's quality.

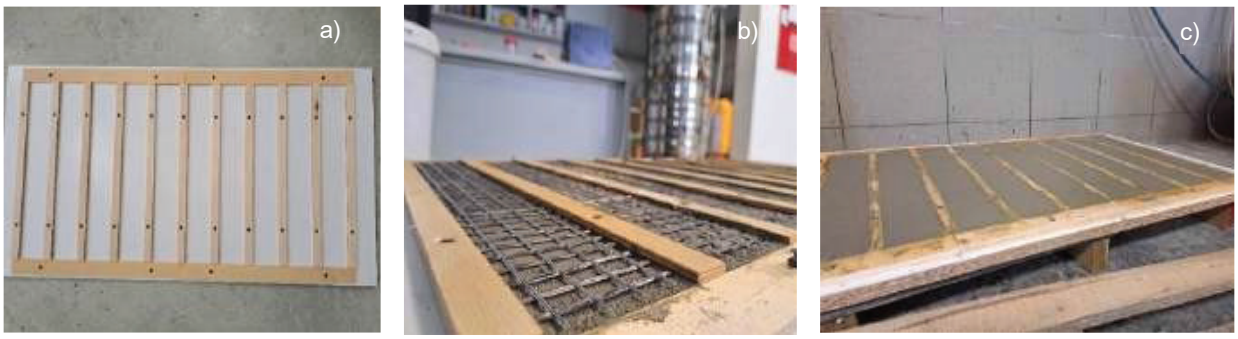

Figure 3. Preparation of the specimens (group II): a) moulds before lay-up procedure, b) embedding of fabric on the 1st mortar layer, c) coupons prepared in molds

EAD 340275-00-0104 [9] requires brick testing according to EN 771-1 (Figure 4) since the compressive strength of brick should not exceed 25 MPa. The tested brick specimens were 50 x 50 x 65 mm and 250 x 120 x 65 mm. The average compressive strength was 33.8 MPa for cubic specimens and 27.6 MPa for prismatic specimens. Although, the measured compressive strength of bricks was higher than required, no negative consequences on the behaviour of the specimens were noticed. The substrate's modulus of elasticity was not tested within this study, although it the determination of this parameter is recommended for the strengthening calculations.

EAD 340275-00-0104 [9] requires testing of mortar joints since the mortar class should not be higher than M5 according to EN 998-2. The mortar used for the joint had a density of 1728 kg/m^3 in a fresh state. During the preparation of masonry elements, six prisms 40 x 40 x 160 mm were made and cured in standard laboratory conditions. Hardened mortar density was measured after 7 and 28 days, as well as mortar flexure and compressive strength. Average values are given in Table 3. Testing results prove that mortar class is not higher than M5 by EN 998-2.

Table 3. Mechanicalproperties of mortar used for joints

Age [days]	Hardened mortar density [kg/m^3]	Flexure strength [MPa]	Compressive strength [MPa]
7	1634	1.10	3.12
28	1607	1.45	4.20

In the third group of specimens, the FRCM system with dimensions 75 x 300 x 10 mm was applied on a masonry element made of 6 half-bricks (125 x 120 x 60 mm) and mortar joints (10 mm thick). Before applying the FRCM system, the masonry substrate had to be prepared appropriately following the manufacturer's pre-treatment guide. The substrate to be strengthened was treated with sand blasting as long as a rough texture with visible pores was achieved. All the masonry surfaces were thoroughly cleaned and dust-free (Figure 5a). Before applying the FRCM system, the substrate was thoroughly pre-wetted to be saturated but surface-dry (Figure 5b).The brick substrate measured 410 x 125 mm, with the FRCM system applied 20 mm shorter at the top and 80 mm shorter at the bottom than the substrate edges (Figure 5c). Bare glass fibre fabric was continuously extended from a bonded system over masonry elements at a 250 mm overhang length. Steel tabs were bonded at the end of the bare fabric in 100 x 75 x 3 mm. Five specimens of the third group were prepared in total (Figure 5c).

The quality of the substrate was tested on individual masonry elements. EAD 340275-00-0104[9] requires testing of substrate quality according to EN 1542. The masonry substrate was properly cleaned by sandblasting before the mortar was applied to a thickness of 10 mm. After the mortar was cured in standard laboratory conditions, steel dollys with a diameter of 50 mm were arranged and bonded on adequately prepared substrate. Repair mortar was drilled using a diamond coring barrel at 5-10 mm depth. „Pull-off" tensile stress was measured on 5 individual dolly-fields (Figure 6). Results of tensile stress measurement and description of failure type are given in Table 4.

Figure 4. Preparation and testing of brick specimens

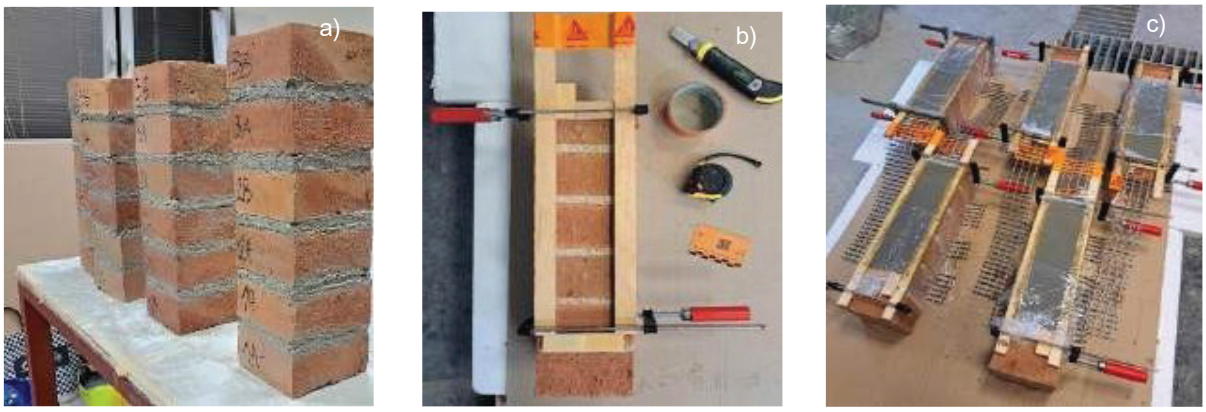

Figure 5. Preparation of the specimens (group III): a) masonry elements, b) area to be strengthened, c) FRCM system applied on masonry element with overhang fabric

Table 4. Substrate quality determination using the „pull-off" method

Dolly no.	Tensile strength [MPa]	Description of failure type	Failure type
1	1.85	Combined failure in substrate and in the 2nd layer	A:C=40:60
2	2.33	Combined failure in substrate and in the 2nd layer	A:C=70:30
3	2.34	Combined failure in substrate and in the 2nd layer	A:C=30:70
4	1.70	Cohesion failure in the 2nd layer	C
5	2.27	Cohesion failure in the 2nd layer	C

Figure 6. Brick specimens after the „pull-off" test was done

Following EN 1542 and EN 1504-3, the adhesion strength of mortar and substrate quality meet the requirements of standards, since all of the results are higher than 1.5 MPa.

3.3 Testing the FRCM system

The study aimed to determine the mechanical properties of the dry fabric (group I) and fabric as part of the FRCM system (groups II and III), as well as the performance of the strengthening system. All specimens were exposed to tensile force, while the strain was measured using extensometers.In group III, the relative displacement between the bare overhang fabric and masonry support was also necessary to measure. For that purpose, one steel profile „L"shape was bonded at the beginning of the overhang fabric length while two LVDTs were bonded on masonry substrate next to each FRCM side and in touch with the „L" profile, forming the 60 mm measuring base.

After considering all of the investigated and available testing methods, the clevis-grip method was adopted as suitable due to the fact that several specimens should be tested and the available testing equipment. A pair of steel plates holds the end of the specimen, while slippage prevention is ensured using rubber sheets. Each pair of steel plates is joined by bolts and fixed into the grips of the standard testing machine, allowing for torsional rotation and thus ensuring specimen alignment before the beginning of the test. This gripping method ensures stress transition by shear, without additional compressive forces perpendicular to the plane of the specimen.

The dimensions of the steel plates used for gripping were defined according to the dimensions of the specimens. The dimensions of the steel plates were adopted to be 100 x 200 x 10 mm so the specimen could be positioned in the central part of the plate. Six Ø15 mm bolt holes were made at each steel plate, ensuring connection by M14 bolts (Figure 7).

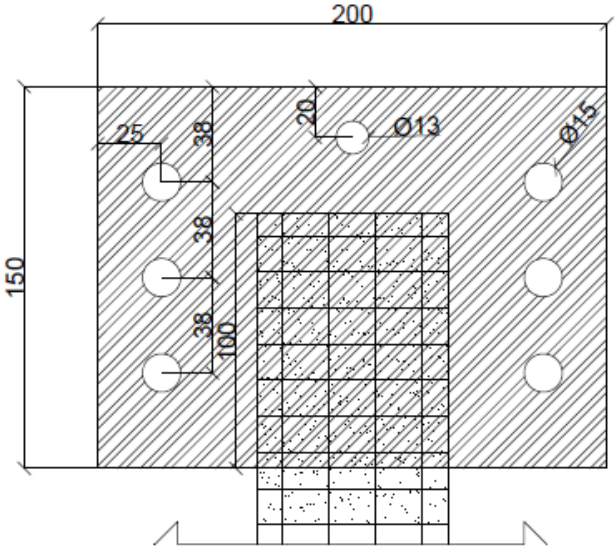

Figure 7. Arrangement of gripp using steel plates (measures are presented in [mm])

The first and the third groups required additional gripping and support equipment. Both groups had a part of dry fabric (without mortar matrix) that should be additionally prepared to ensure additional slippage prevention. A pair of steel tabs with 75 x 100 x 3 mm dimensions were bonded at each end of the fabric using epoxy resin. After the resin was cured, steel tabs were held by steel plates and specimens were exposed to testing (Figure 8).

As previously mentioned, strain measurement is arranged in the central part of the specimens' length using an Epsilon extensometer with gauge lengths of 100 mm and 200 mm for groups I and II, respectively.Slip of the fabric along the overhang length is measured in group III, using a pair of LVDTs („HBM WA-L“, 0-10 mm measurement range) located next to the FRCM bonded area. Tensile tests were performed using the universal testing machine „ShimadzuAG-X plus“ with 300 kN capacity.

4 Results and discussions

4.1 First group of specimens

Tensile tests were performed on three specimens cut from the glass fibre fabric. Based on the stress-strain diagrams (Figure 9), the modulus of elasticity of the fabric was estimated, following the EAD 340275-00-0104[9], referring to the stresses and deformations measured in the range of $F_u/10$ and $F_u/2$.

Based on the mean values of the fabric's ultimate stress and elastic modulus, the ultimate strain of fabric was determined $\varepsilon_{u,f} = (\sigma_{u,f} / E_f)$. These two parameters are crucial when calculating the reinforcement of masonry structures.

Testing the fabric through the clevis-grip method resulted in fibre failure at the clamping area. This failure mode is characteristic of the system in service with insufficient anchorage length. Test results largely correspond to the results from the literature (Table 5).

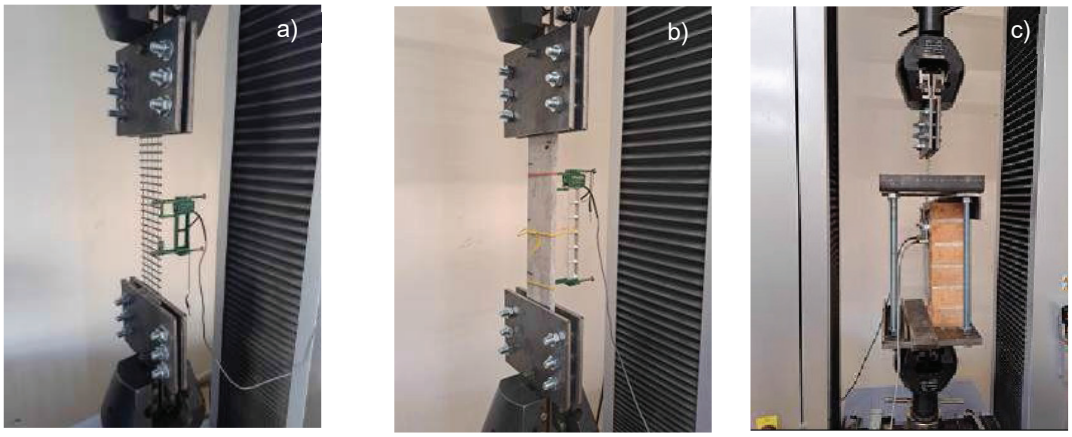

Figure 8. Specimens during the testing a) represent of group I, b) represent of group II, c) represent of group III

Table 5: Comparison of the test results of the first group (I) with results from the literature

SpecimenGroup	$\sigma_{u,f}$[MPa]	E_f [GPa]	$\varepsilon_{u,f}$ [%]
I	742.2	48.4	1.53
ACI 549.6R-20 [8]	750.0	50.0	1.50

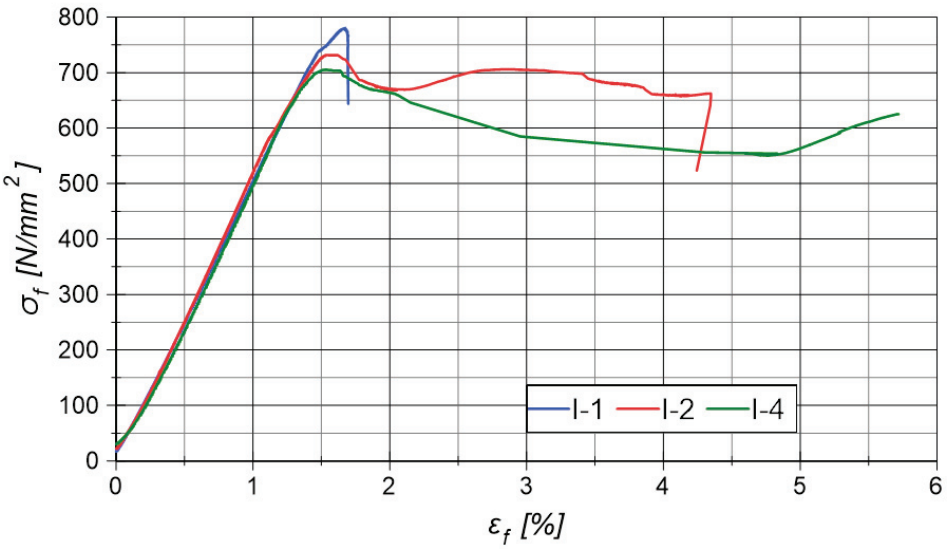

Figure 9. Stress-strain diagram for the first group of specimens [14,15]

4.2 Second group of specimens

This experimental campaign tested 10 prismatic FRCM specimens with 75 × 500 × 10 mm dimensions. The expected behaviour of this type of specimen was described in the section Methodology.

The behaviour of the FRCM composites during the tensile testing is characterised by considerable scattering of test results.The first crack within the extensometer gauge was observed for five specimens, leaving the other five out of the further analysis.

The stress-strain diagrams are presented in Figure 10. Following the EAD, the tensile stiffness moduli of stages A and C are calculated based on the change of stress and strain between the beginning and end of each phase (Tables 6 and 7).The line obtained by connecting the two points chosen for calculating the stiffness modulus should closely follow the trend of the response curve in the region, which was the case for the specimens in question. In stage A, the specimen shows composite behaviour, where the mortar (matrix) prevents the development of deformations in the glass fibres, and mortar and mesh deform together. For the stress-strain diagrams shown in Figure 10, the stress was calculated using cross-sectional area of the dry fabric. In order to determine the slope of the uncracked portion of the stress-strain diagram of the stage A, stresses were calculated both usign the cross-sectional area of dry fabric ($\sigma_{min,f}$ and $\sigma_{mas,f}$) and using the cross-sectional area of the whole specimen ($\sigma_{min,m}$ and $\sigma_{mas,m}$), as shown in Table 6. When the values obtained for fabric are analyzed ($E_{1,f}$), it can be noticed that the values are unusually high. Nevertheless, it is in confinement with the results obtained in the Round Robin test and presented in *ACI 549.6R-20*. The values calculated based on stresses in the mortar matrix ranged between 0.44 GPa and 10.95 GPa.

According to the Aveston-Cooper-Kelly theory (ACK) during the stage A, FRCM obeys the law of mixtures, and modulus of elasticity of composite (E_I) can be calculated as follows:

$$E_I = E_f \cdot v_f + E_m \cdot v_m \tag{3}$$

where E_f, represents Young's modulus of the fabric, E_m is Young modulus of the matrix, and v_f and v_m are the volumetric fractions of the fibers and matrix, respectively. In the presented research the modulus of elasticity for the fabric has been measured for the specimens in group I, while the modulus of elasticity of mortar matrix was not measured. According to Mercedes et al. [16] this modulus can be approximated based on the compressive strength of mortar f_c in [MPa]:

$$E_{ci} = 0.3 \cdot 8500 \sqrt[3]{f_c} \tag{4}$$

If these equations are applied on the obtained results, the modulus of elasticity of mortar matrix is equal to 7.63 GPa, while the modulus of elasticity of the composite (eq.3) is equal to 7.83 GPa.

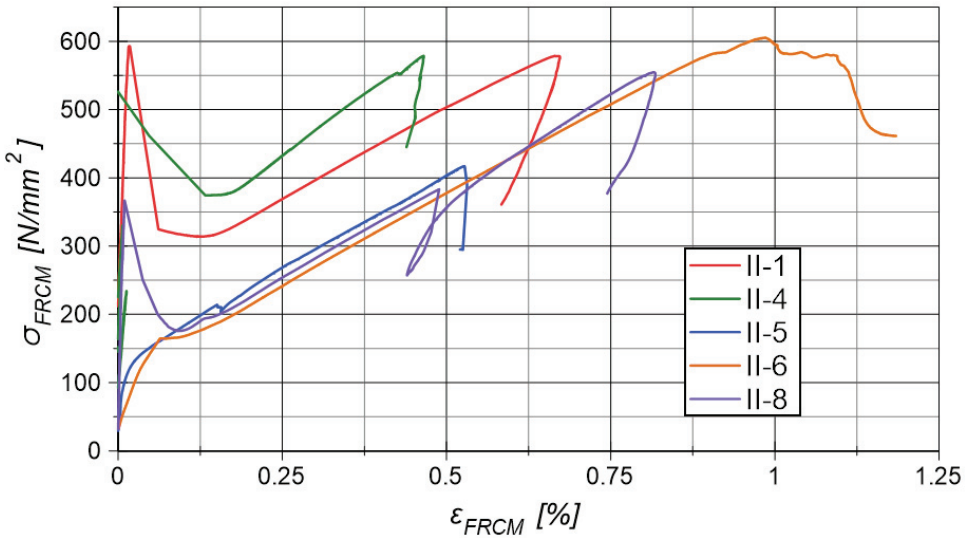

Figure 10. Stress-strain diagram for the second group of specimens [14,15]

Table 6. Measured values of stress, strain and calculated moduli for stage A

	Stage A									
Specimen	F_{min}[kN]	F_{max} [kN]	$\sigma_{min,f}$ [MPa]	$\sigma_{max,f}$ [MPa]	$\sigma_{min,m}$ [MPa]	$\sigma_{max,m}$ [MPa]	ε_{min} [%]	ε_{max} [%]	$E_{1,f}$ [GPa]	$E_{1,m}$ [GPa]
II-1	0.119	2.209	25.3	587.2	0.032	0.737	0	0.0214	2627.3	8.24
II-4	0.444	0.870	93.9	228.8	0.118	0.287	0	0.0124	1090.7	3.41
II-5	0.196	0.805	41.4	91.7	0.052	0.115	0.0029	0.0074	1123.2	2.14
II-6	0.154	0.627	32.8	166.6	0.041	0.209	0	0.0951	140.7	0.44
II-8	0.150	1.441	31.9	361.8	0.040	0.454	0	0.0094	3494.8	10.95

The corresponding stress-strain diagrams show that the stiffness moduli of stage C can be easily obtained from Figure 10 and Table 7. The values presented, and the linear behaviour in stage C align with the fabric's tensile behaviour.

Table 7. Measured values of stress and strain for stage C

	Stage C				
Specimen	σ_{min} [MPa]	σ_{max} [MPa]	ε_{min} [%]	ε_{max} [%]	E_3 [GPa]
II-1	315.1	577.2	0.13755	0.66028	50.1
II-4	377.6	577.0	0.17068	0.46153	68.6
II-5	215.3	416.3	0.16775	0.52731	55.9
II-6	173.3	582.8	0.11655	0.91178	51.5
II-8	197.8	379.0	0.14892	0.48022	54.7
Average					**56.2**

According to the Italian Guide [10], the stiffness moduli of stage A should be recorded if possible. The values calculated within this research exhibita high discrepancy in results.Due to the high scattering of the results, and the fact that in this test the boundary conditions differ from those experienced in the structural applications, the tensile modulus of dry fabric (E_f) is used in calculations, instead of the values measuted for the composite FRCM specimens [8]. Values obtained in the stage C for the stiffness modulus are close to the modulus of elasticity of the dry fabric, measured for the first group of specimens. This is in accordance with the theoretical assumption that in the final phase, the properties of the system rely on the properties of the dry fabric.

In presented stress-strain diagrams, the extensometer readings and the corresponding stress values are proportionally lower than the results from the literature. The smaller strain readings could be caused by insufficient contact between the extensometer and the composite, although much attention was paid to the proper connection of the extensometer to the specimen. On the other hand, estimated stiffness modulus values, as a primary outcome of this test,align with the literature, see Table 8.

Table 8. Comparison of test results of the second group (II) with results from the literature

Specimen Group	σ_u [MPa]	ε_u [%]	E_1 [GPa]	E_3 [GPa]
II	658.0	0.57	2404	56.2
ACI 549.6R-20 [8]	1250.0	1.50	2200	50.0

As confirmed by the tests, this group of specimens shows the highest degree of dispersion of results. Therefore, the requirement of standard EAD 340275-00-0104[9] for testing at least 20 specimens of this group is justified.

4.3 Third group of specimens

Testing the third group of specimens reveals the bond properties of the composite system adhesively applied to a flat masonry substrate. For this purpose, the single-lap shear test was performed as defined by EAD 340275-00-0104[9]. The force-slip diagrams are presented in Figure 11.

During the test, no cracks were observed along the composite, and the load-bearing failure occurred due to the tearing of the exposed part of the fabric (Figure 12). This failure mode designated as "F" in the literature, is expected for this type of reinforcement. As presented in Table 9, stress values are comparable to the corresponding values from the literature. The obtained slip value is lower than expected, although it can be significantly affected by the gauge length.

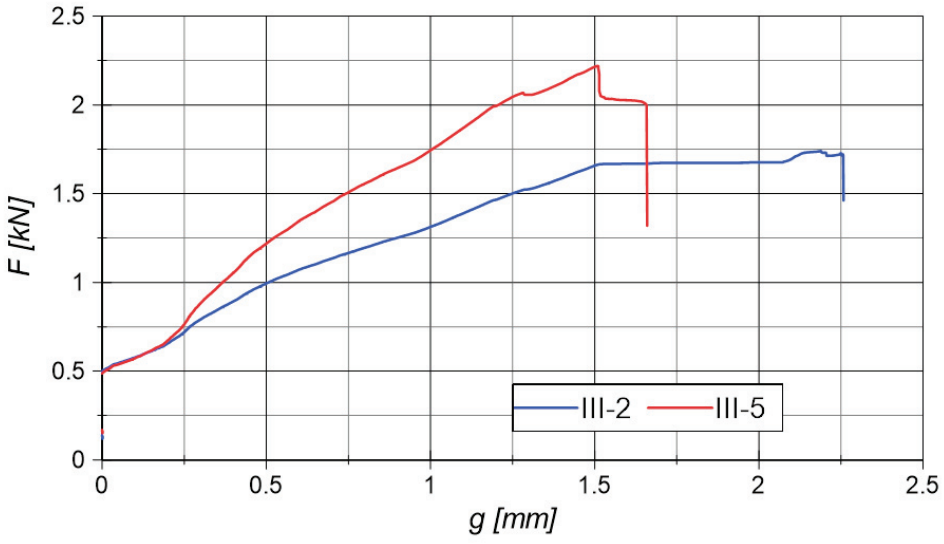

Figure 11. Force-slip diagram for the third group of specimens [14,15]

Figure 12. One specimen of the group III after the failure

The conventional strain was calculated as 1.28% using conventional stress and elastic modulus of dry fabric.

Table 9. Comparison of test results of the third group (III) with results from the literature

Specimen Group	$\sigma_{lim,conv}$ [MPa]	g_{max} [mm]
III	621.4	2.1
ACI 549.6R-20 [8]	620.0	2.8

5 Conclusions

The main objective of this study was to test the most important mechanical properties of the FRCM system used for the strengthening of the masonry elements. To achieve this, first, the components of the systems were tested, followed by the tests performed on the three groups (fibers, fibers in mortar, and masonry system) of specimens. The experiments were designed according to the recommendations found in the literature and using the available equipment and resources. Through the result analysis, different parameters affecting the results were discussed and explained.
The following conclusions can be made:

– Recommended mechanical properties of the component materials used for the specimen production were tested. The compressive strength of the mortar used as a matrix was 26.8 MPa at 28 days, adhesion strength was 2.1 MPa at the same age,and capillary water absorption was 0.218 kg/(m^2·min$^{0.5}$). The compressive strength of the bricks used for the third group of specimens was 33.8 MPa (measured on the cubic specimens cut out from the bricks). At 28 days, the mortar for the wall joints demonstrated a compressive strength of 4.2 MPa.

– Three important parameters obtained from the first group of specimens were ultimate tensile stress of the dry fabric, $\sigma_{u,f}$ = 742,2 MPa, elastic modulus of the dry fabric E_f=48.4 GPa, and ultimate tensile strain of the dry fabric $\varepsilon_{u,f}$=1.53%. Testing the composite specimens (second group) exposed very high dispersion of the results. The unusually high value of the slope of the uncracked phase in stage A is obtained when the stresses are calculated using the cross-sectional area of dry fabric. Although, the used guidelines [8,9] recommend measuring of this value, referred to as stiffness or stiffness moduli of the uncracked stage, the high scattering of the results is still an obstacle to its realistic measurements and application in calculations. When the modulus of elasticity of the stage A is calculated using the ACK model, the obtained value is 7.83 GPa. The ultimate tensile stress for this group of specimens was 658 MPa, while the ultimate strain was 0.57%. The third group of specimens obtained conventional stress at 621.4 MPa, while the conventional strain was 1.28%.

– The obtained results were, in most cases, in accordance with the results presented in the literature, especially the results of the Round Robin test performed within the RILEM TC 250 [8]. The main differences were noticed for the ultimate tensile stress and strain in the second group of specimens. The obtained stress value was 1.8 times lower than values found in the literature, while the strain was 2.6 times lower. The differences were probably the consequence of the different gripping methods applied and the different types of glass-fibre grid dimensions.

– All three groups of specimens used for the mechanical testing of one FRCM system were tested using the clevis-grip method. The chosen geometry of the specimens in different groups enabled the comparison of the obtained results and showed overall satisfying behavior. In the chosen geometry, the anchoring length was reduced to 100 mm, which was not satisfactory for the first group of specimens because the failure was induced near the gripping area. For this group, the recommended anchoring length of 125 mm should be applied in future tests.

– The importance of the way of seizing the specimens (clevis- or clamping-grip) was pronounced in the second group of the specimens. The clevis-grip method used for the performed tests gave realistic results with simpler and less expensive specimen preparation. In this way, most equipment parts may be used multiple times. The ultimate stress values obtained in the second group were lower than in the literature, which may be the consequence of the applied testing method. These specimens in the second group were also quite demanding for preparation.

– The third group of specimens was the most challenging to prepare, but it indicates the whole system's behaviour, which makes it very important. The failure mode in this group was through the fabric, which is expected for this type of FRCM system.

– As an important part of future investigations, different durability properties of the system, and their influence on the durability of the masonry structure should also be tested and discussed.

Creditauthorship contribution statement:

Milica Petrović: Formal analysis, State-of-the-art, Visualization, Writing - original draft. **Marko Popović:** Conceptualization, Methodology, State-of-the-art, Testing, Writing - original draft. **Marina Škondrić:** Conceptualization, Methodology, Funding acquisition, Visualization, Writing - original draft. **Aleksandar Savić:** Methodology, Writing – Control and editing. **Dimitrije Zakić:**Methodology, Writing – Control and editing.

Declaration of Competing Interests:

The authors declare that they have no known competing financial interests or personal relationships that could have appeared to influence the work reported in this paper.

Acknowledgement:

This work was supported by the Ministry of Science, Technological Development and Innovation Republic of Serbia [grant number 200092].

References

[1] C. Elefante, „The Greenest Building Is ... One That Is Already Built“, Forum Journal, vol 27, no 1, pp. 62-42, 2012, 10.1353/fmj.2012.a494514

[2] Ž. Radovanović, S. Dimovski, I.Lalošević, Strengthening masonry walls made of brick blocks with FRCM composites, Building Materials and Structures, 2015, vol. 58, iss. 2, pp. 21-37, Society for Materials and Structures Testing of Serbia

[3] I. Hafner, T. Kišiček, M. Gams, „Review of Methods for Seismic Strengthening of Masonry Piers and Walls“, Buildings, vol. 13, no 6, pp. 1524, 2023, https://doi.org/10.3390/buildings13061524

[4] A. Keshmiry, S. Hassani, U. Dackermann, J. Li, „Assessment, repair, and retrofitting of masonry structures: A comprehensive review“, Construction and Building Materials, vol. 442, no 6, pp. 137380, 2024, https://doi.org/10.1016/j.conbuildmat.2024.137380

[5] CNR – Advisory Committee on Technical Recommendations for Construction, National Research Council Advisory Committee on Technical Recommendations for Construction, Guide for the Design and Construction of Externally Bonded FRP Systems for Strengthening Existing Structures Materials, RC and PC structures, masonry structures; CNR-DT 200 R1/2013, 2014

[6] N. Gattesco, „New Materials for the Rehabilitation of Cultural Heritage“, Czech Technical University in Prague, Faculty of Civil Engineering, 2011.

[7] G. de Felice, M.A. Aiello, C. Caggegi, F. Ceroni, S. de Santis, E. Garbin, N. Gattesco, L. Hojdys, P. Krajewski, A. Kwiecien, M. Leone, G.P. Lignola, C. Mazzotti, D. Oliveira, C. Papanicolaou, C. Poggi, T. Triantafillou, M.R. Valluzzi, A. Viskovic, „Recommendation of RILEM Technical Committee 250-CSM: Test Method for Textile Reinforced Mortar to Substrate Bond Characterization“, Materials and Structures, Vol. 51, No. 4, p. 95 doi: 10.1617/s11527-018-1216-x

[8] ACI 549.6R-20 Guide to Design and Construction of Externally Bonded Fabric-Reinforced Cementitious Matrix (FRCM) and Steel-Reinforced Grout (SRG) Systems for Repair and Strengthening Masonry Structures, prepared by the ACI 549-L – RILEM TC 250 Liaison Subcommittee, American Concrete Institute, ISBN: 978-1-64195-120-3

[9] European Assessment Document- EAD 340275-00-0104, European Assessment Document, „Externally-bonded composite systems with inorganic matrix for strengthening of concrete and masonry structures“, 2018

[10] CNR – Advisory Committee on Technical Recommendations for Construction, Guide for the Design and Constructionof Externally Bonded Fibre ReinforcedInorganic Matrix Systems,for Strengthening Existing Structures, CNR –DT 215/2018, 2020

[11] ConsiglioSuperioredeiLavoriPubbliciServizioTecnico Centrale, Linea Guida per la identificazione, la qualificazione ed ilcontrollo di accettazioe di composite fibrorinforzati a matricepolimerica (FRP) da utillizzarsi per ilconsolidamentostrutturale di costruzioniesistenti, 2019.

[12] D. Arboleda,F. Carozzi, A. Nanni, and C. Poggi, “Testing Procedures for the Uniaxial Tensile Characterization of Fabric-Reinforced Cementitious Matrix Composites”, Journal of Composites for Construction,Vol. 20, No. 3, p. 04015063, 2016 doi: 10.1061/(ASCE)CC.1943-5614.0000626

[13] RILEM Technical CommitteeTC 232-TDT (Chairman W. Brameshuber), Recommendation of RILEM TC 232-TDT: test methodsand design of textile reinforced concrete, Materials and Structures, 2016, DOI 10.1617/s11527-016-0839-z

[14] M. Petrović, M. Popović, M. Škondrić, A. Savić, D. Zakić, Načini ispitivanja cementnih kompozita ojačanih staklenom mrežicom kod zidanih konstrukcija, Zbornik radova sa nacionalnog simpozijuma DGKS, p. 381-390, 2024.

[15] M. Petrović. Testing methods and possible applications of the glass fiber reinforced cement composites in masonry structures, Master thesis, University of Belgrade, Faculty of Civil Engineering, 2023.

[16] L. Mercedes, G. Castellazzi, E. Bernat-Maso, L. Gil, Matrix and fabric contribution on the tensile behaviour of the fabric reinforced cementitious matrix composites, Construction and Building Materials, 363, 129693, 2023. https://doi.org/10.1016/j.conbuildmat.2022.129693

Građevinski materijali i konstrukcije
Building Materials and Structures
journal homepage: www.dimk.rs

https://doi.org/10.5937/GRMK2500001D UDK: 666.972.1:661.666

Original scientific paper

Assessment of the development of strains/cracks in carbon-short-fiber-reinforced concrete (CSFRC) under static tensile loading using strain gauges and light-beam micrometer

Ante Džolan[*1)], Oliver Fischer[2)], Marino Jurišić[3)]

[1)] *Department of Structural Engineering, Faculty of Civil Engineering, University of Rijeka, 51000 Rijeka, Croatia*
[2)] *Chair of Concrete and Masonry Structures, Technical University of Munich, 80333 Munich, Germany*
[3)] *Department of Mechanics, Materials and Structures, Faculty of Civil Engineering, Architecture, and Geodesy, University of Mostar, 88000 Mostar, Bosnia and Herzegovina*

Article history
Received: 10 January 2025
Received in revised form: 04 February 2025
Accepted: 12 February 2025
Available online: 10 March 2025

Keywords
CSFRC,
light-beam micrometer (LBM),
ductile behavior,
strain, crack

ABSTRACT

Concrete is the most widely used material in the world today, but its extensive use also poses environmental risks due to high CO_2 emissions. To mitigate these emissions, reducing concrete consumption in construction is crucial. Enhancing its mechanical properties, particularly low tensile strength, can accomplish this. Enhancing tensile strength allows for the construction of smaller cross-sections of concrete elements, resulting in more efficient material utilization. One effective method for strengthening concrete is through fiber reinforcement. In this study, short carbon fibers are used to reinforce the concrete, creating a material known as short-carbon-fiber-reinforced concrete (CSFRC). The objective of this research is to advance the understanding of CSFRC's behavior under tensile stress. To do this, strain gauges and a light-beam micrometer (LBM) are used to track crack and strain growth, which gives information about how well the CSFRC is working overall.

1 Introduction

Buildings, bridges, and other infrastructure are essential for modern society to function effectively. Different types of infrastructure require various construction materials, with concrete being one of the most important. According to some sources, concrete is the most widely used man-made material and the second most used material overall, after water [1]. As a result, global concrete production has reached approximately 30 billion tons annually [2]. However, this extensive use of concrete has significant environmental consequences, as it accounts for 4 to 8% of total CO_2 emission [3]. To mitigate concrete's environmental impact, it is crucial to reduce the quantity of concrete used in construction. This can be achieved by minimizing concrete cross-sections, which requires addressing its main weakness—low tensile strength. The higher the tensile strength of concrete, the less material is needed for construction.

The tensile strength of concrete can be enhanced by incorporating various fibers (such as natural, steel, PVA, cellulose, glass fibers, etc.) into the fresh concrete mixture during the mixing process [4-17]. In this study, the addition of carbon fibers during the mixing phase improves the mechanical properties of concrete.Carbon fibers possess several advantageous characteristics, including the ability to withstand high stresses under both quasi-static and dynamic loading conditions, a high elastic modulus, creep resistance, low specific weight, high tensile strength, non-corrosiveness, a low thermal expansion coefficient, chemical stability, high thermal conductivity, and low electrical resistivity [18-21]. Due to their low electrical resistivity, concrete reinforced with carbon fibers also exhibits low electrical resistivity (i.e., high electrical conductivity). This makes carbon-fiber-reinforced concrete self-sensing, which lets cracks be found and concrete degradation be evaluated without damaging the concrete [22–31]. For this reason, some researchers refer to carbon-fiber-reinforced concrete as "smart concrete." In addition to these sensing capabilities, the inclusion of carbon fibers enhances the mechanical properties of concrete, as detailed below.

Concrete generally has significantly higher compressive strength than tensile strength, but the addition of carbon fibers further enhances its compressive strength. In [32], the design of M25 grade concrete, with a compressive strength of 28.13 MPa, followed IS 10262-2009 was used as the reference concrete. Specimens reinforced with 0.75 vol%, 1.00 vol%, and 1.25 vol% of carbon fibers showed compressive strength increases of 46.80%, 60.00%, and 32.40%, respectively, compared to the reference concrete. The optimal result was observed with 1.00 vol% of carbon fibers. In [33], the reference concrete had a compressive strength of 43.80 MPa and was reinforced with carbon fibers ranging from 0 to 2.40 vol%. The greatest increase in

* Corresponding author:
E-mail address: ante.dzolan@uniri.hr

compressive strength was seen with 0.2 vol% of carbon fibers, achieving 90.10 MPa—an increase of 105.70%. But as the amount of carbon fibers went above 0.2 vol%, the compressive strength steadily went down. The lowest value (17.40 MPa) was found in the mixture with 2.40 vol% carbon fibers. Similarly, the results in [34] indicate that compressive strength increases only up to a certain carbon fiber content, beyond which it begins to decline. For instance, plain concrete with a compressive strength of 40.88 MPa increased to 46.40 MPa (13.50% increase) with 1.00 vol% carbon fibers. At 1.50 vol%, the strength was 41.66 MPa (1.91% increase), while 2.00 vol% resulted in 39.48 MPa (3.55% decrease).

It looks like these results show that there is not a single way to tell if carbon-fiber-reinforced concrete will get stronger because it depends on both the concrete mix and the type of carbon fibers that are used [21]. A higher content of carbon fibers does not automatically result in higher compressive strength, and there is concern about over-reinforcing concrete with carbon fibers. To avoid this, the optimal fiber content for each concrete mixture must be determined.

The tensile strength of concrete can be measured directly or indirectly (through splitting tensile strength tests). In reference [35], the carbon fiber content in the concrete mixture is expressed as the fiber-cement ratio (f-c ratio). Splitting tensile strength was measured for f-c ratios of 0%, 4%, 8%, and 12%. The results show a continuous increase in splitting tensile strength as the f-c ratio rises from 0% to 8%. The peak value, 4.60 MPa, is reached at an f-c ratio of 8%, representing a 62% increase compared to the f-c ratio of 0% (2.84 MPa). However, further increasing the f-c ratio reduces the beneficial effect of carbon fiber reinforcement, with the splitting tensile strength at a 12% f-c ratio dropping to around 4.25 MPa—a 7.60% decrease compared to the strength at 8%.

Similarly, the results in [34] show the splitting tensile strength for various fiber contents: 0 vol%, 0.50 vol%, 1.00 vol%, 1.50 vol%, and 2.00 vol%. A near-linear increase in splitting tensile strength is observed as carbon fibers are added, with the highest value of 3.42 MPa at 2.00 vol% of fibers, which represents a 132.60% increase over plain concrete. In [32], plain concrete has a splitting tensile strength of 3.20 MPa, which increases steadily as the carbon fiber content rises to 1.00 vol%. At this level, the splitting tensile strength reaches 5.00 MPa, an increase of 56.25%. But at 1.25 vol%, the strength drops to 3.50 MPa, which is only 9.40% more than plain concrete. This shows that the tensile strength decreases as the carbon fiber content rises above 1.00 vol%.

As with compressive strength, these findings suggest that there is an optimal carbon fiber content, beyond which the benefits diminish or even become negative. Also, the results in [36] show that concrete reinforced with carbon fibers has higher splitting tensile strengths of 16.30% compared to concrete reinforced with glass fibers and 12.80% compared to steel fibers.

In [21], the tensile strength of plain concrete, concrete reinforced with steel fibers (SF), Zoltek carbon fibers (zCF), Hexcel carbon fibers (hCF), and recycled carbon fibers (rCF) were measured directly. It turns out that concrete reinforced with rCF has a tensile strength of 6.89 MPa, which is about 27.80% higher than plain concrete (5.21 MPa), 4.60% higher than concrete reinforced with SF (6.58 MPa), 26.30% higher than concrete reinforced with hCF (5.29 MPa), and 26.40% lower than concrete reinforced with zCF (8.99 MPa). In [37, 38], the directly measured tensile strength of concrete reinforced with 1.00 vol% zCF is reported to be around 15.00 MPa. These studies used a high-performance concrete (HPC) mixture, which was then reinforced with carbon fibers. According to [39], the tensile strength of HPC alone is approximately 7.90 MPa, meaning the addition of zCF increases the tensile strength by 90.00%.

The findings in [21, 37, 38] reveal varying degrees of improvement in tensile strength depending on the type of concrete mixture and carbon fibers used. These improvements are significantly influenced by the alignment angle between the carbon fibers and the direction of applied loads (stresses) [20, 37, 40, 41]—the smaller the alignment angle, the greater the improvement in mechanical properties, including tensile strength.

References [32-35, 42] demonstrate the improvement of flexural strength through the reinforcement of concrete with carbon fibers. However, careful attention must be given to avoid over-reinforcing the concrete According to studies [32, 33, 35], the flexural strength goes up up to a certain point where the optimal amount of carbon fibers is reached. After that, the benefits start to fade, and too many fibers can even make the flexural strength lower than in plain concrete. According to [37], the flexural strength of carbon-fiber-reinforced concrete increases by approximately 2.70-fold and 4.65-fold for concrete containing 1.00 vol% and 3.00 vol% of carbon fibers, respectively, when the fiber alignment angle relative to the applied stress is 0°. However, when the alignment angle increases to 30°, the improvement is reduced to around 1.13-fold for 1.00 vol% and 1.57-fold for 3.00 vol%.

These results show that carbon fiber reinforcement has less of a positive effect as the angle between the fibers and the direction of stress increases. At a 30° alignment angle, the impact is minimal, while at angles up to 20°, the positive effects are still noticeable. Beyond 40°, no improvement in flexural strength is observed [37].

In addition to enhancing mechanical properties, reinforcing concrete with carbon fibers alters the behavior of carbon-fiber-reinforced concrete under tension. Specifically, carbon fibers bridge cracks in the concrete [21], contributing to the pseudo-ductile behavior of carbon-fiber-reinforced concrete under tension [37, 38, 43]. This study contributes to the further understanding of the pseudo-ductile behavior of carbon-fiber-reinforced concrete under tensile loading. To this end, dog-bone-shaped specimens reinforced with short carbon fibers (3 mm in length) were prepared for direct static tensile tests. Due to the short length of the fibers, this material is referred to as carbon-short-fiber-reinforced concrete (CSFRC). The static tests were performed on specimens of different ages at the time of loading (28 and 70 days). For each age group, three specimens were tested, and their strain during the tests was measured using two techniques—strain gauges and a light beam micrometer (LBM). When measuring with strain gauges, the strain is measured in one point (micro-region), so that the results of different strain gauges can disagree to each other and it cannot be expected that the results of a single strain gauge correctly describe the behaviour of the entire testing area. Therefore, four different strain gauges were attached to the specimens in the testing area, and the behaviour of the testing area is described by the average value of these four strain gauges. However, the question arises as to whether this method of describing the behaviour of the testing area based on the average results from different points is reliable. To test this, the LBM micrometre was also used to measure the strain in the testing area. In contrast to strain gauges, the LBM measures the strains in a larger area (in this work in the entire testing area) and not in one point. Therefore, its results

are more relevant for describing the behaviour of the testing area than the results obtained with strain gauges. The main objective of this work is to investigate the reliability of the description of the behaviour of the test area based on the average results of several strain gauges. For this purpose, the average results of strain gauges are compared with the results measured with LBM.

2 Materials and methods

2.1 Raw materials and mixing procedure

The raw materials for the preparation of the CSFRC specimens are listed in Table 1:

Table 1. List of raw materials

Component	Type of Component	wt%
Cement	Holcim Sulfo 52.5 R	34.70
Silica fume	Sika Silicol P	21.70
Quartz powder	SF 500	21.70
Quartz sand	H33	7.70
Water	--	11.70
Superplasticizer	BASF ACE 460	2.50
Carbon fibers	Zoltek (Toray) PX35, 3 mm	1.00 (vol%)

Carbon fibers were uniformly cut to a length of 3 mm, with the following properties: diameter of 7 µm, elastic modulus of 242 GPa, tensile strength of 4137 MPa, and ultimate tensile strain of 1.5%. To enhance the dispersion of the fibers in the concrete mixture and improve adhesion between the fibers and the concrete, the fibers were oxidatively heated for 2 hours in an open furnace at 425°C before being incorporated into the cement paste [19]. The addition of carbon fibers decreases the workability of the concrete [34, 42]. However, workability can be improved by adding a superplasticizer to the cement matrix prior to incorporating the carbon fibers [33, 44]. The superplasticizer also aids in achieving better dispersion of the carbon fibers within the concrete. Furthermore, the addition of silica fume to the concrete mixture enhances the interfacial adhesion and dispersion of the fibers [19, 45]. Care should be taken when adding silica fume, as it can negatively affect the concrete, such as increasing shrinkage [45-49]. To achieve high early strength in the concrete paste, CEM 52.5 R cement was selected as the binder. Other components of the concrete mixture included quartz powder, quartz sand, and water.The maximum grain size of the sand is 0.6 mm, making it suitable for use in 3D concrete printing.

The mixing process consists of several phases. In the first phase, all dry components—cement, quartz powder, quartz sand, and silica—were placed into the mixer and thoroughly mixed. Once the dry components were well combined, water and superplasticizer were gradually added. The mixing continued until the air content in the mixture was minimized. Afterward, carbon fibers were incorporated into the mixture, and two mixing cycles lasting approximately 30 to 45 seconds were conducted to ensure uniform dispersion.

2.2 Printing process and curing procedure

To achieve optimal alignment between the carbon fibers and the applied stresses, a 3D printing technique was employed for the production of the specimens [50]. After completing the mixing procedure, the concrete mixture was transported in plastic bags to a 3D printer developed at the Technical University of Munich (TUM) for specimen fabrication [51]. Good fiber alignment was accomplished by extruding the concrete mixture through a nozzle with a diameter of 4 mm (Figure 1a). As a result, the deviation in the angle between the carbon fibers and the tensile stresses remained primarily within the range of ±10° [37]. A more detailed description of the printing process can be found in [52, 53].

The tested specimens were shaped like dog bones, measuring approximately 445 mm in height, 100 mm in width at both the upper and lower ends, and 50 mm in width in the testing area, which was also 50 mm in height. The specimens had a consistent depth of 50 mm (Figure 1b).

After the specimens were produced, they were placed in formwork and kept in an environment with 100% relative humidity (RH) for 1 day. Subsequently, for the following 6 days, the specimens were cured underwater. Following this 7-day curing period, the specimens were stored in a controlled environment with an RH of 65±5% and a temperature of 20±2°C until the day of testing.

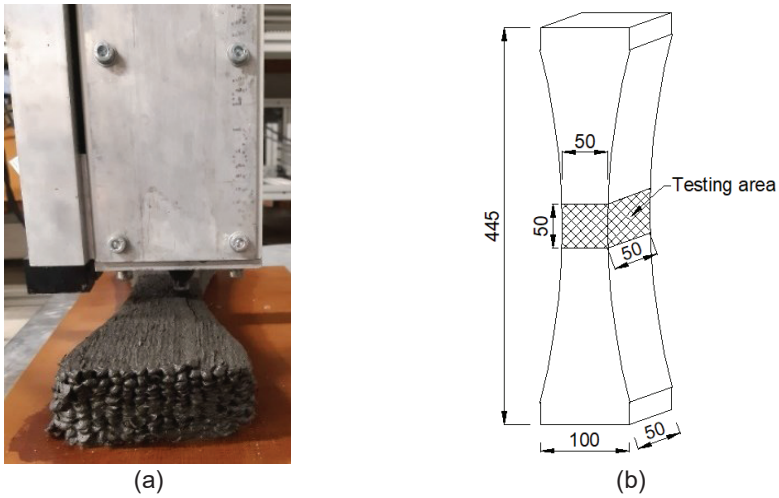

(a) (b)

Figure 1. Printing process (a); Shape and dimensions (measurement units are in mm) of the tested specimens (a) [38]

2.3 Testing procedure

One day before testing, strain gauges were attached to the specimens. Immediately afterward, the specimens were positioned in the testing device (Figure 2a). They were secured to the device using a two-component adhesive that required 24 hours to cure . Each specimen had four strain gauges put on it in the direction of the tensile load. Two gauges were placed on the top and bottom edges of the testing area (Figure 2b).

After the two-part glue had dried, two light beam micrometer (LBM) devices were attached to the test device and the samples (Figure 2) so the tests could begin.The specimens were subjected to uniaxial tensile loading in a displacement-controlled manner, with a loading rate of 0.003 mm/s. The load was gradually increased until the specimens fractured.

Three specimens were tested at 28 days of age, while another three specimens were tested at 70 days.

3 Results and discussion

3.1 Specimens tested at the age of 28 days

As mentioned earlier, four strain gauges were installed on each specimen to measure the development of strains. For the specimens loaded at 28 days, three specimens—designated as S37, S44, and S57—were tested. The results from all four strain gauges on specimen S57 are presented in Figure 3, from which an average line was derived.

Based on the average line, it is evident that the average first crack strength of specimen S57 (position A) is 9.11 MPa, corresponding to a strain of 0.24‰. The average ultimate tensile strength (position B) is 15.11 MPa, and the average ultimate tensile strain (position C) is 1.56‰ [38] (Figure 3). The average first crack strength, average tensile strength, and average ultimate tensile strain for specimens S37 and S44 were determined in the same manner and are presented in Table 2.

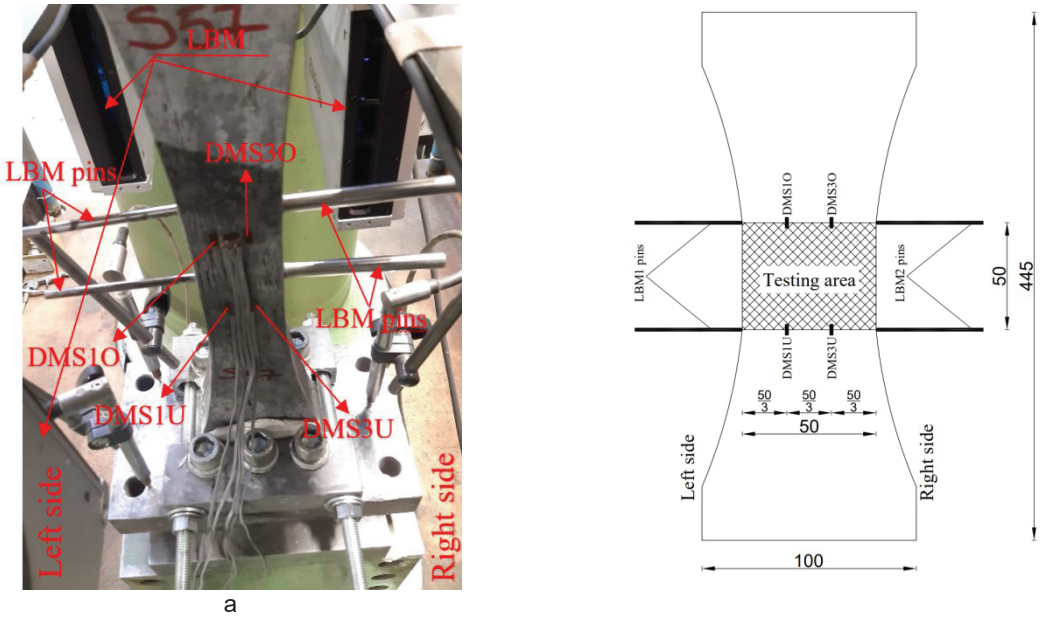

Figure 2. View of the specimen installed to the test device (a); Schematic representation of the measuring equipment's position (measurement units are in mm)(b)

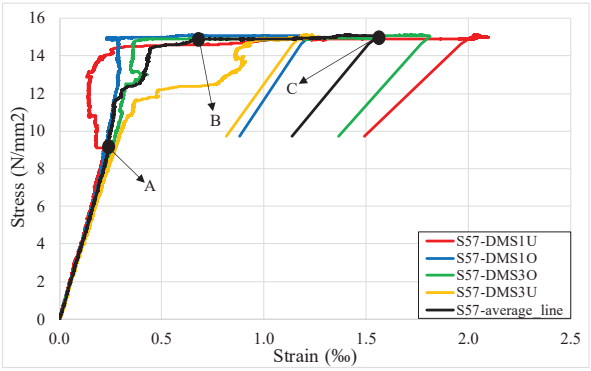

Figure 3. Results measured by strain gauges in the specimen S57

Table 2. Mechanical properties of the specimens S37 and S44 [38]

Specimen	First crack strength (MPa)	Tensile strength (MPa)	Ultimate tensile strain (‰)
S37	8.30	14.64	3.42
S44	9.20	15.01	2.28

Figure 4 presents a comparison of the average lines for all three specimens: S37, S44, and S57.

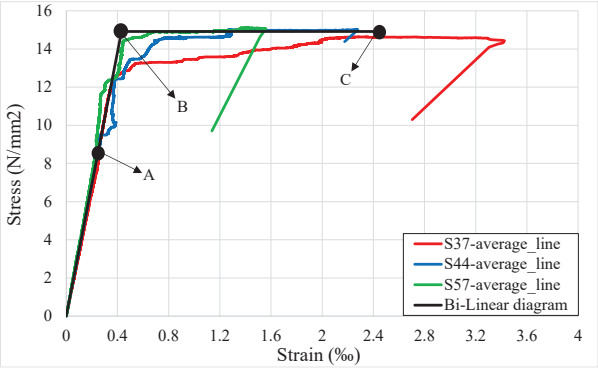

Figure 4. Stress-strain curves of the specimens loaded at the age of 28 days [38]

To see how carbon-short-fiber-reinforced concrete (CSFRC) acts when it is loaded at the age of 28 days [38], a bi-linear diagram can be made from the average lines.The bi-linear diagram indicates linear behavior until the stress reaches the tensile strength of 14.92 MPa [38] (position B in Figure 4), after which CSFRC yields until the ultimate tensile strength of 2.42‰ [38] (position C in Figure 4) is attained. However, Figure 4 reveals a slight discrepancy between the experimental results and the bi-linear diagram from position A (first crack strength of 8.87 MPa [38]) to position B. This discrepancy arises from micro-nonlinearity (micro-cracks) that occurs between positions A and B, which doesn't disrupt the global linearity of the specimens, i.e., the testing area. The strain measured by the strain gauge reflects the strain development at a specific point (a narrow local area), and the micro-nonlinearity at that point does not necessarily influence the global linearity of the specimen. This is evident in the results presented in Figure 3.

The blue (DMS1O) and green (DMS3O) lines in Figure 3 behave almost linearly until the tensile strength is reached. This means that there were no cracks at the locations of these two strain gauges or nearby. In contrast, the red line (DMS1U) demonstrates strain relaxation between positions A and B, suggesting that a micro-crack opened near the location of that strain gauge, leading to the observed strain relaxation. Unlike the red line, the yellow line (DMS3U) shows a sudden increase in strain at approximately 12.00 MPa. After the strain reaches around 0.80‰, the slope of the stress-strain curve closely resembles the slope before position A. This indicates that a micro-crack opened at the location of the strain gauge (reflected in the sudden increase of strain), which likely closed after some time as another micro-crack formed nearby.

The results presented in Figure 3 illustrate all possible types of strain development at the locations of the strain gauges. Similar trends were observed for specimens S37 and S44, which contributed to the average lines shown in Figure 4. These average lines are what the bi-linear diagram is built on, which lets us figure out how carbon-short-fiber-reinforced concrete (CSFRC) acts in a bigger picture.

A pertinent question arises: can these localized, somewhat mediocre results accurately predict the macro (i.e., global) behavior of CSFRC? To address this question, the results in Figure 4 are compared with those obtained using the light beam micrometer.

Figure 2 illustrates that the light beam micrometer (LBM) measures the distance—specifically, the change in distance—between the upper and lower edges of the testing area on both sides of the specimens during the tensile static test. From this distance change, the macro (i.e., global) strains (ΔL/L) of the testing area can be calculated. The LBM results for specimens S37 and S57 are presented in Figures 5a and 5b, respectively. However, specimen S44 experienced a lack of LBM data due to the LBM pins becoming unglued at the very beginning of the test.

Figures 5a and 5b present the LBM stress-strain curves alongside the bi-linear diagram from Figure 4. There is a strong link between the results when you look at the LBM curves (Figures 5a and 5b) and the average lines from the strain gauges (Figure 4).This indicates that the mediocre micro-results obtained from the strain gauges can reliably represent the global behavior of carbon-short-fiber-reinforced concrete (CSFRC), allowing the bi-linear diagram to serve as an effective tool for predicting CSFRC behavior. The coordinates of the bi-linear diagram are listed below:

Table 3. Coordinates of the bi-linear diagram.

Stress (MPa)	Strain (‰)
0.00	0.00
14.92	0.43
14.92	2.42

A comparison of the results in Figure 5 with those in Figure 3 clearly demonstrates that relying on data from a single strain gauge within the testing area is not sufficient for accurately predicting the behavior of carbon-short-fiber-reinforced concrete (CSFRC).

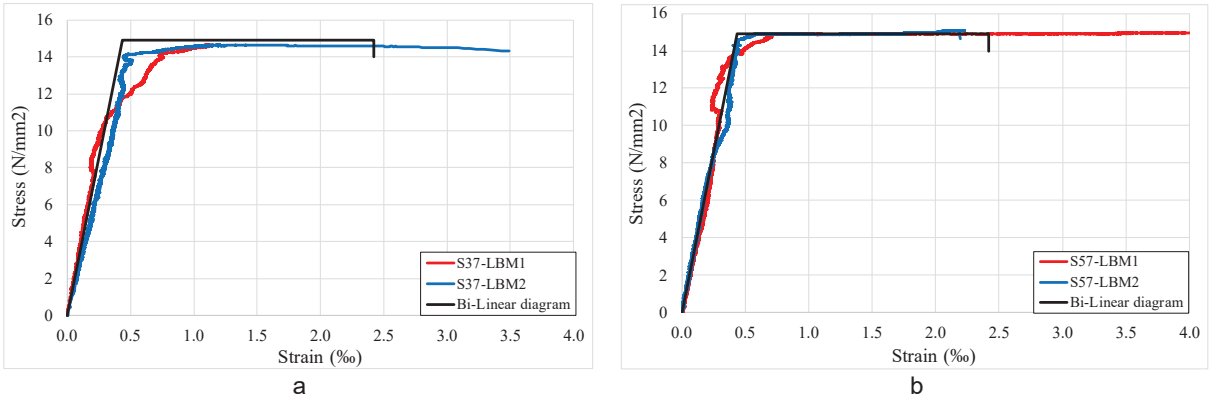

Figure 5. LBM Stress-strain curves of the specimens S37 (a); and S57 (b)

3.2 Specimens tested at the age of 70 days

Specimens identified as S53, S56, and S59 were tested at 70 days of age. Figure 6 presents the results for specimen S56.

According to the results in Figure 6a, a linear relationship between stress and strain can be observed in all strain gauges until the stress reaches an average first crack strength of 11.35 MPa for the specimen [38]. After this point, strain relaxation occurs in all four strain gauges (Region A in Figure 6a). This strain relaxation indicates that the damage process—characterized by the opening of micro- and macro-cracks—occurs outside the testing area. This assertion is supported by Figure 6b, which shows that the main crack developed at the bottom edge of the testing area. The presence of these micro and macro cracks outside the testing area and along the specimen's edges fully relaxes the strain and crack state within the testing area. When the stress reaches the tensile strength of the specimen at 14.72 MPa, the CSFRC begins to yield (Figure 6a). The average ultimate strain for specimen S56 is recorded at 1.56‰ [38].

The failure of specimens S53 and S59 also occurred outside the testing area. In contrast to specimen S56, specimen S53's main crack formed well above the testing area (Figure 7a), while specimen S59's main crack formed well below the testing area (Figure 7b).

Since the main cracks in specimens S53 and S59 are located farther away from the testing area than in specimen S56, they do not relax the strain and crack state of specimens S53 and S59 as significantly as in specimen S56. This is illustrated in Figure 8, which presents the results for specimen S53.

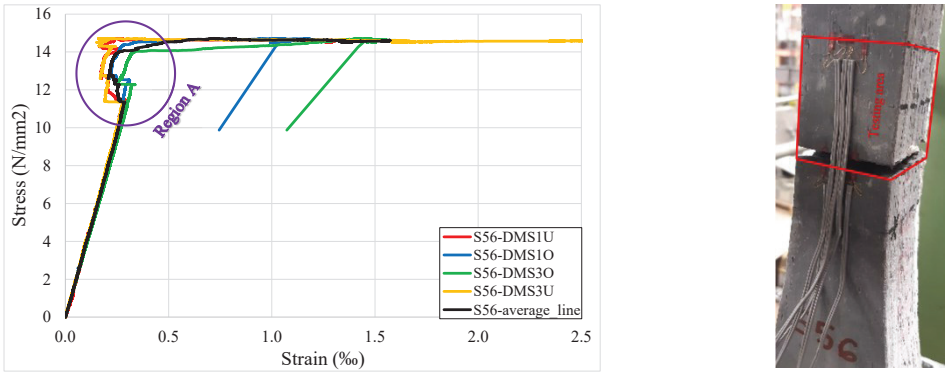

a b

Figure 6. Results measured by strain gauges in the specimen S56 (a); View of the specimen after failure (b)

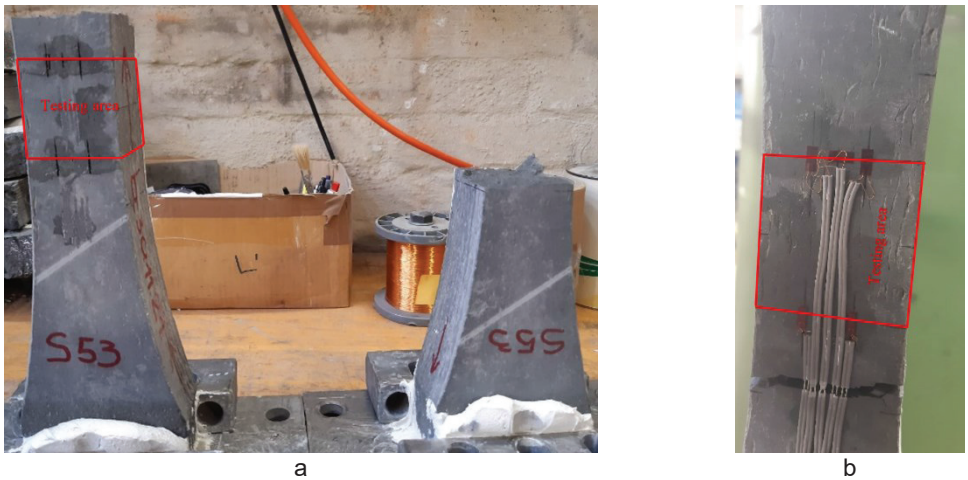

a b

Figure 7. View of the specimen S53 (a); and specimen S59 after failure (b)

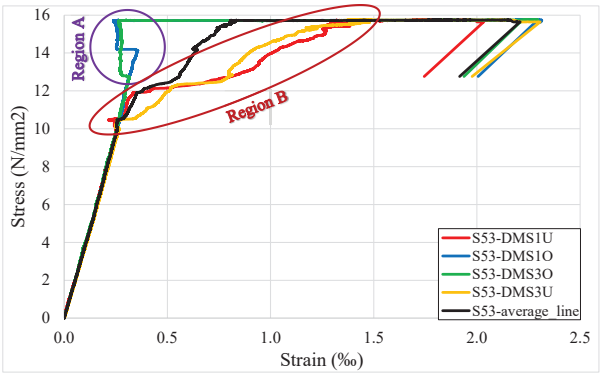

Figure 8. Results measured by strain gauges in the specimen S53

In region A (Figure 8), a soft relaxation of strains can be observed in the strain gauges DMS1O and DMS3O. These gauges are positioned closer to the main crack than DMS1U and DMS3U (Figure 7a). Therefore, the soft relaxation in these strains may be attributed to the proximity of the main crack to the strain gauges or the presence of micro- or macro-cracks nearby. In contrast, no relaxation effect is observed in strain gauges DMS1U and DMS3U.

Once the stress reaches the first crack strength (the average value for specimen S53 is 10.10 MPa [38]), the slope of the stress-strain curve in region B (Figure 8) is lower than before reaching the first crack strength. This means that global (macro) cracks are starting to appear at the locations of strain gauges DMS1U and DMS3U. These cracks keep getting bigger as the stress rises to the tensile strength (15.75 MPa [38]). Indeed, region B (Figure 8) indicates the hardening behavior of CSFRC when stress is between the first crack strength and the tensile strength. After the stress reaches the tensile strength, CSFRC begins to yield, and upon reaching the ultimate tensile strain (the average value for specimen S53 is 2.20‰), the specimen ultimately breaks.

The behavior of specimen S59 is similar to that of specimen S56, and its mechanical properties are provided in Table 4.

Table 4. Mechanical properties of the specimens S59 [38]

Specimen	First crack strength (MPa)	Tensile strength (MPa)	Ultimate tensile strain (‰)
S59	10.20	15.69	1.76

In Figure 9, alongside the average lines of the tested specimens, two prediction models—the bi-linear diagram and the stress-strain curve in four points—are also presented. The stress-strain curve in four points effectively simulates the experimental results of specimens S53 and S59. In contrast, the behavior of specimen S56 is more accurately represented by the bi-linear diagram. The coordinates of these two prediction models are provided in Table 5:

For each specimen, the average stress-strain curves were generated based on the results from four different strain gauges, as illustrated in Figure 9.

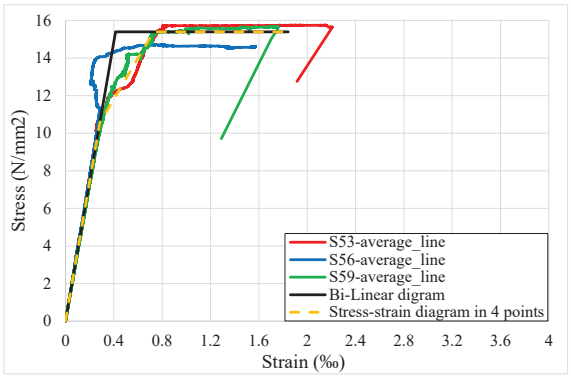

Figure 9. Stress-strain curves of the specimens loaded at the age of 70 days [38]

The results presented in Figure 9 are derived from averaging the data collected at various points, allowing for the prediction of the global (macro) behavior based on these local (micro) results. To validate the prediction models illustrated in Figure 9 and Table 3, a comparison is made between these results and those obtained through Light Beam Micrometer (LBM) measurements. The global (macro) results for the testing area of specimens S53 and S56, as obtained by LBM, are displayed in Figure 10. Unfortunately, for specimen S59, the LBM pins detached from the specimen at the beginning of the test, resulting in a lack of LBM data for this specimen.

Table 5. Coordinates of the bi-linear diagram

Bi-Linear diagram			***Stress-strain curve in 4 points***	
Stress (MPa)	Strain (‰)		Stress (MPa)	Strain (‰)
0.00	0.00		0.00	0.00
15.39	0.41		10.55	0.28
15.39	1.84		15.39	0.73
			15.39	1.84

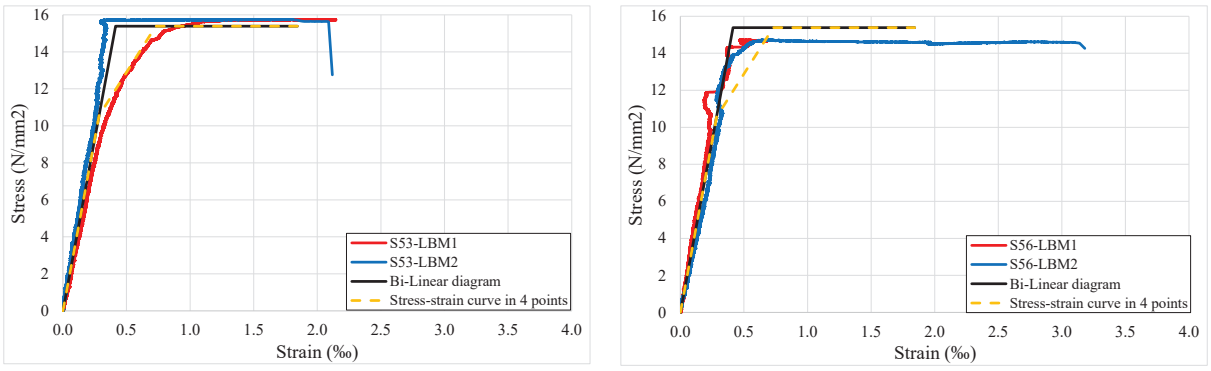

Figure 10. LBM Stress-strain curves of the specimens S53 (a); and S56 (b)

The results in Figure 10a show that both the bi-linear diagram and the stress-strain curve in four points can accurately predict how Carbon-Short-Fiber-Reinforced Concrete (CSFRC) will behave on a larger scale. These are based on the local (micro) results from four different points in the testing area (shown in Figure 9). Additionally, Figure 10b confirms that the bi-linear diagram reliably characterizes the behavior of specimen S56.

The LBM results presented in Figure 10a reveal a distinct behavior between the left side of specimen S53 (LBM1) and the right side (LBM2). On the left side, the stress-strain curve remains nearly linear until the stress reaches the tensile strength, after which the CSFRC begins to yield. In contrast, the stress-strain curve on the right side is linear only until the stress hits the first crack strength. Following this, the CSFRC exhibits hardening while the stress is between the first crack strength and tensile strength. Once the tensile strength is achieved, the CSFRC starts to yield. This disparity in results between the left and right sides of the specimen suggests the location of the first global (macro) crack within the testing area and indicates the direction of its propagation. Specifically, the global crack in the testing area initiates on the right side of the specimens and propagates towards the left side as the load increases.

3.3 Comment on the CSFRC behavior

Based on the previously described results, CSFRC clearly demonstrates a highly ductile behavior under tension. However, notable differences in this behavior emerge concerning the age of the loaded specimens. Specifically, specimens loaded at the age of 28 days exhibit an almost linear behavior until the stress reaches the tensile strength. While the global behavior remains nearly linear, a local (micro) non-linearity can be observed in the testing area when the stress is between the first crack strength and the tensile strength. Once the stress surpasses the tensile strength, CSFRC begins to yield.

When the stress is between the first crack strength and the tensile strength, the specimens loaded at 70 days show a tendency for CSFRC to harden. This is not the case with the specimens loaded at 28 days. Accordingly, their behavior can be divided into three distinct phases. Initially, until the stress reaches the first crack strength, they exhibit a linear behavior. Once this happens, and the stress is between the first crack strength and the tensile strength, something similar to CSFRC hardening happens. Finally, after the stress surpasses the tensile strength, CSFRC begins to yield.

4 Conclusions

Based on the presented results, the following conclusions can be drawn:

- **HighTensile Strength**: Carbon-short-fiber-reinforced concrete (CSFRC) exhibits relatively high tensile strength, nearly twice that of high-performance concrete and approximately six times greater in comparison with normal-strength concrete.
- **Ductile Behavior**: CSFRC demonstrates highly ductile behavior, regardless of the age at the time of loading. This characteristic enhances its fatigue performance.
- **Prediction of 28-Day Behavior**: The behavior of CSFRC loaded at 28 days can be accurately predicted using a bi-linear diagram. This behavior can be divided into two distinct phases: a predominantly linear behavior until the tensile strength is reached, followed by yielding once the tensile strength is exceeded. While no global cracks are present before reaching the tensile strength, a network of micro-cracks (micro-nonlinearity) develops between the first crack strength and tensile strength, contributing positively to the fatigue performance of CSFRC.
- **70-Day Behavior**: In contrast, CSFRC loaded at 70 days exhibits a tendency toward CSFRC hardening when the stress is between the first crack strength and the tensile strength. This behavior can be reliably predicted using a stress-strain curve with four points, which is divided into three distinct phases: a linear behavior until reaching the first crack strength, CSFRC hardening indicating the opening of global cracks between the first crack strength and tensile strength, and yielding after reaching the tensile strength. The global cracks that form enhance the fatigue performance of CSFRC compared to the specimens loaded at 28 days.
- Prediction **of Global Behavior**: **Relying on a single strain gauge in the testing area to predict global (macro) behavior is not feasible.** Increasing the number of strain gauges improves the accuracy of predictions for global behavior. The global behavior predicted by averaging the results from four strain gauges aligns closely with the global results obtained from light-beam micrometers (LBM).
- **Utilizationof LBMs**: Employing two LBMs on opposite sides of the specimens facilitates the prediction of where the global crack will appear and the direction of its propagation.
- **Hardening of the testing area:** All three specimens tested at 28 days broke within the testing area, while those tested at 70 days broke outside the testing area. This indicates that the ageing of CSFRC has a positive effect on the hardening of the testing area and on the improvement of its energy dissipation capacity.
- **Limitations of the study and directions for future research:** This study investigared only the CSFRC with one amount of carbon fibers. It did not look at what happens when this material is reinforced with more carbon fibers.

Therefore, future research should shed light on how effective the reinforcement of concrete with carbon fibers is when the content of carbon fibers increases.

CRediT authorship contribution statement:

Project administration, O.F.; supervision, O.F.; writing-review and editing: O.F., A.D., M.J.; conceptualization, A.D.; data curation: A.D.; formal analysis investigation: A.D.; methodology: A.D.; visualization: A.D.; validation: A.D.; writing – original draft preparation: A.D., M.J. All authors have read and agreed to the published version of the manuscript.

Declaration of competing interest:

The funders had no role in the design of the study; in the collection, analyses or interpretation of data; in the writing of the manuscript or in the decision to publish the results.

Funding: This research is funded by the German Research Foundation (DFG) as part of the Priority Program SPP2020: “Cyclic deterioration of High-Performance Concrete in an experimental-virtual lab” (Grant Numbers FI1720/7-1, GR1664/13-1, PE1464/6-1, VO829/13-1)

Acknowledgments:

The researcher express their gratitude to everyone involved in the priority program SPP2020, as the working atmosphere between the groups is created by fruitful collaboration.

References

[1] Concrete: the most destructive material on Earth, https://www.theguardian.com/cities/2019/feb/25/concrete-the-most-destructive-material-on-earth (accessed on 2 October 2024).

[2] There Will Soon Be More Concrete Than Biomass on Earth, https://heatmap.news/economy/the-planet-s-jaw-dropping-astonishing-downright-shocking-amount-of-concrete (accessed on 2 October 2024).

[3] Environmental Go!: 9 Environmental impacts of Cement Production, https://hr.environmentgo.com/utjecaj-proizvodnje-cementa-na-okoli%C5%A1/#google_vignette (accessed on 2 October 2024).

[4] A.M.Brandt,Fibre reinforced cement-based (FRC) composites after over 40 years of development in building and civil engineering,*Compos. Struct.*86 (2008) 3–9. doi.org/10.1016/j.compstruct.2008.03.006

[5] X.Guo,G. Xiong, Resistance of fiber-reinforced fly ash-steel slag based geopolymer mortar to sulfate attack and drying-wetting cycles,*Constr. Build. Mater.*269 (2021) 121326. doi.org/10.1016/j.conbuildmat.2020.121326

[6] H.M.Hamad,J.Shi,M.S.Al Jawahery,A.Majdi,S.T.Yousif,G. Kaplan, Application of natural fibers in cement concrete: A critical review,*Mater. Today Commun.*35 (2023) 105833. doi.org/10.1016/j.mtcomm.2023.105833

[7] K.Hannawi,H.Bian,W.Prince-Agbodjan,B. Raghavan, Effect of different types of fibers on the microstructure and the mechanical behavior of Ultra-High Performance Fiber-Reinforced Concretes,*Compos. Part B Eng.*86 (2016) 214–220. doi.org/10.1016/j.compositesb.2015.09.059

[8] G.L.Insaurriaga,C.C.Gomes,F.V.Ribeiro,G.L.Calegaro ,T.A.Silveira,L.F.Cruz,J.A.Cruz,S.C.Amico,RA. Belucis, Effect of Hybridization of Carbon Fibers on Mechanical Properties of Cellulose Fiber-Cement Composites: A Response Surface Methodology Study,*C-J Carbon. Res.*10 (2024) 41. doi.org/10.3390/c10020041

[9] S.H.Kosmatka,W.C.Panarese,B. Kerkhoff, Design and Control of Concrete Mixtures. Portland Cement Association Skokie: Skokie, IL, USA, 2002; Volume 5420.

[10] I.L.Larsen,R.T. Thorstensen, The influence of steel fibres on compressive and tensile strength of ultra high performance concrete: a review,*Constr. Build. Mater.*256 (2020) 119459. doi.org/10.1016/J.CONBUILDMAT.2020.119459

[11] J.Liu,C. Lv, Durability of Cellulosic-Fiber-Reinforced Geopolymers: A Review,*Molecules.*27 (2022) 796. doi.org/10.3390/molecules27030796

[12] J.Liu,C. Lv, Properties of 3D-Printed Polymer Fiber-Reinforced Mortars: A Review,*Polym.*14 (2022) 1315. doi.org/10.3390/polym14071315

[13] J.Liu,C. Lv, Research progress on durability of cellulose fiber-reinforced cement-based composites,*Int. J.Polym. Sci.*2021 (2021) 1014531. doi.org/10.1155/2021/1014531

[14] L.Mohammed,M.N.M.Ansari,G.Pua,M.Jawaid,M.S. Islam, A review on natural fiber reinforced polymer composite and its applications,*Int. J.Polym. Sci.*2015 (2015) 1–15. doi.org/10.1155/2015/243947

[15] J.A.Sainz-Aja,M.Sanchez,L.Gonzalez,P.Tamayo,G.Garcia del Angel,A.Aghajanian,S.Diego,C. Thomas, Recycled Polyethylene Fibres for Structural Concrete,*Appl. Sci.*12 (2022) 2867. doi.org/10.3390/app12062867

[16] S.F.A.Shah,B.Chen,S.Y.Oderji,M.A.Haque,M.R. Ahmad, Comparative study on the effect of fiber type and content on the performance of one-part alkali-activated mortar,*Constr. Build. Mater.*243 (2020) 118221. doi.org/10.1016/j.conbuildmat.2020.118221

[17] P.Zhang,X.Han,Y.Zheng,J.Wan,D. Hui, Effect of PVA fiber on mechanical properties of fly ash-based geopolymer concrete,*Rev. Adv. Mater. Sci.*60 (2021) 418–437. doi.org/10.1515/rams-2021-0039

[18] S.C. Chen,X.L. Shi,X.M. Yu,Effect of voltage on mechanical properties of carbon fiber reinforced concrete,*J. Phys: Conf. Ser.*2680 (2024) 012022. doi:10.1088/1742-6596/2680/1/012022

[19] H.Gao,Y. Xia, Research on the dispersion of carbon fiber and recycled carbon fiber in cement-based materials: a review,*Front. Mater.*10 (2023) 1243392. doi.org/10.3389/fmats.2023.1243392

[20] T.V.Muthukumarana,M.A.V.H.M.Arachchi,H.M.C.C.So marathna,SN. Raman, A review on the variation of mechanical properties of carbon fiber-reinforced concrete,*Constr. Build. Mater.*366 (2022) 130173. doi.org/10.1016/j.conbuildmat.2022.130173

[21] A.Patchen,S.Young,D. Penumadu, An Investigation of Mechanical Properties of Recycled Carbon Fiber Reinforced Ultra-High-Performance Concrete,*Mater.*16 (2023) 314. doi.org/10.3390/ma16010314

[22] D.M. Bontea,D.D.L. Chung,G.C. Lee Damage in carbon fiber-reinforced concrete, monitored by electrical resistance measurement,*Cem.Concr. Res.*30 (2000) 651-659. doi.org/10.1016/S0008-8846(00)00204-0

[23] B.Chen,J. Liu, Damage in carbon fiber-reinforced concrete, monitored by both electrical resistance measurement and acoustic emission analysis,*Constr. Build. Mater.*22 (2008) 2196-2201. doi.org/10.1016/j.conbuildmat.2007.08.004

[24] P.W. Chen,D.D.L. Chung,Carbon fiber reinforced concrete for smart structures capable of non-destructive flaw detection,*Smart. Mater. Struct.*2 (1993) 22-30. doi.org/ 10.1088/0964-1726/2/1/004

[25] D.D.L. Chung, Cement reinforced with short carbon fibers: a multifunctional material,*Compos. B: Eng.*31 (2000) 511-526. doi.org/10.1016/S1359-8368(99)00071-2

[26] Y.Hao,C.Shi,Z.Bi,Z.Lai,A.She,W. Yao, Recent Advances in Properties and Applications of Carbon Fiber-Reinforced Smart Cement-Based Composites,*Mater.*16 (2023) 2552. doi.org/10.3390/ma16072552

[27] A.Loukidis,I.Stavrakas,D. Triantis, Electrical Methods for Sensing Damage in Cement Mortar Beams Combined with Acoustic Emissions,*Mater.*15 (2022) 4682. doi.org/10.3390/ma15134682

[28] Z.Q.Shi,D.D.L. Chung, Carbon fiber-reinforced concrete for traffic monitoring and weighing in motion,*Cem.Concr. Res.*29 (1999) 435-439. doi.org/10.1016/S0008-8846(98)00204-X

[29] M.Sun,Z.Li,Q.Mao,D. Shen, Thermoelectric percolation phenomena in carbon fiber-reinforced concrete,*Cem.Concr. Res.*28 (1998) 1707-1712. doi.org/10.1016/S0008-8846(98)00161-6

[30] M.Sun,Q.Liu,Z.Li,Y. Hu, A study of piezoelectric properties of carbon fiber reinforced concrete and plain cement paste during dynamic loading,*Cem.Concr.Res.*30 (2000) 1593-1595. doi.org/10.1016/S0008-8846(00)00338-0

[31] W.Wang,S.Wu,H. Dai, Fatigue behavior and life prediction of carbon fiber reinforced concrete under cyclic flexural loading,*Mater. Sci.Eng: A*434 (2006) 347-351. doi.org/10.1016/j.msea.2006.07.080

[32] H.A.Navya,N.N. Patil, Experimental studies on behaviour of carbon fiber reinforced concrete. *IJCIET*9 (2018) 1461.1469. https://iaeme.com/Home/issue/IJCIET?Volume=9&Issue=7

[33] J.Zhang,A.Heath,R.J.Ball,K. Paine, Effect of fibre loading on the microstructural, electrical, and mechanical properties of carbon fibre incorporated smart cement-based composites,*Front. Mater.*9 (2022)1055796. doi: 10.3389/fmats.2022.1055796

[34] S.Y.Ghanem,J. Bowling, Mechanical Properties of Carbon-Fiber-Rinforced Concrete,*Adv. Civ. Eng.Matls.*8 (2019) 224-234. doi.org/10.1520/ACEM20180089

[35] G.J.Liu,E.L.Bai,J.Y.Xu,N. Yang, Mechanical Properties of Carbon Fiber-Reinforced Polymer Concrete with Different Polymer-Cement Rations,*Mater.*12 (2019)3530. doi:10.3390/ma12213530

[36] O.S. Khan,S. Sohu,M.Z. Jamali,S.Ahmed,S. Nagapan,Improving mechanical properties of concrete by using fibrous materials,*Eng. Solid. Mech.*12 (2024)437-446. doi: 10.5267/j.esm.2024.4.001

[37] M. Rutzen,P. Lauff,R. Niedermeier,O. Fischer,M. Raith,C.U. Grosse, U. Weiss,M.A. Peter,D. Volkmer, Influence of fiber alignment on pseudoductility and microcracking in a cementitious carbon fiber composite material,*Mater. Struct.*54 (2021) 58. doi.org/10.1617/s11527-021-01649-2

[38] A.Džolan,P.Lauff,O.Fischer,G. Šunjić, Influence of Concrete Shrinkage on the Behavior of Carbon Short-Fiber-Reinforced Concrete (CSFRC) under Tension,*Appl. Sci.*13 (2023) 7081. doi.org/10.3390/app13127081

[39] Y.Kusumawardaningsih,E.Fehling,M.Ismail,A.A.M.Abo ubakr, Tensile strength behaviour of UHPC and UHPFRC,*Procedia. Eng.*125 (2015) 1081-1086. doi.org/10.1016/j.proeng.2015.11.166

[40] M. Hambach,H. Möller,T. Neumann,D. Volkmer,Portland cement paste with aligned carbon fibers exhibiting exceptionally high flexural strength (>100 MPa),*Cem.Concr. Res.*89 (2016) 80–86. doi.org/10.1016/j.cemconres.2016.08.011

[41] P. Lauff,P. Pugacheva,M. Rutzen,U. Weiß,O. Fischer,D. Volkmer,M.A. Peter,C.U. Große,Evaluation of the Behavior of Carbon Short Fiber Reinforced Concrete (CSFRC) Based on a Multi-Sensory Experimental investigation and a Numerical Multiscale Approach,*Mater.*14 (2021) 7005. doi.org/10.3390/ma14227005

[42] V.Bellary,B.Khartode,M.Shewale,S.R.Arangi,N. Shinde, Experimental Investigation of Randomly Distributed Carbon Fibers in Concrete Beams,*E3S Web of Conf.*559 (2024) 04052. https://doi.org/10.1051/e3sconf/202455904052

[43] D.L.Nguyen,D.K.Thai,DJ. Kim, Direct tension-dependent flexural behavior of ultra-high-performance fiber-reinforced concretes,*J. Strain Anal. Eng. Des.*52 (2017) 121-134. doi.org/10.1177/0309324716689625

[44] M.Safiuddin,G.Abdel-Sayed,N. Hearn, Absorption and strength properties of short carbon fiber reinforced mortar composite,*Buildings*11 (2021) 300. doi.org/10.3390/buildings11070300

[45] S.Ivorra,P.Garces,G.Catala,L.G.Andion,E. Zornoza, Effect of silica fume particle size on mechanical properties of short carbon fiber reinforced concrete,*Mater. Des.*31 (2010) 1553–1558. doi.org/10.1016/j.matdes.2009.09.050

[46] P.W. Chen,D.D.L. Chung,Low-drying-shrinkage concrete containing carbon fibers,*Compos. B Eng.*27 (1996) 269–274. doi.org/10.1016/1359-8368(95)00020-8

[47] P.Lura,O.M.Jensen,K. van Breugel, Autogenous shrinkage in high-performance cement paste: An evaluation of basic mechanisms,*Cem.Concr. Res.*33 (2003) 223–232. doi.org/10.1016/S0008-8846(02)00890-6

[48] L.Wu,N.Farzadnia,C.Shi,Z.Zhang,H. Wang, Autogenous shrinkage of high performance concrete: A review,*Constr. Build. Mater.*149 (2017) 62–75. doi.org/10.1016/j.conbuildmat.2017.05.064

[49] L.Yang,C.Shi,Z. Wu, Mitigation techniques for autogenous shrinkage of ultra-high-performance concrete—A review,*Compos. B Eng.*178 (2019) 107456. doi.org/10.1016/j.compositesb.2019.107456

[50] V.N.Nerella,H.Ogura,V. Mechtcherine, Incorporating reinforcement into digital concrete construction. In Proceedings of the IASS Symposium 2018: Creativity in Structural Design, Boston, MA, USA, 16–20 July 2018.

[51] TUMuenchen. 3D Printing in Concrete. Additive Manufacturing at TUM, https://www.youtube.com/watch?v=H3aD0VZ3ESU (accessed on 3 October 2024).

[52] O.Fischer,D.Volkmer,P.Lauff,M.Hambach,M. Rutzen, Zementgebundener Kohlenstofffaserverstärkter Hochleistungswerkstoff (Carbonkurzfaserbeton); Forschungsinitiative Zukunft Bau, Band F 3178; Fraunhofer IRB Verlag: Stuttgart, Germany, 2019.

[53] P.Lauff,O. Fischer, Effizienter Ultrahochleistungsbeton mit innovativer trajektorienorientierter „Bewehrung “,*Ce Pap.*3 (2019) 82–88. doi.org/10.1002/cepa.976

Građevinski materijali i konstrukcije
Building Materials and Structures
journal homepage: www.dimk.rs

https://doi.org/10.5937/GRMK2400015G UDK: 624.014.2.078.4

Preliminary report

Practical issues in slip-resistant bolted connections for steel structures

Tzvetan Georgiev[*1)]

[1)] *Department of "Steel, timber and plastic structures", University of Architecture, Civil Engineering and Geodesy UACEG, "Hr. Smirnenski" blvd. 1, 1046 Sofia, Bulgaria*

Article history
Received: 29 September 2024
Received in revised form:
15 December 2024
Accepted: 11 January 2025
Available online: 12 February 2025

Keywords
slip factor,
slip-resistant bolted connections,
testing,
practical safety issues

ABSTRACT
The application of slip-resistant bolted connections is necessary to prevent the contribution of slippage due to bolt-hole-diameter clearances in the lateral displacements of high-rise steel-braced frames or other high-rise structures. The safety and reliability of these connections rely on the reliable value of the slip factor in calculations. Despite the clear guidelines provided by European standards for connection design and execution, certain issues frequently arise in current construction practices. In this article, the author investigates two cases he found in his practice. For that reason, an experimental campaign with slip determining tests to annex G of EN 1090-2 is conducted at the University of Architecture, Civil Engineering and Geodesy (UACEG). The problems which are pointed out and investigated are: how a lack of knowledge about the k-class K_2 can impact the slip factor test results, and how various surface treatments, such as fabrication errors, impact the slip factor.

1 Introduction

The use of slip-resistant bolted connections is widespread in the design and construction of high-rise steel structures for the industry (Figure 1a, b). Steel or composite bridges also utilize these connections, with fatigue dictating the design (Figure 1c). Their advantages for structures subjected to cyclic loads are well known and reflected in fatigue calculation standards [1], and logically they are the preferred choice of the designers for dynamically or seismically loaded structures. Furthermore, even for relatively tall structures that are primarily subjected to wind (Figure 1a, b), the application of slip-resistant bolted connections is essential for controlling lateral displacement. Such structures, for example, are telecommunication towers, trestle structures for high industrial belt conveyors, towers for power transmission, or process towers (Figure 1a). If the non-preloaded bearing type bolted connections are used within the vertical bracing system (specifically between diagonals and the main frame) at a certain level of lateral load, below the serviceability limit state, slip will occur.

The total elongation of the connection without resistance can reach up to 2 mm, and in the worst case, up to 4 mm. This is due to the standard clearance between the bolt shank and plate hole, which is 2 mm for the most frequently used bolts, M16, M20, and M24 [2]. Experiments [3] reveal that, due to various factors, the theoretical slip of 4 mm never reaches its maximum. However, even if it reaches half or a third of its maximum, the actual horizontal displacements at each storey level significantly increase. This could potentially compromise the structure's serviceability, lead to irreversible horizontal storey drifts, or trigger second-order effects that were not considered in the structural analysis.

At present, slip-resistant bolted connections are well known and often used. They have their technological and market advantages over other alternatives such as injection bolts, fit bolts [2, 4], or field welds. Design guidelines are available in standards [2, 4, 6] or literature [3, 5, 7]. Eurocode 3 [4] classifies bolted connections that transmit shear forces through friction between contact surfaces as either category C or B, based on whether the ultimate or serviceability limit state determines their no-slip response. Eurocode 8 [8] mandates the use of these bolted connection categories in the joints connecting dissipative elements to non-dissipative ones, such as the diagonal connections of Concentrically Braced Frames (CBFs) to columns or beams. Furthermore, as mentioned in [2], the combination of slip-resistant bolted connections and long or short slotted holes provides an excellent combination of liberalized fabrication tolerances, ease of erection, and a clear and reliable force-transmitting path. All this, combined with the significant progress in the field of high-strength bolt fabrication and the development of building chemistry, implies the increasingly widespread use of slip-resistant bolted connections on the steel construction market even within typologies of steel structures outside their traditional fields of application.

Achieving the required bolt preloading and slip factor is crucial for the safety of slip-resistant bolted connections. During the inspection of bolt preloading, the engineer can use either direct or indirect site control methods, such as the torque method, the combined method, direct tension

[*] Corresponding author:
E-mail address: cvgeorgiev_fce@uacg.bg

a) High-rise industrial steel structure with CBFs

b) Belt conveyer with high-rise trestle

c) Steel road bridge

Figure 1. Steel structures with application of slip-resistant bolted connections

indicators, the HRC method [2] or sensorized structural bolts [9]. When controlling the slip factor, the engineer primarily depends on the technical specifications provided by the vendor for surface preparation and coating application, as well as the alignment between the prescribed actions and their actual execution.

A brief review of the literature highlights the various aspects of research interest in the field of slip-resistant bolted connections. The Bulletin 37 of ECCS [10] is of particular interest to European steel construction. The main results of the study include the analysis of factors related to surface preparation and conservation, correlated to the achieved friction coefficient. The study concludes that blast-cleaning the steel surfaces to a minimum of Sa 2½ degree is necessary. The best slip factors are achieved when a 75- to 100-µm-thick coating is applied.

Since 1951, comprehensive studies that periodically reflect and update design recommendations, has been conducted in North America [5]. As different steel grades with increased strength or improved durability become more widely used, there is a growing interest in studying the methods of cleaning their surfaces, coating them, and exploring the results of their slip factor. The publication [11] addresses this issue by testing S275, S690, and S355 weather-resistant steel and determining their respective slip factors. Following the implementation of EN 1090-2 [12] and, more specifically, Annex G for slip factor determination, several research studies have examined various factors, including test loading speed, slip criteria, preload force determination method, and the location of displacement transducers within the test sample [13, 15]. Researchers draw comparisons between procedures in Europe and North America [14]. Consequently, recommendations were made for improving Annex G.

The presented brief literature review indicates that the primary focus of research is on the impact of factors such as surface preparation, steel grades, coating type, and testing procedures on the slip factor. Researchers focus on this classic set of topics to some extent. This article takes a different approach. The article identifies and discusses two common issues faced by practitioners. There is no table in EN 1090-2 [2, 12] with prescribed values for tightening moments in the torque method. Only k-class K_2 permits this tightening procedure in Europe. Therefore, the engineer must calculate the torque moment separately for each bolt batch. Nevertheless, engineers often encounter surprises within the execution phase due to the lack of information for the value of K_2. This could be attributed to the manufacturer's longer delivery terms for bolts with a k-class K_2 specification, or it could simply be the result of routine practices from earlier times (before EN 1090-2 [12]). In such a situation, under the pressure of deadlines and circumstances, designers and supervisors are forced to work only with the k-class K_1, where its range is from 0.10 to 0.16 wide [16]. This is the first problem that the author encountered in his practice, and which is discussed in this article.

The second practical problem addressed is the following. It is a matter of interest to explore how a possible error in the coating technology affects the coefficient of friction. Most often, this can happen when the surfaces with the already applied conservation primer (Figure 2) are painted by mistake with the anti-corrosion coating for the structure. This

is not a rare thing to happen, according to the author's practice, because the corrosion protection is applied mostly manually. In addition, the worker's body is covered with a protective suit and face mask. Seeing is tough and high personal concentration is required in a dirty work environment. In such a case, after painting by mistake, the flying surfaces for the slip-resistant bolted connection must be cleaned locally and the conservation primer applied again.

The formulated practical problems necessitate further investigation through an experimental campaign. It is conducted by the Research Laboratory of the department of "Steel, timber and plastic structures" of UACEG. The main goals of this campaign are (a) to find out the real coefficients of friction that are achieved by using the same vendor product to preserve the surface and k-class K_1 as per [2, 12] for torque moment calibration; (b) to see how using different ways to prepare the surfaces of contact plates affects the real coefficients of friction; and (c) to obtain a force-displacement diagram for the pre-slip and post-slip connection response as a starting point for more research.

2 Experimental setup and experimental specimens

The experimental set-up used is entirely dictated by the recommendations and requirements of Annex G of [2]. The test is carried out using a universal testing machine type UMM-50 which has a force range of 500 kN. The components for the test specimens are fabricated and the surfaces coated in a professional workshop under strict quality control of the author and an independent specialized laboratory. They are assembled in the workshop, while the bolts are preloaded by the lab staff. About 15 days pass between the bolt preloading and the testing day, achieving the expected initial relaxation. Only short-time tests are conducted while a creep test was not planned. The specimens are being loaded in tension with a force that increases smoothly with a speed of 0,20 kN/sec for specimens with bolts M16 and 0,50-0,60 kN/sec for specimens with bolts M20. The value of the applied force is measured by a sensor connected to the measuring mechanism of the testing machine (force sensor #0). Four displacement transducers (DT) with a range of 0-10 mm are mounted on both sides of each of the cover plates of the test specimen, along the longitudinal axis. They measure the mutual slippage between the inner plate and fixed angle to the cover plates. In this way, four relative displacement values between the cover plates and the inner plates are measured from each specimen, two on the left and two on the right (Figure 3, indicated as 1, 2, 3 and 4). Figure 3 illustrates the geometry and type of test specimens, while Table 1 and Table 2 provide the dimensions for Groups 1 and 2, respectively. The lab staff measures only the dimension L_1 for the test specimens of Group 1 while the rest of the dimensions are assumed to be equal to the nominal. All dimensions for the test specimens of Group 2 are measured by the lab staff, Table 2.

a) Flying surface in hot-rolled profile b) Flying surface in gusset plate

Figure 2. Flying surface coated by conservation coat for slip-resistant bolted connections

Table 1. Geometric dimensions of the specimens, Group 1

Specimen (group-series-specimen #) / bolt diameter	L, mm	L_1, mm	a, mm	b_1, mm	c_1, mm	t_1, mm	t_2, mm
Specimen 01-01-01 / M16	700	250	80	35	50	16	8
Specimen 01-01-02 / M16	700	250	80	35	50	16	8
Specimen 01-01-03 / M16	700	248	80	35	50	16	8
Specimen 01-02-01 / M20	780	289	100	40	60	20	10
Specimen 01-02-02 / M20	780	288	100	40	60	20	10
Specimen 01-02-03 / M20	780	287	100	40	60	20	10
Specimen 01-03-01 / M20	780	288	100	40	60	20	10
Specimen 01-03-02 / M20	780	289	100	40	60	20	10
Specimen 01-03-03 / M20	780	287	100	40	60	20	10

Table 2. Geometric dimensions of the specimens, Group 2

Specimen (group-series-specimen #) / bolt diameter	L, mm	L_1, mm	a, mm	b_1, mm	c_1, mm	t_1, mm	t_2, mm
Specimen 02-01-01 / M16	792	293	100.8	39.6	61.5	20.2	10.5
Specimen 02-01-02 / M20	786	293	100.0	39.2	60.9	20.4	10.6
Specimen 02-01-03 / M20	788	290	100.8	37.8	60.8	20.1	10.4
Specimen 02-02-01 / M20	786	290	100.4	38.0	61.5	20.1	10.1
Specimen 02-02-02 / M20	786	290	100.8	37.4	62.0	20.0	10.4
Specimen 02-02-03 / M20	783	292	100.4	39.6	62.1	20.1	10.3
Specimen 02-03-01 / M20	788	292	100.0	38.2	61.5	20.1	10.3
Specimen 02-03-02 / M20	789	293	100.6	38.5	60.9	20.4	10.3
Specimen 02-03-03 / M20	788	290	99.7	37.9	61.3	20.2	10.3

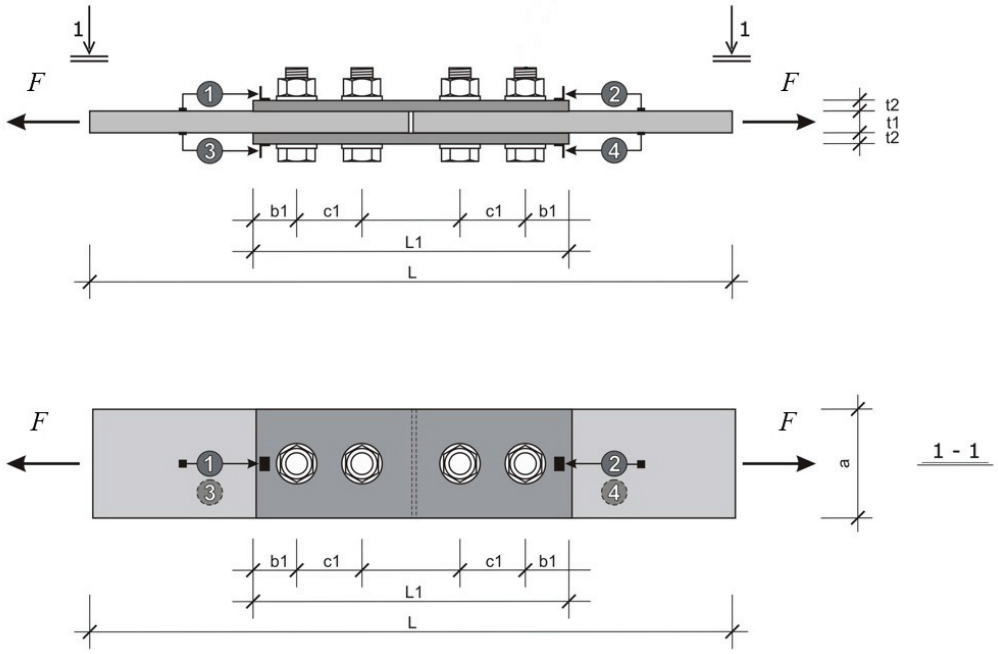

Figure 3. Test specimens' geometrical parameters and DTs location and numbering

The time for testing one specimen with bolts M16 is about 20 minutes, while for specimens with bolts M20, it is about 10 minutes. A computer-aided system records data readings every second (Figure 4).

The specimens are made of steel grade S235JR in accordance with the EN 10025-2 [17]. All bolts are HV type grade 10.9, according to EN 14399-4 [18] having an oxidized surface (no hot deep galvanizing). All bolts and nuts are supplied in the lab with an applied lubricant.

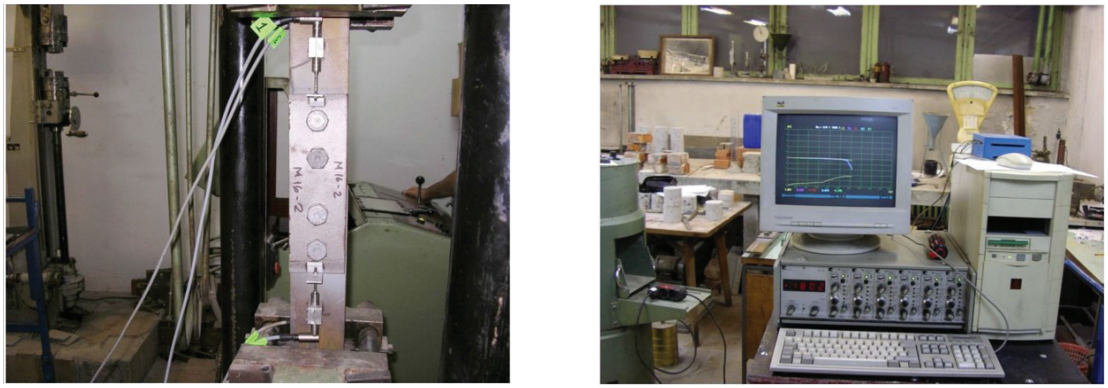

Figure 4. Experimental set-up and data recording system

3 Experimental campaign

Two groups of tests, named Group 1 and Group 2, are conducted within the experimental campaign, Figure 5. Group 1 involves the execution of three series of experimental specimens. The first three with bolts M16-10.9 are named Series 1-1, and the second and third with bolts M20-10.9 are named Series 1-2 and Series 1-3. The samples' surfaces are grit-blasted to grade Sa 2½, which is medium roughness (G), according to ISO 8503-1 [19]. They are then covered with a zinc silicate primer that is about 80 µm thick. The first objective of the tests in Group 1 is to obtain the value of the coefficient of friction. The second objective is to investigate whether k-class K_1 (Series 1-2) and k-class K_2 (Series 1-3) can determine the preloading force and produce reliable slip factor results. The workshop fabricates all experimental specimens of Group 1 using the same technology, and prepares the steel plates of all six specimens in an almost identical manner. The conservation primer is a two-component zinc silicate coat, which falls into the friction coefficient class B according to EN 1090-2 Appendix G.

Testing Group 2 comprises nine tests, arranged in three series (Figure 5), each of which includes three standard specimens (Figure 7), namely Series 2-1, Series 2-2, and Series 2-3. All 9 tests use bolts M20-10.9, fabricated by the same (European) manufacturer from a single delivery batch. The objective of testing Group 2 is to investigate how the surface preparation affects the slip factor. For this purpose, the specimens of Series 2-1 are grit blasted to Sa $2^{1/2}$ grade and then coated with an anti-corrosion primer. The primer is then cleaned using a mechanical wire brush, Bristle Blaster (Figure 6, b), again to grade Sa $2^{1/2}$ and medium roughness (G) according to ISO 8503-1 [19]. After that, a conservation coat is put on the contact surfaces. This is a one-component zinc dust paint based on ethyl silicate (the primer is tested and approved in accordance with EN 1090-2 appendix G for friction coefficient class B, vendor datasheet). The layer should be up to 80 µm thick. The purpose of the steps prior to the testing of Series 2-1 is to simulate an error in the fabricator's painting workshop regarding the treatment of the friction surfaces (see Figure 6) and the subsequent application of cleaning and coating manipulation. It should be emphasized that only the side plates of 10 mm thickness were subjected to these manipulations, and not the inner plates of 20 mm. This implies that only 50% of the flying surface is cleaned and repainted.

Series 2-2 specimens are grit blasted to Sa 2½ and medium roughness (G) according to [19]. After cleaning, the plates are assembled in the specimen. The contact surfaces remain uncoated (Figure 7, b). The purpose of Series 2-2 is to determine the coefficient of friction, which solely depends on the level of cleaning. Here it is relevant to clarify that from the time of cleaning to the time of assembly, the steel plates were in a room with a relatively dry environment, and therefore no intensive rust should be expected on the contact surfaces.

Series 2-3 specimens were grit blasted to Sa 2½ grade and medium roughness (G) according to ISO 8503-1 [19]. The specimens receive a conservation coating (one-component zinc-based metallizing primer) after cleaning, with a nominal layer thickness of up to 80 m. The purpose of Series 2-3 is to obtain the slip factor (coefficient of friction) after following the technical specifications of the manufacturer of the conservation coat.

Group	Series	Spesimen	Bolt diameter / class	Objectice of the test
01	01-01	01-01-01	M16 / 10.9	Evaluation of the influence of the method of determining the bolt preload force
		01-01-02		
		01-01-03		
	01-02	01-02-01	M20 / 10.9	
		01-02-02		
		01-02-03		
	01-03	01-03-01	M20 / 10.9	Same as Series 01-02, but after bolt preload force assessed by testing
		01-03-02		
		01-03-03		
02	02-01	02-01-01	M20 / 10.9	Simulation of mistake done during painting operation in the fabricators workshop
		02-01-02		
		02-01-03		
	02-02	02-02-01	M20 / 10.9	Evaluation of the influence of the roughness of cleaned contact surfases
		02-02-02		
		02-02-03		
	02-03	02-03-01	M20 / 10.9	Evaluation of the influence of the surface roughness + concervation primer coat
		02-03-02		
		02-03-03		

Figure 5. Flow chart of the conducted experimental campaign

a) simulating an error by applying an anti-corrosion primer;
b) cleaning with a mechanical wire brush;
c) flying surfaces before applying conservation coat;

Figure 6. Steps for processing the Series 2-1 specimen

a) Series 2-1, simulation of mistake in painting shop
b) Series 2-2, no conservation coating applied
c) Series 2-3, surface preparation and conservation coating

Figure 7. Specimens of Group 2

4 The data elaboration methodology and experimental results

Each of the eighteen tests directly yields the slip force F_S [kN]. The tensile force F (Figure 3) is constantly measured throughout the whole test, by force sensor #0 connected to the measuring mechanism of the testing machine and the recording system controlled by software (Figure 4). The value assigned as F_S is that corresponding to a recorded slip of 0.15 mm or for a very close smaller value between the side plate and the inner plate in each of the four DTs (Figure 3). Tables 3 and 5 present the average values of the forces *F*s for sensors #1 and #3 and correspondingly for sensors #2 and #4. The final average value of *F*s is from the readings of all DTs.

The two parameters the slip force *FS* depends on are the contact pressure (preloading) and the coefficient of friction between the slipping surfaces. Each bolt's contact pressure equals the preload force $F_{p,C}$. This implies that this force must be defined precisely. Regardless for the *Series 1-1* and *Series 1-2* tests the preload force is calculated by formula (1), based on k-class *K*1 . The value of 0,16 is selected according to the practice before EN 1090-2 [12]. The value K_1=0.16 is applied to the two bolt sizes, M16 and M20, resulting in tightening moments of 280 Nm and 550 Nm, respectively. The value of the tightening moment, $M_{r,2}$ [Nm], is measured by a calibrated dynamometric wrench. Despite its widespread use in real construction, this approach lacks precision and is prohibited by [2, 12]. For this reason, it is one of the subjects of research in this article.

$$F_{p,C} = \frac{M_{r,2}}{d \cdot K_1} \tag{1}$$

where *d* is the diameter of the bolts in meters.

K-class K_2 having a value of 0,17 obtained through testing, is used to achieve the preloading in the Series 1-3 and to compare the results with Series 1-2.

The preload force based on k-class K_2 only is used for all the tests belonging to Group 2. For this purpose, the K_2 factor for specimens in Group 2 is obtained after testing.

It is also assumed that the preload force $F_{p,C}$ within all four bolts of an experimental specimen is the same since they are tightened with the same torque moment and wrench. Therefore, formulas (2) and (3) yield the mean value of the coefficient of friction μ_m.

$$\mu_i = \frac{F_{S,i}}{4 \cdot F_{p,C}} \quad (2)$$

where μ_i is the coefficient of friction obtained by testing the *i*-th specimen.

$$\mu_m = \frac{\Sigma \mu_i}{n} \quad (3)$$

where μ_m *is* the mean value of the coefficient of friction for each series and *n* is the number of values obtained through testing. Formulas (4) and (5) calculate the standard deviation S_μ and the coefficient of variation V, respectively.

$$S_\mu = \sqrt{\frac{\Sigma \left(\mu_i - \mu_m \right)^2}{n-1}} \quad (4)$$

$$V = \frac{S_\mu}{\mu_m} \quad (5)$$

The characteristic value of the coefficient of friction μ_{car} is obtained as the 5% fractile value with a confidence level of 75%, through calculation by equation (6) [2, 11].

$$\mu_{car} = \mu_m - 2.05 \cdot S_\mu \quad (6)$$

After following the methodology thus described, the elaborated data for slip factor values are obtained. The results of the conducted experiments from Group 1 are summarized in Tables 3 and 4, while the results of the conducted experiments from Group 2 are summarized in Tables 5 and 6.

After processing the data from Table 3, the calculated parameters presenting the coefficient of friction for series belonging to Group 1 are summarized in Table 4.

As can be seen from Table 4, there is a significant scatter in the obtained values and the coefficient of variation is high (*V*=13,36%) for Series 1-2 compared to Series 1-1. Not surprisingly, the characteristic value for the coefficient of friction obtained for Series 1-2 is lower and differs significantly from that obtained from Series 1-1. It is worth

Table 3. Group 1, testing results

Series number	**Specimen (group-series-specimen) / bolt diameter**	**Slip Force F_S, [kN]**	**Coefficient of friction, μ_i**
1-1	Specimen 01-01-01 / M16	205,90	0,4705
		201,7	0,4609
	Specimen 01-01-02 / M16	211,3	0,4829
		217,3	0,4966
	Specimen 01-01-03 / M16	193,3	0,4417
		200,5	0,4582
1-2	Specimen 01-02-01 / M20	237,0	0,3447
		238,2	0,3465
	Specimen 01-02-02 / M20	301,1	0,4380
		265,8	0,3866
	Specimen 01-02-03 / M20	315,4	0,4588
		318,4	0,4632
1-3 (conducted after measurement of preload force)	Specimen 01-03-01 / M20	278,0	0,4293
		287,7	0,4443
	Specimen 01-03-02 / M20	282,7	0,4365
		302,6	0,4673
	Specimen 01-03-03 / M20	284,9	0,4399
		273,3	0,4220

Table 4. Group 1, elaborated data

Series	**Mean slip force, F_{sm}, kN**	**Mean Coefficient of friction, μ_m**	**Standard deviation, S_μ**	**Coefficient of Variation, (V%)**	**Characteristic Coefficient of friction, μ_{car}**
1-1	205,0	0,4685	0,0194	4,138	0,4287
1-2	279,3	0,4063	0,0543	13,360	0,2950
1-3	284,9	0,4399	0,0156	3,539	0,4080

reminding that the surfaces of the steel plates of Series 1-1 and 1-2 were cleaned in an identical manner and the same conservation coat was applied identically. There should be no physical reason for such a large difference in the results for the coefficient of friction. In searching for an answer to these deviations, it is concluded that applying the same K_1 factor for bolts M16 and M20 is misleading. That is why the last three specimens in *Series* 1-3 are tested after the preload force is obtained by k-class K_2. The execution of specimens is done by the same fabricator, using the same dimensions as for specimens from Series 1-2. The bolt preload force is obtained by measurements in a similar manner to the set-up used in [20]. Since the publication [20] is in Bulgarian only, the experimental setup will be presented very briefly hereafter. The bolt is placed on a specially designed stand so that its head is stationary. A cylindrical compression force gauge (measuring device) with a central hole is put and the bolt body stays in the hole. Washers are placed between the bolt head, the force gauge, and the nut (Figure 8a). The bolt nut is tightened with a torque wrench, with steps of 35 Nm increasing tightening torque. The force gauge provides information about the compressive force obtained in it, which is assumed to be equal to the preload force in the bolt. In addition to the tightening torque at each step, the angle of rotation of the torque wrench is also measured and reported [20]. An illustration of the results of the measurements are presented in Figure 8b.

Table 5 presents the testing results of the specimens from Group 2, while Table 6 presents the elaborated data. Recall that the preload force is obtained from measurements, following the same process as Series 1-3. Its value is 161 kN related to a torque moment 450 Nm.

a) Setup for preload forcemeasurements

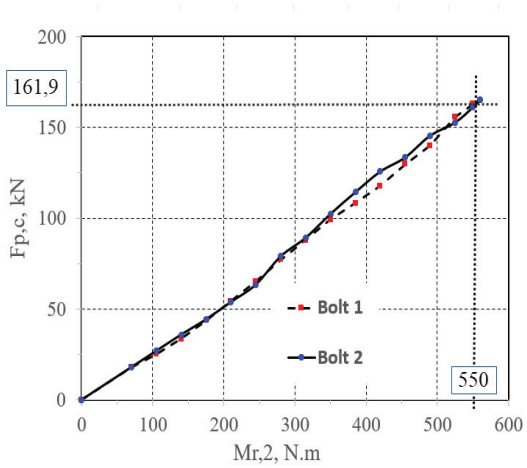

b) Relation preload force – torque moment

Figure 8. Testing for preload force determining for the bolts in Series 1-3

Table 5. Group 2, testing results

Series number	**Specimen (group-series-specimen) / bolt diameter**	**Slip Force F_S, [kN]**	**Coefficient of friction, μ_i**
2-1	Specimen 02-01-01 / M20	263,6	0,4093
		261,0	0,4053
	Specimen 02-01-02 / M20	270,9	0,4207
		269,6	0,4186
	Specimen 02-01-03 / M20	267,2	0,4149
		262,7	0,4079
2-2	Specimen 02-02-01 / M20	274,2	0,4258
		292,8	0,4547
	Specimen 02-02-02 / M20	332,2	0,5160
		347,8	0,5401
	Specimen 02-02-03 / M20	356,7	0,5539
		328,3	0,5098
2-3	Specimen 02-03-01 / M20	312,8	0,4857
		297,1	0,4613
	Specimen 02-03-02 / M20	331,2	0,5143
		322,6	0,5009
	Specimen 02-03-03 / M20	304,3	0,4725
		309,4	0,4804

Table 6. Group 2, elaborated data

Series	Mean slip force, F_{sm}, kN	Mean Coefficient of friction, μ_m	Standard deviation, S_μ	Coefficient of Variation, (V%)	Characteristic Coefficient of friction, μ_{car}
2-1	265,8	0,4128	0,0062	1,504	0,4001
2-2	322,0	0,5000	0,0498	9,969	0,3978
2-3	312,9	0,4859	0,0192	3,953	0,4465

Another important aspect of the behaviour of these bolted connections is the force-displacement diagram that clearly indicates the pre-slip and post-slip connection behaviour. The experiments carried out made it possible to record both values namely connection tensile force *F* and relative displacements in DTs #1, #2, #3 or #4. Graphical illustration of one these records is presented in Figure 9. which shows expected behaviour of bolts in preloaded shear connections (category *B* or *C*) according to Eurocode 3 [4]. After reaching the slipping force Fs the connection slips without resisting until some clearances are exhausted. The connection starts working as category *A* until bolt shear failure or steel net section capacity is reached.

Some observations can be outlined from the graph from Figure 9. The following three specific stages are recognized in the relation force-displacement. They are distinguished by the points 0, 1, 2 and 3 in Figure 10. The phase of elastic and rigid response is between points 0 and 1. The displacements are due only to the elastic elongations in the connected plates. When the force F reaches the value of Fs, then the friction is overcome, and the connection elongates without resisting. This stage can be named "*major slip*" [3], and it is characterized by an almost constant value of the force and with the margin of the elongation D_{MS}. The conducted tests clearly show that the magnitude of D_{MS} is smaller than the theoretical value of the clearances between the bolt body and the diameter of the hole. Other researchers have also noted and reported on that specialty [3].This can be attributed to the fact that geometric imperfections in the fabrication and erection and the unavoidable small misalignments of the elements cause some bolts to come close to the steel surfaces of the holes. Thus, a given bolt meets the surface of the steel in the hole and begins to work on the bearing and shear. From this moment (after point 2), the connection enters the post-slip phase and begins to resist but also to elongate. The behaviour of the bolted connection after point 2 towards point 3 is of interest. The tests conducted had another purpose. With the sensors used and the experimental setup, a realistic picture of the force-displacement relationship in the branch 2-3 cannot be presented. This should be a question for future research. Of interest will be the tangential stiffness (whether there is a hardening branch or a softening branch). Of interest is also what criteria for the ultimate displacement and corresponding force will be found in the state of connection failure or the structural ultimate limit state.

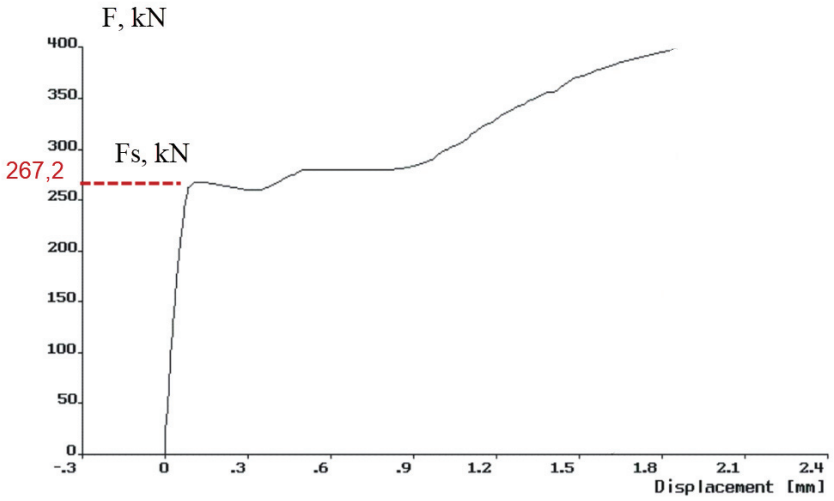

Figure 9. Relation tensile force F – relative displacement between side and inner plate. Raw data from DTs #1, Specimen 02-01-03

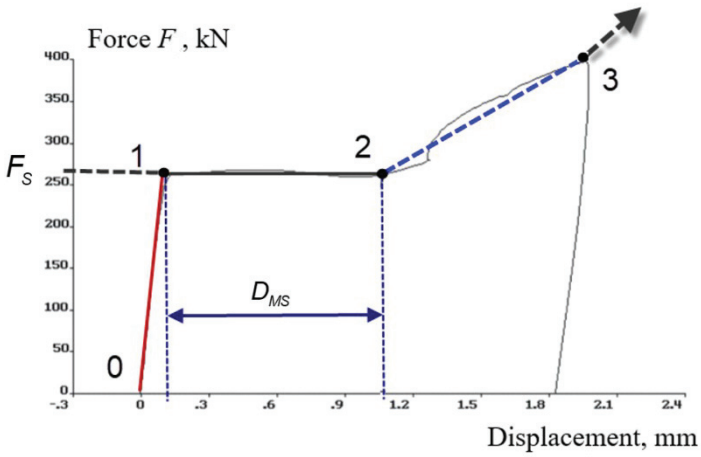

Figure 10. Characteristic phases in the behavior of a slip-resistant bolted connection

5 Conclusions

From the nine tests conducted in Group 1, it was clearly seen that when one of the governing parameters, namely the preload force in the bolt, is assumed theoretically, based on k-class K_1 , the results are not reliable. The differences in the obtained characteristic values of the slip factor between Series 1-1 and Series 1-2 and the improvement achieved after testing Series 1-3 prove this thesis. Testing is necessary to determine both the sliding force (F_S) and the preload force ($F_{p,C}$) in the bolts, ensuring a reliable determination of the coefficient of friction for a specific prepared conservation coat.

In practice, we must avoid determining torque moments based on theoretical data (k-class K_1), even from authoritative product-oriented sources like [21]. When using the tightening method, it is strictly mandatory to work with k-class K_2 [2]. In such cases, one must obtain K_2 factors either from the bolt kit manufacturer's certificates or after testing some bolt assemblies from delivered batches.

Testing Group 2 aims to investigate the technological aspects of conservation coating application. Based on the elaborated data and results presented in Table 6, it can be concluded that the highest average value of the coefficient of friction appears in Series 2-2, at which no conservation coating is applied. Conversely, the largest variation of the reported results is observed in this series. In the end, the characteristic value of the coefficient of friction is lower than that of Series 2-1 and Series 2-3. The occurrence of some corrosion between the time of cleaning the steel plates and the connection assembly can explain this controversial result. The use of cleaned and uncoated surfaces for such bolted joints is assumed and allowed in [2, 12], but the engineer should bear the following in mind. Using friction surface class *A* of the standard [2, 12] for slip-resistant connection design means that the organized execution process must ensure the absence of rust between the friction surfaces. Only a strict and rigorous site-oriented organization for cleaning and assembly can accomplish this. Such a strict organization of work is difficult, and therefore the engineer should take advantage of this option only when he is convinced that it is technologically and managerially feasible.

Comparing the results of Series 2-1 and Series 2-3 is of particular interest for the practice. This comparison focuses on the correct application of surface treatment and coating, which Series 2-3 simulates, and how Series 2-1 simulates a fabrication error and the subsequent repair of that error. Testing determines the preload force for both series, and the bolts originate from the same manufacturing batch. This implies that the sole distinction between the two series lies in the treatment of the plates' friction surfaces.

Workshop painting errors are a common occurrence in professional practice. In the author's engineering practice, workshop painting errors have frequently occurred in structures fabricated in Europe, specifically in Bulgaria, Slovenia, or the Czech Republic, by fabricators with high reputations, a strong technological culture, and EXC3 certificates in accordance with EN 1090-2 [2, 12]. One should prepare for such an unexpected situation in any design project that uses a slip-resistant bolted connection.

Comparing the results of Series 2-1 and Series 2-3 (Table 6) shows that the mean value of the slip factor is 17.7% lower for Series 2-1. The difference in characteristic values is 11.6%. These findings need the following comment. Only the side plates, which account for half of the contacting surfaces in Series 2-1, simulate fabrication error. Should the error encompass all surfaces, we anticipate a more significant reduction. This reduction is explained by the fact that cleaning with a mobile brush does not provide the surface roughness required for this conservation coat.

Formulating the following design recommendations is possible. In case of a mistake in applying the primers, it is best to repeat the cleaning technology using a grit blasting machine. This is not always possible for scheduling or technological reasons. In case of using a mobile mechanical brush for cleaning, the engineer should anticipate a reduction of 25% in the coefficient of friction for 100% affected contact surfaces and 15% for 50% affected. To achieve more accurate results, more experimental investigations similar to those presented in this article should be conducted.

Investigating the post-slip behavior of the slip-resistant bolted connections requires a constitutive behavior model. The proposed model, according to Figure 10, is an approximation but still not sufficient. It can be interpreted as an initial framework for further refinement. Future research should focus on conducting experiments with an advanced test setup to track the force-displacement relationship after the major slip and establish failure criteria. We can successfully apply these bolted connection models to a wide variety of structural archetypes and various limit states. These include, for instance, seismic analysis for significant damages or near-collapse limit states (seismic analysis), key structural element loss scenarios (robustness of structures),

fire design situations (fire engineering), and other similar scenarios.

CRediT authorship contribution statement

Tzvetan Georgiev: Conceptualization, Formal analysis, Investigation, Methodology, Supervision, Validation, Visualization, Writing.

Declaration of competing interest

As the sole and corresponding author, I declare that I have no financial or personal relationships with other people or organizations that could inappropriately influence my work related to this research. I declare that I have no potential conflicts of interest related to consultations, stock ownership, honoraria, paid expert testimony, patent applications/registrations, and grants or other funding that may be relevant to the research presented in the manuscript.

Acknowledgments

The current research work is carried out with the financial support of the "New Lead Plant" project management team of KCM AD. The author thanks them for the trust and support they have provided him. All experimental studies are carried out by the Center for Scientific Research and Design at the UACEG in the Research Laboratory of the Department of "Steel, Timber and Plastic Structures" under the direction of Eng. Ognyan Ganchev. I sincerely thank him for his professionalism, without which this would not have been possible.

References

[1] CEN, EN 1993-1-9: Eurocode 3: Design of steel structures - Part 1-9: Fatigue, European Committee for Standardization, Brussels, 2005.

[2] CEN, EN 1090-2: Execution of steel structures and aluminium structures — Part 2:Technical requirements for the execution of steel structures, European Committee for Standardization, Brussels, 2018.

[3] *G. Kulak, J. Fisher, J. Struik*, Guide to Design Criteria for Bolted and Riveted Joints. Second Edition, ISBN 1-56424-075-4, Research Council on Structural Connections, 2001.

[4] CEN, EN 1993-1-8: Eurocode 3: Design of Steel Structures - Part 1-8: design of joints, European Committee for Standardization, Brussels, 2005.

[5] RCSC — Specification for Structural Joints Using High-Strength Bolts, Research Council on Structural Connections, c/o AISC, Chicago, December 2009.

[6] Ordinance No. RD-02-20-1 of October 5, 2022 “Execution of steel structures”, State Gazette, No. 83 of October 18, 2022, Ministry of Regional Development and Public Works (in Bulgarian).

[7] *Tzankov, M*. Execution of construction steelwork according to Eurocode, KIIP publishing house, 2012, ISBN 978-954-92275-6-7 (in Bulgarian).

[8] CEN, EN 1998-1: Eurocode 8: Design of structures for earthquake resistance - Part 1 : General rules, seismic actions and rules for buildings, European Committee for Standardization, Brussels, 2004.

[9] https://tokbo.it/en/applications/ (last assessed 15.12.2024)

[10] ECCS, Slip factors of connections with H. S. F. G. bolts, European Convention for Constructional Steelwork, TC 10 - Bolted and Welded Connection, n. 37, Brussels, 1984.

[11] Cruz A., Simões R., Alves R., Slip factor in slip resistant joints with high strength steel. Journal of Constructional Steel Research 70 (2012) 280–288.

[12] CEN, EN 1090: Execution of steel structures and aluminium structures - Part 2: Technical requirements for the execution of steel structures, European Committee for Standardization, Brussels, 2008.

[13] Natalie Stranghöner, Nariman Afzali, Jörn Berg, Markus Schiborr, Frans Bijlaard, NolGresnigt, Peter de Vries, Ralf Glienke, Andreas Ebert, INFLUENCE OF DIFFERENT TESTING CRITERIA ON THE SLIP FACTOR OF SLIP-RESISTANT CONNECTIONS, Nordic Steel Construction Conference 2015, Tampere, Finland, 23-25 September 2015

[14] Maiorana, E., Zampieri, P., Pellegrino, C., Experimental tests on slip factor in friction joints: comparison between European and American Standards, Frattura ed IntegritàStrutturale, 43 (2018) 205-217.

[15] Natalie Stranghöner, Markus Schiborr, Ralf Glienke, PROCEDURE TEST OF SLIP-RESISTANT CONNECTIONS ACCORDING TO EN 1090-2, EUROSTEEL 2014, September 10-12, 2014, Naples, Italy.

[16] CEN, EN 14399: High-strength structural bolting assemblies for preloading, European Committee for Standardization, Brussels, 2005

[17] CEN, EN 10025 - Hot rolled products of structural steels - Parts 1 to 6, European Committee for Standardization, Brussels, 2004.

[18] CEN, EN 14399-4: High-strength structural bolting assemblies for preloading - Part 4: System HV - Hexagon bolt and nut assemblies, European Committee for Standardization, Brussels, 2005

[19] ISO 8503-1: Preparation of steel substrates before application of paints and related products - Surface roughness characteristics of blast-cleaned steel substrates - Part 1: Specifications and definitions for ISO surface profile comparators for the assessment of abrasive blast-cleaned surfaces, 2012.

[20] *GeorgievTzv*., Relation torque moment – tension force in high strength bolts. // Godishnikna UACEG ISSN 1310-814X, 2014, Fifth National Symposium on Steel, Timber and Composite Structures, UACEG, 2014, http://hdl.handle.net/20.500.12641/66440 (in Bulgarian

[21] https://www.peiner-ut.com/wp-content/uploads/2021/06/Peiner-HV-Montagehilfe_2021_deutsch.pdf , PEINER Umformtechnik GmbH. Montagehilfezu „HV-Schraubengarnituren“ nach DIN EN 14399, DIN EN 1090-2, DIN EN 1993-1-8/NA Vorspannkräfte und Anziehmomente, Klemmlängen, Nennmaße, Anwendungshinweise, last accessed at 11.12.2024.

Građevinski materijali i konstrukcije
Building Materials and Structures
journal homepage: www.dimk.rs

https://doi.org/10.5937/GRMK2400014K UDK: 72.071 Балгач Е.

Technical paper

Culture of memory - Prof. Edmund Balgač and his (un)forgotten building opus

Dragan Kostić[1)], Predrag Radomirović[2)], Vuk Milošević[*1)], Radomir Folić[2)]

[1)] *Faculty of Civil Engineering and Architecture, University of Niš, Aleksandra Medvedeva 14, Niš, Serbia*
[2)] *Faculty of Technical Sciences, University of Novi Sad, Trg Dositeja Obradovića 6, Novi Sad, Serbia*

Article history
Received: 27 October 2024
Received in revised form:
06 December 2024
Accepted: 25 December 2024
Available online: 10 February 2025

Keywords
Building Heritage,
Suspended Cable Structural Systems,
Edmund Balgač

ABSTRACT

The tendency to cover large areas led to the adoption of saddle-shaped geometric forms as the optimal solution for suspended roof systems. The development of suspension systems in the early 1950s was facilitated by advancements in numerical methods for solving complex systems of differential equations. Fred Severud (USA) and David Jawerth (Sweden) provided analytical solutions that enabled the optimal application of these systems. Edmund Balgač (Yugoslavia) enhanced existing models with his theoretical knowledge and practical skills, applying them in the construction of several halls in Serbia. Professor Balgač achieved the uniqueness of his solutions by combining aesthetic and structural requirements for covering large areas. Even today, many buildings utilizing this structural system continue to fascinate with their appearance and functionality. This paper analyzes the theoretical contributions of Prof. Balgač through the calculation of the roof structure of the Great Hall of the Textile Fair in Leskovac and the Fair and Sports Hall in Subotica, highlighting his creativity and the importance of these suspension cable structures as cultural and architectural heritage. Simultaneously, we remember Professor Balgač as a versatile engineer with a special gift for solving specific tasks using the most modern methods and techniques from global practice, thanks to his proficiency in German and English.

We dedicate this work to Edmund Balgač, an engineer, professor, and renowned researcher committed to the progress and development of construction in Yugoslavia during the second half of the 20th century. The unique works of suspended and catenary structures by Prof. Balgač are widely recognized, but much of his theoretical contributions have yet to be fully acknowledged.

1 Introduction

Suspended structures represent specific architectural and construction systems praised for their elegant form and ability to cover large spans. In civil engineering, suspended cable structures embody a fusion of theoretical excellence and practical application, often defining modern cityscapes with their graceful appearance and engineering challenges. These challenges necessitate innovative solutions in architectural design, calculation, material selection, and construction technology to achieve a balance between aesthetics, load-bearing capacity, and functionality. Understanding the principles of prestressing in suspended cable systems, along with the unique challenges posed by suspended cable systems, is particularly crucial. A comprehensive grasp of the benefits and challenges associated with cable structures is essential for design and construction. Despite the structural efficiency, large spans, and material savings offered by these systems, they present challenges such as cable maintenance, dynamic behavior, and construction costs.

The enduring presence of suspended structures in urban landscapes attests to their lasting influence. One of the key figures in this field is Professor Edmund Balgač, whose name is closely associated with the theoretical understanding and practical application of suspended cable systems.

The aim of this paper is to remind the professional and scientific community of the construction achievements that remain iconic in Leskovac and Subotica, and to express gratitude for Balgač's extensive translation work across all areas of construction. The research and analysis of Professor Balgač's contributions to the theoretical understanding and application of suspended cable systems in former Yugoslavia demonstrate how his work shaped the modern interpretation and use of these architectural and engineering innovations. The paper focuses on analyzing his theoretical contributions, with particular attention to projects such as the Great Hall of the Textile Fair in Leskovac and the Fair and Sports Hall in Subotica. Professor Balgač built upon the works of Jawerth from Sweden and Severud from the

* Corresponding author:
E-mail address: vukamer@yahoo.com

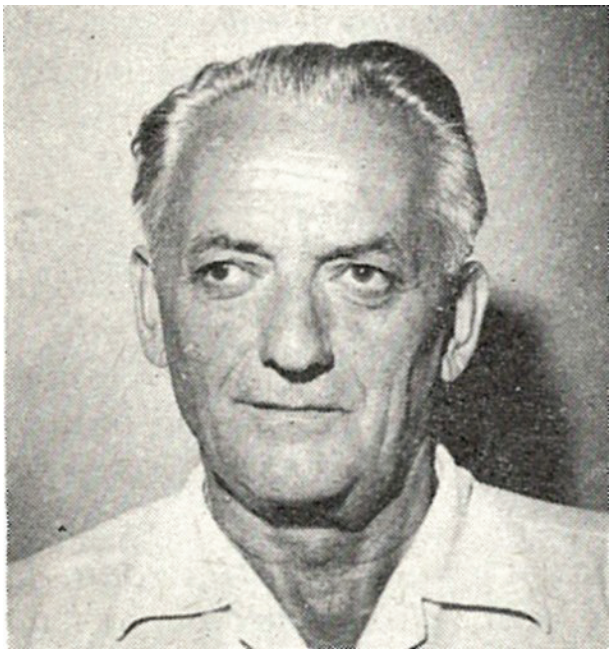

Figure 1. Professor Balgač and his authentic signature [1]

USA, enhancing and expanding the method whose foundations were laid by Kačurin [2]. This work aims to deepen the understanding and appreciation of Professor Balgač's contributions to the theoretical advancement of suspended cable systems through analytical calculation, recalling his constructed works and translation efforts, and honoring the 110th anniversary of his birth.

2 Biography

Edmund Balgač was born on May 24, 1913, in Sombor in the former Austro-Hungarian Monarchy. His high intelligence and inclination toward natural-mathematical and technical sciences directed him to study civil engineering, which he completed in 1939 at the Faculty of Civil Engineering in Belgrade. Throughout his illustrious career, he worked in construction companies in Sombor, Srbobran, Novi Sad, and Belgrade. For a significant portion of his career, he served as a construction manager in the complex construction companies "Trudbenik" and "Rad." His extensive work experience, professional knowledge, proficiency in German, and extraordinary ability to synthesize qualified him for the position of professor at the Higher Technical Construction School in Subotica (1965-70). In 1982, he was appointed a full professor by invitation at the Faculty of Civil Engineering in Subotica.

During his time in the operational department, he collaborated closely with leading experts such as Milan Krstić, PhD, Đorđe Lazarević, PhD, and Milorad Ivković, PhD. He learned from them and together they developed and applied new knowledge and modern global achievements. He made significant contributions through his research and teaching work, as well as with numerous realized projects that continue to impress with their function and form. A significant professional and scientific contribution was also made through his exceptional translation work.

As a professor, he left behind a considerable body of research in all areas of civil engineering, especially suspended cable systems, construction, and foundation theories [3-11]. With his theoretical contributions, he earned the reputation of being one of the pioneers and originators of suspended systems in the former Yugoslavia, as well as in Europe and the world. One of his most significant contributions to science was the introduction of numerical analysis into the geometrically nonlinear problem of prestressed suspended systems. He improved and applied the existing analytical methods of Prof. Nowicki and Severud (Dorton Arena) and Jawert (Johannesov Arena) for facilities in Leskovac, Zemun, and Subotica. His research laid the foundations for future advancements in the construction of these structures. As a researcher, he made significant contributions to numerous scientific works, including the textbook "Engineering Structures: Reinforced Concrete Structures," which was published at the Higher Technical School of Construction in Subotica in 1966.

In addition to his theoretical work, Prof. Balgač was one of the most outstanding civil engineers of his era. As an engineer at "Rad" from Belgrade, Balgač left behind many buildings that continue to serve as benchmarks in the urban landscape. Among his notable projects are the Great Hall of the Textile Fair in Leskovac, the Fair and Sports Hall in Subotica, and the Sports and Cultural Center "Pinki" in Zemun [12, 13]. In the company Kosovo Project, he addressed the interaction of the foundation with the soil for the bridge over the Tisa River near Novi Kneževac. He demonstrated his versatility and ability to synthesize in concise works that addressed the issues dominating Yugoslav congresses of constructors and geotechnicians. At the same time, he enjoyed the respect of all his colleagues, and his insights on the work of professors and meritorious engineers were appreciated and valued.

Prof. Edmund Balgač passed away at the age of 77 on September 12, 1990, in Belgrade, leaving behind an indelible legacy with his theoretical work and constructed projects that continue to remind us of his greatness and importance.

3 Contribution in translating literature

Through his translation work, Prof. Balgač significantly improved the education of many generations of students at technical faculties in Yugoslavia. During his career, Prof. Balgač translated several important works and books in the fields of spatial structural systems, concrete structures, and traffic construction. Some of his notable translations include:

- "Spatial Roof Constructions: Details and Execution. Concrete, Wood, Ceramics, Steel, Plastic Material." Part 1 and Part 2, Construction Library - Herman Rile with a group of authors, translated by Edmund Balgač, 1977, Construction Book (488 pages).
- "Prestressed Concrete in Practice" (Spannbeton für die Praxis) - Leonhardt Fritz, translated by Edmund Balgač, 1959, Construction Book Belgrade (526 pages).
- "Traffic Engineering Manual" - Ludvig Kirgs, translated by Edmund Balgač, 1962, Construction Book Belgrade (635 pages).
- "Theory of Reinforced Concrete Structures" - Gothart Franz, translated by Edmund Balgač, 1979, Construction Book Belgrade (390 pages).

4 The theoretical contribution of Prof. Balgač

4.1 Historical overview of the works that contributed to the development of the analytical solution

When discussing the theoretical work of Prof. Balgač in the field of suspended cable structures, it is essential to mention pioneers like Fred Severud [14, 15] and David Jawerth [16], who laid the basics for further advancements in the calculation of cable systems. Prof. Balgač continued to refine the analytical method for calculating geometrically non-linear structures established by Severud and Jawerth. The first major breakthrough in creating suspended constructions was the optimization of analytical calculations, wherein the stabilization of catenaries by weight was replaced by prestressing, introducing a revolutionary concept in this field [1, 14, 17].

Swedish engineer David Jawerth developed an innovative system to mitigate the undesirable swaying of cable trusses - a hanging prestressed system in the vertical plane - using the analytical model of Kačurin [2]. A cable truss system, composed of two tensioned cables of opposite curvature, is often referred to as a Jawerth system. Due to its tensioned nature, it prevents excessive movement and swaying of the roof. The cable system is interconnected by rods, forming a truss, while the anchor structure with diagonal stay cables ensures the immovability of the support nodes and balances the forces within the cable structure. According to Jawerth's recommendation, the ratio of the added load (v) to the total gravity load (q) should be taken as $v/q < 0.6$ for the calculation. This theoretical solution was applied in the design of the Ice-Skating Rink in Johannesov, Stockholm (Figure 2), with the project carried out by architect Hedquist and the calculations by engineer Jawerth. The skating rink in Johannesov, Sweden, was the first facility built with a system of prestressed cable trusses. It was designed in 1956 and completed in 1964, with a capacity of 16,000 spectators [1, 18].

A real revolution in the construction of suspended systems with a spatial arrangement of prestressed catenaries was brought about by the construction of the state fair hall in Raleigh, North Carolina. The ingenuity of the idea in its geometric, constructive, and conceptual solution came from Nowicki [14, 15, 19, 20].

Maciej Nowicki, an architect and professor, was born in Chita, Siberia, in 1910. After World War II, he worked on the reconstruction of Warsaw. As a delegate of Poland, he went to New York in December 1945 to work on rebuilding Poland's infrastructure. From 1948 until his tragic death in 1950, he taught and worked in the department of architecture at the newly formed "North Carolina State College School of Design." As a teacher, designer, and urbanist of international repute, his legacy is mainly reflected in the inspirational influence he exerted at the School of Design, the lost potential to change the course of contemporary architectural and planning thinking and practice, and in the radical design of his only completed project in North Carolina, the famous Dorton Arena, completed after his death. In collaboration with engineer Fred Severud, Nowicki drew up the plan for the arena in Raleigh (Dorton Arena) (Figure 3). The shape of the arena is determined by two inclined parabolic arches of reinforced concrete that meet near the ground, connected below ground level by braces. A net of prestressed cables between the arches supports the roof and forms the surface of a hyperbolic paraboloid. Dorton Arena has gained wide and lasting admiration, becoming one of the few North Carolina facilities to achieve international recognition. The extraordinary hyperbolic-paraboloid structure became a model for a series of later buildings designed in the "saddle dome" form around the world during the 1950s and 1960s. For North Carolina in the mid-20th century, it became a bold symbol of modernity and progress, a celebrated icon of modern architectural design from the day it was built. With his concept, Professor Nowicki also influenced the development of an analytical solution for the calculation of cable structures, together with Fred Severud. The calculation of the suspended roofs of several important halls in the USA was carried out by the project bureau known today as Severud Associates (Madison Square Garden 1968, Dorton 1953, Ingalls Hockey Rink 1958).

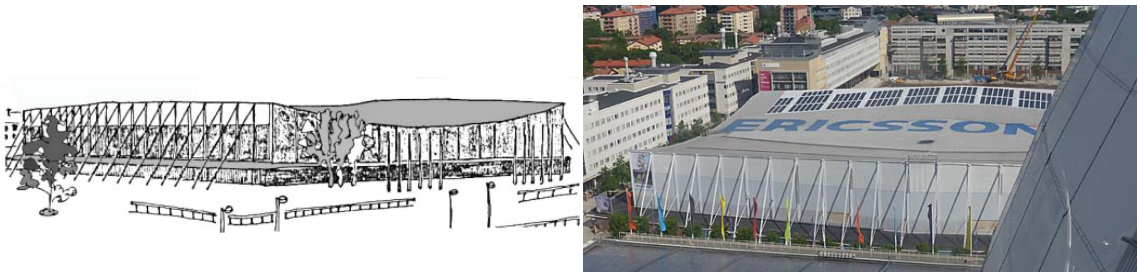

Figure 2. Ice-Skating Rink in Johanneshov, Sweden, 1956. (David Jawerth), today Hovet arena (author's drawing – left, author's photograph – right)

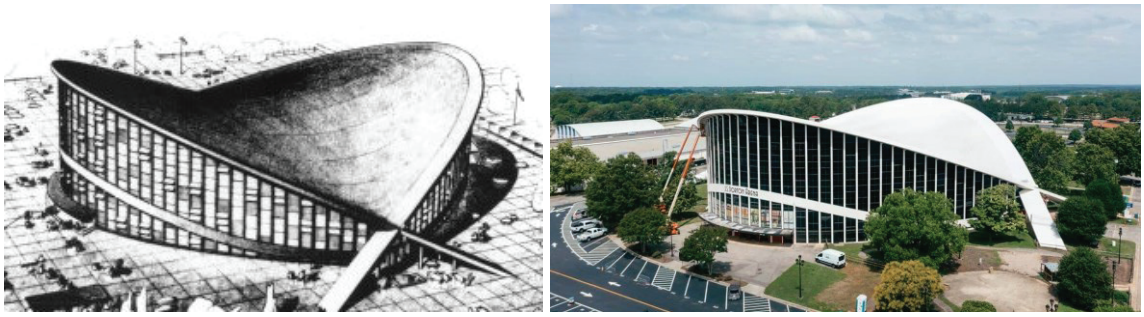

Figure 3. Dorton Arena, Raleigh, North Carolina, USA, 1952 [21] and today (Maciej Nowicki, Fred Severud) [22]

After the construction of Dorton Arena, Prof. Balgač used the analytical procedure applied by Fred Severud, advanced the analytical part of the method, and applied it to the construction of three halls: Pinki in Zemun in 1973, the Textile Fair Hall in Leskovac in 1959, and the Fair and Sports Hall in Subotica in 1968 [1, 14, 17, 23, 24, 25].

4.2 Basic principles of analytical solution

The main feature of the theoretical work of Prof. Balgač is reflected in the introduction of numerical methods into the analytical techniques applied by Jawerth and Severud. Professor Balgač based the calculations for achieving roof stability on his original method, which, for prestressed networks, implied an additional load on the supporting cables. The establishment of balance was obtained by applying additional load to the supporting cables in direct contact with the prestressing cables. In this way, the reactive load between the supporting and prestressing cables was introduced into the calculation, which changes intensity depending on the load phase of the roof. In the no-load phase, the reactive load causes the highest tensile forces in the stabilizing cables. By loading the roof net, in the load-bearing and stabilizing cables, the greatest forces will occur in the phase of the greatest gravity load, and the least in the phase of prestress. Conversely, in the stabilizing cables, the greatest forces will occur in the phase of prestress, and the least in the phase of full workload. For the input data of the calculation, the principle of identical change of deflections in the carrying and prestressing cables in all phases of the load was applied. The calculation of the loads acting on the cables takes into account the accurately calculated values of the reactive forces k during loading, i.e. k1 when the roof is unloaded. According to the Professor's method, the additional load of the supporting cables (v) should have an intensity of 0.15 kN/m^2 to 0.20 kN/m^2 [1, 14, 17].

Prof. Balgač based his calculation of the forces in the cables on the assumptions that load - bearing and prestressing cables in the unloaded state, and later under continuous load, have the shape of a parabola. During the calculation of the hanging roof of the Great Hall of the Leskovac textile fair, for the calculation of the geometry of the supporting cables, a deviation of 2% occurred.

4.3 The practical application of Balgač's analytical procedure

Starting from the assumption that the cables of the prestressed net are affected by equally distributed vertical loading, the characteristic phases through which the roof will pass during construction and exploitation are defined as:

- **(0)** the phase without loading;
- **(1)** the prestress phase;
- **(2)** the prestress and self weight phase;
- **(3)** the prestress, self weight, snow, and pressure or suction of the wind phase.

The calculation procedure could be divided into two phases [1, 14, 17, 26-28]:

I The previous calculation of the form of the load-bearing and stabilizing cable for the aforementioned phases of loading

This procedure includes the determination of the changes in the sags of the main cables due to the loading or unloading of the construction, by using formulas (1), (2) and (3) [1,14, 17, 26-28]. We assume that the sags f_0 and f_{p0} occur during phase (2), during the so-called designed state. Due to complete unloading, phase (0), a change will occur in the sags of the load-bearing cables for Δf_0 whose value can be determined using the formula (2).

The structure of the load d uring phase (2) is:

$g = g_{nos.} + g_{pom.}$,

where: $g_{nose.} = a \cdot v_p + k_{ver.} + a \cdot g_p - k_{1,ver.}$; $Mr._{Pom.} = a \cdot v_p + k_{ver.} - k_{1,ver.}$

The probable increased pressure, with which the stabilizing cable presses onto the load-bearing one, due to the unloading of the roof $k_{ver.} \approx g_p \cdot a$, that is, the probable decrease in pressure of the load-bearing cable on the stabilizing one due to the load of the roof $k_{1,ver.} \approx v_p \cdot a$ (based on author's personal experience) must be assumed precisely enough so the previous calculation would not have to be repeated. Due to full loading, the unloaded roof moves into the phase of the greatest gravitational load (phase **(3)**), while changes in the arrows are calculated using formula (1). By means of the successive unloading of the roof for the value of the load of the wind and snow, that is, the weight of the roof itself, the roof moves into phase **(2)** of the loading, that is (1), and the change in the arrow is calculated using the formula (2). The obtained arrows of the load-bearing cables over the phases of loading are input into formulas (4), (5) and (6) [13, 16, 17, 24-27], which leads to the expected values for k and k_1 . If $k_{ver.} \neq k$ and $k_{1,ver.} \neq k_1$, the previous calculation must be repeated with adjusted values of $k_{ver.}$ and $k_{1,ver.}$.

$$\Delta f^3 + \Delta f^2 (3f - A) + \Delta f (2f^2 - 2Af) - A(B + f^2) = 0$$
$$A = \frac{q l^2}{4EF} \qquad B = \frac{3}{16}(l^2 + h^2) \tag{1}$$

$$\Delta f_{0p}^2 \left(\frac{f_{0,qv}}{m_G} - \frac{3 f_{p0}}{m_P} \right) - \Delta f_{0,p} \left(\frac{2 f_{0,qv}^2}{m_G} + \frac{2 f_{p0}^2}{m_P} \right) + p = 0 \tag{2}$$

$$\Delta f_0^2 \left[\frac{3 f_0}{m_G} - \frac{f_{p0}}{m_P} \right] + \Delta f_0 \left[\frac{2 f_0^2}{m_G} + \frac{2 f_{p0}^2}{m_P} \right] - p = 0 \tag{3}$$

$$k = p - \frac{2 f_{0,qv}^{2} \Delta f_{0,p} - f_{0,qv} \Delta f_{0,p}^{2}}{m_G} \tag{4}$$

$$m_G = m + m_I + m_{II} \quad m = 3\frac{l_0^4}{64\,E\,F} \quad m_I = \frac{f_{0,qv}^{2} l_0^{2}}{4\,E\,F} \quad m_{II} = \frac{3\,l_0^{2}\,h^2}{64\,E\,F}$$

$$k = \frac{2\,f_{p0}^{2}\Delta f_{0,p} + 3\,f_{p0}\Delta f_{0,p}^{2}}{m_P} \tag{5}$$

$$m_P = m_p + m_{pI} \qquad m_p = \frac{3\,l_{p0}^{4}}{64\,E\,F_p} \qquad m_{pI} = \frac{l_{p0}^{2} f_{po}^{2}}{4\,E\,F_p}$$

$$k_I = p - \frac{f_0}{m_G}\,\Delta f_0\,(\,2 f_0 + 3\Delta f_0\,) \quad tj. \quad k_I = \frac{f_{p0}\Delta f_0}{m_P}\,(\,2 f_{p0} - \Delta f_0\,) \tag{6}$$

II The calculation of the geometry and forces in the cables

By using the equation (7) and the equations (8) and (9) [1, 14, 17, 26-29] we obtain the geometry of the prestressed net, that is, the force in the load-bearing cables.

It is clear that in the load-bearing cables, the greatest force will be found during the greatest gravitational load, and the smallest during the prestressing phase, while in the stabilizing cable the greatest force will occur during the prestressing phase, and the smallest in the full load phase.

Stabilizing cables, even under the greatest gravitational load, must retain within them the tensioning force which will, using its vertical component, press down on the load-bearing cables with a certain load *v.* Professor Balgač recommends that the intensity of this load, the so-called "contact force", should be *v= 0.15 - 0.20 kN/m²*. In this way, the stability of the prestressed net roof, that is, the tensioning force in all the members of the system is guaranteed. This represents the quality of this method of calculation, in addition to the simplification which was introduced into the calculation.

This budget model was first published in the scientific literature [14] in 1961, with full explanations and mathematical expressions. Balgač himself states in the bibliography of the work [14] that he used the model according to which the Dorton Arena was designed (Severud's model) [15, 30]. Later published works by Sobotka [31], Kasilov, Bandel, Irvine [32], Leonhardt [33], Schlight [34], Jawerth [16] and others show similar equations used for calculation due to static loading and temperature changes. It is clear that Prof. Balgač was among the pioneers of the application of a successful analytical solution for which we have no evidence that it is completely original, but it was certainly reduced to an applicable procedure by which many hanging halls were built in Europe and of course in our country. Collaborating with professors from the Faculty of Civil Engineering in Belgrade, the constructed roof of the Great Fair Hall in Leskovac was checked in relation to the calculated values, by on-site testing [14]. The geometrical parameters as well as the measured forces in the cables showed minimal deviations that can be considered within the limits of the expected deviations, so the calculation model was thus verified.

5 Engineering contribution

Conventional space-surface structural systems (shells) have proven to be expensive from a technical perspective due to the complexity of formwork and scaffolding, and from a technological standpoint due to the challenges of installing concrete on curved and sloping roof surfaces. The idea of introducing hanging systems with identical geometric forms arose as a vision of Nowicki, with the calculation model applied by Severud at Dorton Arena. This approach maintained the geometric form of the hyperbolic paraboloid, satisfying aesthetic requirements, while the introduction of chain prestressed systems liberated the roof surface from complicated scaffolding and formwork. This resulted in the construction of highly aesthetic, attractive, functional, and economical medium- and large-span buildings.

$$z = 4\,f_0\,\frac{x}{l_0}\left(\,\frac{x}{l_0} + \frac{h}{4\,f_0}\,\right) \tag{7}$$

$$H_0 = \frac{q\,l_0^2}{8\,f_0} \quad V_2 = H_0\,tg\,\alpha_2 = \frac{q\,l_0}{2}\left(1 + \frac{h}{4\,f_0}\right) \quad V_I = -\,H_0\,tg\,\alpha_I = \frac{q\,l_0}{2}\left(1 - \frac{h}{4\,f_0}\right) \tag{8}$$

$$S_2 = \sqrt{H_0^2 + V_2^2} = \frac{q\,l_0^2}{8\,f_0}\sqrt{1 + \left(\frac{4\,f_0 + h}{l_0}\right)^2} \qquad S_I = \frac{q\,l_0^2}{8\,f_0}\sqrt{1 + \left(\frac{4\,f_0 - h}{l_0}\right)^2} \tag{9}$$

The modern approach allowed for the replacement of shells with catenaries, optimizing construction with minimal material use and faster building times. These systems enable the elegant covering of large spans without the need for internal supports, utilizing high tensile strength materials. Architecture later embraced hanging systems, leading to diverse variations. Steel ties, ropes, and cables became standard materials, manufactured to high steel standards. Research improved the efficiency of building structures, encouraging further exploration.

The use of suspended roof systems to cover large areas brings innovative, bold, and economical solutions. These systems are integrally tensioned structures, resulting from the geometric characteristics of load-bearing roof elements (cables and ropes). Cables do not transmit pressure forces, only tension forces, and they are extremely long with small cross-sections, making their bending stiffness negligible. Their carrying capacity is maximally utilized, making them economical structural elements. Advantages of hanging systems compared to other constructions for covering large spans include fast preparation through CAD and CAM technology, cheap transportation, and simple connection of elements with less qualified labor. However, suspended roofs are subject to aerodynamic challenges due to loads such as self-weight, snow, wind, earthquakes, and other vibrations. Ensuring the stability of the structure is crucial to prevent negative effects like roof swaying, ceiling cracking, and installation damage.

Modern cable truss systems are stabilized by applying weight loading, preload, and a combination of bending elements. A modern approach involves prestressing by introducing tensile forces into the roof cables during construction. These cables, when pre-tensioned, exert pressure on the structural elements, and stabilization is achieved using high compressive strength elements and cables of opposite curvature in different spatial arrangements [1, 14, 17, 23-28, 35, 36].

The multitude of advantages characterizing hanging chain systems led to their massive application in the mid-20th century, both globally and in the former Yugoslavia. Among the engineers who created halls using this system, Prof. Edmund Balgač stands out, having left behind several halls built with prestressed chain links. This work includes case studies on the Great Textile Fair Hall in Leskovac and the Sports Fair Hall in Subotica. These halls continue to captivate with their aesthetic value even after 6-7 decades, serving as landmarks in the cities where they are located.

5.1 The Great Hall of the Textile Fair in Leskovac

The Great Hall of the Leskovac Textile Fair, also known as the Round Pavilion or "Šajkača" (Serbian traditional hat) was designed by Prof. Edmund Balgač and architect Milorad Cvetić. The pavilion is the second facility in the world and the first in Europe built according to the revolutionary design and construction principles pioneered by the famous "Dorton Arena" in the United States of America. The building was constructed in 1959 in the eastern part of the Fair complex and has a characteristic circular shape (Figure 4).

The roof's structural system is a prestressed net of steel cables in the shape of a hyperbolic paraboloid. The main cables have a cross-section of 8Φ5 mm, while the auxiliary cables are 3Φ5 mm. Reinforced concrete clamped arches with a cross-section of 70/300 cm are inclined outwards and serve as supports for the prestressed cable network. This forms an approximately circular base with a diameter of 60 m. The perimeter supports are slender columns with a cross-section of 40/90 cm and variable height. The facade consists of 180 cm high parapets made of brick and glass surfaces up to the arched supports. The gallery, in the form of an inner ring separated from the main structure, is 8 meters wide with staircases on the north and south sides. Although originally planned to be covered with copper, the pavilion is actually

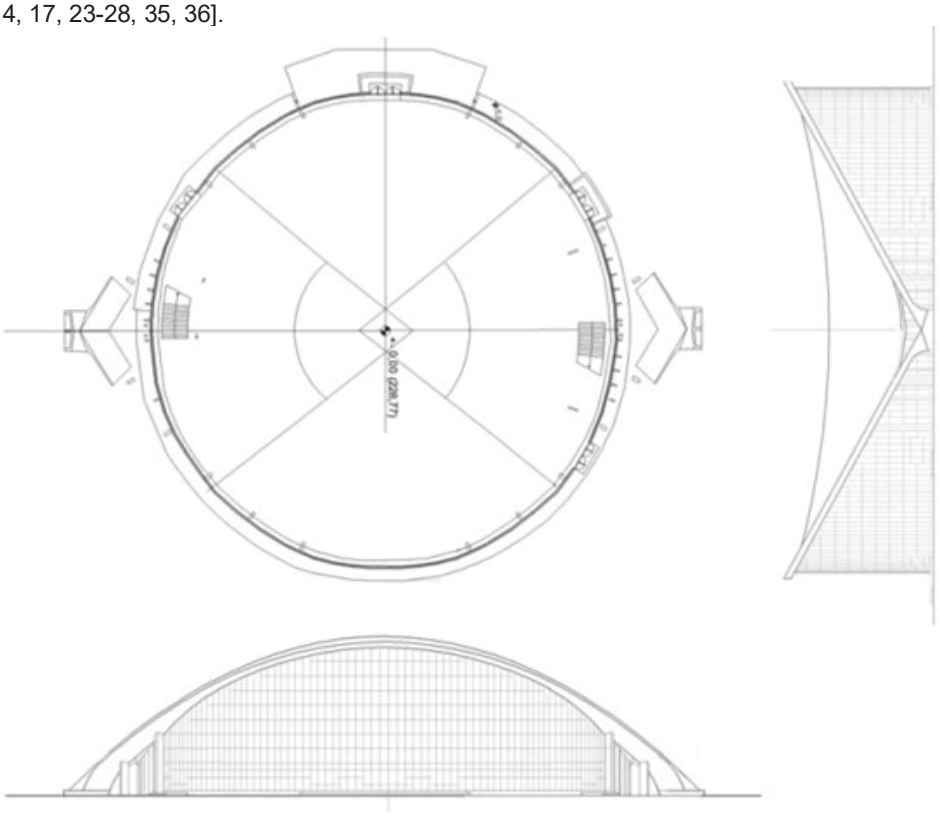

Figure 4. Basis and facades of the Large Hall of the Textile fair in Leskovac, Serbia, 1959 [37]

covered with galvanized sheet metal. The ceiling is made of lightweight volcanic tuff concrete with an average thickness of 6 cm. The total usable area of the building is 3440 m², with the ground floor covering 2375 m² and the gallery 1065 m² [1, 14, 17, 24, 26-28].

Revitalization of the building partially started in 2017, and in 2021 the building was given a new look and restored its shine. The pavilion was reopened in 2021, now serving as a shopping center (Figure 5 right). Unfortunately, the inner ring of the gallery space was permanently removed due to the new function of the building. During renovation, the roof structure made of concrete elements and the cover were renewed, while the cables were preserved, maintaining the unique geometric form of the roof structure [37].

5.2 The Sports Fair Hall in Subotica

According to the project of Prof. Edmund Balgač and architect Ivan Antić, the Sports Fair Hall in Subotica was realized in 1969 (Figure 6). The location of Dudova Šuma was chosen for the new hall. The building has a square base with sides of 57.6 m, dominated by an attractive roof structure with the geometric shape of a hyperbolic paraboloid. The new facility was intended for multifunctional use with simple adaptation for fair exhibitions, sports events, and cultural and artistic events. The hyperbolic paraboloid construction was realized in the form of a hanging structure of a prestressed cables net, similar to the hall in Leskovac. Steel cables with a cross-section of 6Φ5 mm placed at 50 cm intervals form the supporting cable structure, while auxiliary cables have a cross-section of 3Φ5 mm. A network of prestressed ropes is tensioned on a clamped spatial framework made of reinforced concrete. The frame consists of two clamped triangular concrete elements measuring 80/380 cm in section. The triangular structure has different slopes, resulting in different roof heights at opposite ends. The edge construction of the concrete frame is supported by columns placed at 7.2 m intervals. Edge posts have variable height and cross-section, with the tallest column having a cross-section of 50/120 cm [25, 36].

From the very beginning, the hall faced issues with the small capacity of the atmospheric sewage system, leading to overflows on the low supports of the roof, and the large volume of space created difficulties in heating. Consequently, the hall underwent two reconstruction processes. The first reconstruction in 1988 involved installing prefabricated stands, giving the building a purely sporting character. The hall was divided into two parts, creating two separate courts and increasing spectator capacity. In 2011, the stands were reconstructed again. Although the spectator capacity was reduced, the reconstruction addressed the discomfort of the existing seating area. The existing bleachers had non-standard dimensions, necessitating the reconstruction after 2011. The hall's area remains unchanged, with hopes for future solutions to improve space utilization.

The Sports Fair Hall in Subotica is an exceptional example of architecture and cultural heritage that reflects the city's rich history and development. This imposing sports hall features a striking architectural style, recognizable by its elegant roof structure and adaptive function. It has served as a venue for sporting events and a central gathering place for citizens during cultural events and manifestations, making it a vital part of Subotica's cultural life. Its architectural value lies in balancing aesthetics and functionality, contributing to its status as a cultural monument. In January 2022, the Institute for the Protection of Cultural Monuments considered

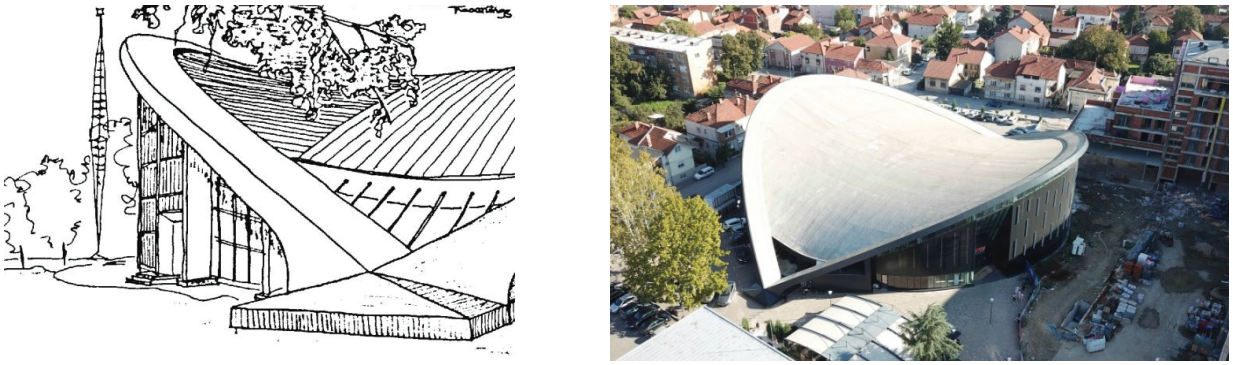

Figure 5. The Large Hall of the Textile fair in Leskovac: Original building view 1959 (author's drawing – left), Reconstructed new purpose shopping mall, 2024 (author's photograph – right)

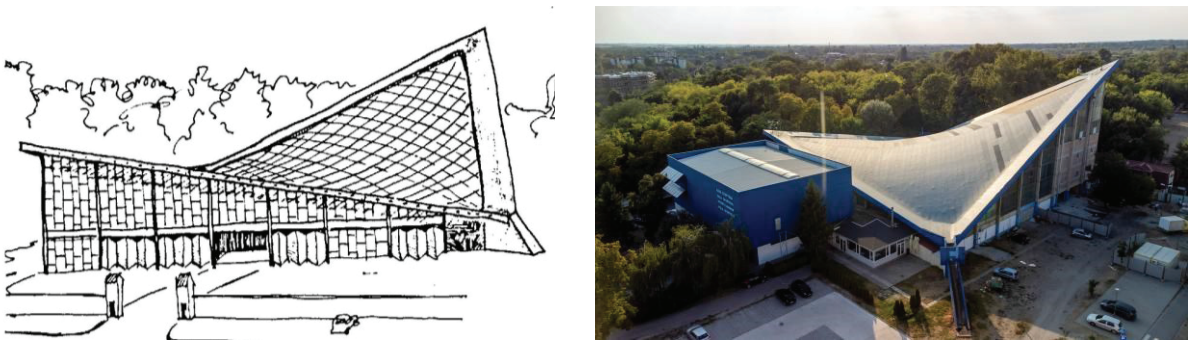

Figure 6. Sports and fair hall in Subotica, Serbia, 1969 (author's drawing – left)
Aerial view after seies of reconstructions (Marko Bulatović – right)

the hall, but it was not included in the list of Immovable Cultural Properties after assessing its historical, artistic, and cultural value.

6 Conclusion

Professor Edmund Balgač's contributions to the field of suspended cable structures are both profound and enduring. Through his innovative application of numerical methods to the analysis and design of geometrically non-linear structures, Balgač advanced the theoretical understanding and practical implementation of these systems. His work, particularly in projects such as the Great Hall of the Textile Fair in Leskovac and the Fair and Sports Hall in Subotica, exemplifies the successful integration of aesthetic and structural principles, creating iconic landmarks that continue to impress with their elegance and functionality.

Balgač's ability to build upon and refine the analytical models introduced by his predecessors, such as Fred Severud and David Jawerth, highlights his role as a key figure in the evolution of suspended cable structures. His pioneering efforts in applying numerical analysis to prestressed systems not only advanced engineering practices but also facilitated the construction of large-span structures with minimal material use and reduced construction complexity.

As we commemorate the 110th anniversary of his birth, it is evident that Professor Balgač's legacy endures through the buildings he designed and the principles he established. His work remains a testament to the harmonious blend of theoretical rigor and practical application, continuing to inspire and guide the field of structural engineering. The enduring presence and functionality of his projects stand as a tribute to his vision and expertise, cementing his place in the annals of architectural and engineering history.

CRediT authorship contribution statement

Conceptualization – DK; Data curation - PR, DK, RF; Investigation - DK, PR; Methodology – DK; Supervision – RF; Visualization – DK; Writing - original draft – PR, DK; Writing - review & editing – VM, PR.

Declaration of competing interest

Authors declare no conflict of interest.

Acknowledgement

This research was supported by the Science Fund of the Republic of Serbia, br.7363, Project title: IMPROVEMENT OF FUNCTIONAL, ENERGETIC, LIGHTENING AND STRUCTURAL CHARACTERISTICS OF CLOSED AND SEMI CLOSED HALLS COVERED BY STRUCTURAL TEXITILE MEMBRANES, ACRONYM: BALLOON-HALL-Optima.

References

[1] E. Balgač, Distribution of forces in the cables of the pre stressed network of suspended roofs in the form of a hyperbolic paraboloid, Izgradnja 69, No 11, 5-14 (1969).

[2] В. К. Качурин, Гибкие нити с малыми стрелками, Государственное издательство теоретической литературы, Moscow, 1956.

[3] E. Balgač, The influence of the five-fold distribution of pressure in the soil on the calculated value of the moments in the foundation beam, Izgradnja 8, 1-13 (1974).

[4] E. Balgač, Could teaching be organized like this at the faculties of civil engineering? A proposal for the inclusion of business in education, for shortening studies until entry into professional practice and for extending education to the entire professional life of engineers, Izgradnja, 11, 40-51 (1974).

[5] E. Balgač, VI Congress of the Yugoslav Society of Construction, Izgradnja 1, 46-48 (1979).

[6] Š. Bači, E. Balgač, R. Janjetov, The work of the SAP Vojvodina Institute of Civil Engineering on the industrialization of residential construction in Vojvodina, Izgradnja 9, 41-62 (1979).

[7] E. Balgač, Milutin-Mika Maksimović-75 years of life, Izgradnja 1, 21-30 (1980).

[8] E. Balgač, Advice: O quality and assortment of domestic cement, Izgradnja 5, 45-47 (1980).

[9] E. Balgač, Calculation of a floor slab loaded with an equally distributed load, Izgradnja 10, 3-5 (1980).

[10] E. Balgač, III Consultation of the Society for Soil Mechanics and Foundations, Izgradnja 1, 48-51 (1985).

[11] E. Balgač, XVIII Congress of Yugoslav Societies for Materials and Construction Research in Portorož, Izgradnja 1, 31-35 (1987).

[12] D. Milašinović, I. Marić, Exhibition Ivan Antić – architectural, BINA, Belgrade, 2018.

[13] M. Petrović, L. Skansi, An architect's relation to structure: analysis of Pinki Cultural sports center by Ivan Antić, Spatium 40, 33-41 (2018).

[14] E. Balgač, Die neue Ausstellungshalle der Textilmasse in Leskovac, Beton und Stahlbetonbau 7, 157-163 (1961).

[15] O. Frei, Die Arena in Raleigh, USA, Bauwelt 5, 89-93 (1953).

[16] D. Jawerth, H. Schulz, Ein beitrag zur eigenschwingungen, windanfachenden krafte und aerodinamischen stabilitat bei hangenden dachern, Der Stalbau, 1-8 (1966).

[17] E. Balgač, Suspended roof of the large exhibition hall of the Leskovac textile fair, Special edition: Concrete prestressed constructions – Construction, 227-235 (1969).

[18] D. Kostić, V. Milošević: Stability analysis of some constructed cable trusses, Building materials and structures 58, Vol 2, 39-57 (2015).

[19] N.S. Moskalev, Construction of suspended ceilings, Stroizdat, 1980.

[20] M. Ristić, Contribution to the analysis of elastic prestressed networks, Doctoral dissertation, Belgrade, 1982.

[21] Baker Roofing, Dorton Arena, BakerRoofing.com, https://bakerroofing.com/dorton-arena/, 2023 (accessed 4 December 2024).

[22] Arcaro, Dorton Arena, Arcaro.org, http://www.arcaro.org/tension/album/dorton.htm, 2023 (accessed 18 December 2023).

[23] E. Balgač, Hanging roof of the Youth and Sports Center in Zemun, Izgradnja 7, 12-18 (1971).

[24] E. Balgač, Two cases of application of suspended roofs, Izgradnja 1, 26-28 (1975).

[25] E. Balgač, Hall for sport and recreation in Subotica, Izgradnja 4, 5-11 (1988).

[26] D. Kostic, Contribution to the solution of the problem of stress-deformation states of suspended structures in the building industry, master's thesis, GF Niš, 1994.
[27] D. Kostić, Contribution to the solution of the stability problem of the double layered catenary systems, Faculty of civil engineering and architecture, University of Niš, Niš, 2007.
[28] D. Kostic, V. Milosevic, The use of an analytical-numerical method for the calculation of elastic prestressed roof systems, TTEM 9, No 2, 422-432 (2014).
[29] E. Balgač, Blocks for anchoring the cables of the suspension road bridge over the Tisa River near Novi Kneževac, Izgradnja 6, 1-6 (1976).
[30] Nowicki, Deitrick, Severud, Elstad, Krueger, Livestock Judging Raleigh Arena, NC USA, Architectural forum 97, No 10, 134 (1952).
[31] Z. Sobotka, Zavešené strechy, Státní Nakladatelství Technické Literatury Praha, 1962.
[32] I. Max, Analytical Solutions for Pretensioned Cable Nets, Journal of the Engineering Mechanics Division 102, No 1, 43-57 (1976).
[33] J.W. Leonard, Tension Structures-Behavior & Analysis, McGraw Hill Book Company, 1988.
[34] F. Leonhardt, J. Schlaich, Structural design of roofs over the sports arenas for the 1972 Olympic games: Some problems of prestressed cable net structures, The Structural Engineer 50, No 3, 113-120 (1972).
[35] G. Radivojević, D. Kostić, Suspended structural systems in high-rise construction, University of Niš, Serbia, 1998.
[36] L. Stipić, Fair Sports Hall in Subotica, Construction 2, 20-33 (1975).
[37] S. Dimitrijević, D. Petković, D. Pavlović, M. Rangelov, D. Madžarac-Savić, D. Lazić, G. Mitić, Preliminary business plan for the revitalization of the Round Pavilion in Leskovac, EPuS-Leskovac, 2015.

Building Materials and Structures

GUIDE FOR AUTHORS

In the journal *Building Materials and Structures*, the submission and review processes take place electronically. Manuscripts are submitted electronically (online) on the website **https: // www.dimk.rs.** The author should register first, then log in and finally submit the manuscript which should be in the form of editable files (e.g. Word) to enable the typesetting process in journal format. All correspondence, including Editor´s decision regarding required reviews and acceptance of manuscripts, take place via e-mail.

TYPES OF ARTICLES

The following types of articles are published in *Building Materials and Structures:*

Original scientific article. It is the primary source of scientific information, new ideas and insights as a result of original research using appropriate scientific methods. The results are presented briefly, but in a way to enable readers to assess the results of experimental or theoretical/numerical analyses, so that the research can be repeated and yield with the same or results within the limits of tolerable deviations.

Review article. It presents the state of science in particular area as a result of methodically systematized, analyzed and discussed reference data. Only critical review manuscripts will be considered as providing novel perspective and critical evaluation of the topics of interest to broader BMS readership.

Preliminary report. Contains the first short notifications of research results without detailed analysis, i.e. it is shorter than original research paper.

Technical article. Reports on the application of recognized scientific achievements of relevance to the field of building materials and structures. Contain critical analysis and recommendations for adaption of the research results to practical needs.

Projects Notes. Project Notes provide a presentation of a relevant project that has been built or is in the process of construction. The original or novel aspects in design or construction should be clearly indicated.

Discussions. Comment on or discussion of a manuscript previously published in *Building Materials and Structures*. It should be received by the Editor-in-Chief within six months of the online publication of the manuscript under discussion. Discussion Papers will be subject to peer review and should also be submitted online. If Discussion Paper is selected for publication the author of the original paper will be invited to respond, and Discussion Paper will be published alongside any response that the author.

Other contributions

Conference Reports. Reports on major international and national conferences of particular interest to *Building Materials and Structures*. Selected and/or awarded papers from the ASES Conferences are published in Special issues.

Book Reviews. Reviews on new books relevant to the scope of *Building Materials and Structures*.

PREPRINTS

These are the author's own write-up of research results and analysis that has not been peer reviewed, nor had any other value added to it by a publisher (such as formatting, copy-editing, technical enhancements and the like). Authors can share their preprint anywhere at any time. If accepted for publication, we encourage authors to link from the preprint to their formal publication via its Digital Object Identifier (DOI). Preprints should not be added to or enhanced in any way in order to appear more like, or to substitute for, the final versions of articles.

MANUSCRIPT STRUCTURE

The manuscript should be typed one-sided on A4 sheets. Page numbers should be included in the manuscript and the text should be single spaced with **consecutive line numbering** - these are essential peer review requirements. The figures and tables included in the single file should be placed next to the relevant text in the manuscript. The corresponding captions should be placed directly below the figure or table. If the manuscript contains Supplementary material, it should also be submitted at the first submission of the manuscript for review purposes.

There are no strict rules regarding the structure of the manuscript, but the basic elements that it should contain are: Title page with the title of the manuscript, information about the authors, abstract and keywords, Introduction, Materials / Methods, Results and Conclusions.

The front page

The front page contains the title of the manuscript which should be informative and concise; abbreviations and formulas should be avoided.

Information about the authors are below the title; after the author's name, a superscript number is placed indicating his/her affiliation, which is printed below the author's name, and before the abstract. It is obligatory to mark the corresponding author with superscript *) and provide his/her e-mail address. The affiliation should contain the full name of the institution where the author performed the research and its address.

Abstract

Abstract should contain 150-200 words. Motivation and objective of the conducted research should be presented; main results and conclusions should be briefly stated as well. References and abbreviations should be avoided.

Keywords

Keywords (up to 10) should be listed immediately after the abstract; abbreviations should be used only if they are generally accepted and well-known in the field of research.

Division into chapters

The manuscript should be divided into chapters and sub-chapters, which are hierarchically numbered with Arabic numbers. The headings of chapters and sub-chapters should appear on their own separate lines.

At the end of the manuscript, and before the references, it is obligatory to list the following statements:

CRediT authorship contribution statement

For transparency, we require corresponding authors to provide co-author contributions to the manuscript using the relevant CRediT roles. The CRediT taxonomy includes 14 different roles describing each contributor's specific contribution to the research output. The roles are: Conceptualization; Data curation; Formal analysis; Funding acquisition; Investigation; Methodology; Project administration; Resources; Software; Supervision; Validation; Visualization; Roles/Writing - original draft; and Writing - review & editing. Note that not all roles may apply to every manuscript, and authors may have contributed through multiple roles.

Declaration of competing interest

Corresponding authors, on behalf of all the authors of a submission, must disclose any financial and personal relationships with other people or organizations that could inappropriately influence their work. Examples of potential conflicts of interest include employment, consultancies, stock ownership, honoraria, paid expert testimony, patent applications/registrations, and grants or other funding. All authors, including those *without* competing interests to declare, should provide the relevant information to the corresponding author (which, where relevant, may specify they have nothing to declare).

Declaration of generative AI in scientific writing

This guidance only refers to the writing process, and not to the use of AI tools to analyze and draw insights from data as part of the research process. Where authors use generative artificial intelligence (AI) and AI- assisted technologies in the writing process, authors should only use these technologies to improve readability and language. Applying the technology should be done with human oversight and control, and authors should carefully review and edit the result, as AI can generate authoritative-sounding output that can be incorrect, incomplete or biased. AI and AI-assisted technologies should not be listed as an author or co-author, or be cited as an author. Authorship implies responsibilities and tasks that can only be attributed to and performed by humans. Authors should disclose in their manuscript the use of AI and AI- assisted technologies in the writing process by following the instructions below. A statement will appear in the published work. Please note that authors are ultimately responsible and accountable for the contents of the work.

Disclosure instructions

Authors must disclose the use of generative AI and AI-assisted technologies in the writing process by adding a statement at the end of their manuscript in the core manuscript file, before the References list. The statement should be placed in a new section entitled 'Declaration of Generative AI and AI-assisted technologies in the writing process'.

Statement: During the preparation of this work the author(s) used [NAME TOOL / SERVICE] in order to [REASON]. After using this tool/service, the author(s) reviewed and edited the content as needed and take(s) full responsibility for the content of the publication.
This declaration does not apply to the use of basic tools for checking grammar, spelling, references etc. If there is nothing to disclose, there is no need to add a statement.

Acknowledgments

State the institutions and persons who financially or in some other way helped the presented research. If the research was not supported by others, it should also be stated in this part of the manuscript.

Appendices

The manuscript may have appendices. If there is more than one appendix, they are denoted by A, B, etc. Labels of figures, tables and formulas in appendices should contain the label of the appendix, for example Table A.1, Figure A.1, etc.

ABBREVIATIONS

All abbreviations should be defined where they first appear. Consistency of abbreviations used throughout the text should be ensured.

MATH FORMULAE

Formulae should be in the form of editable text (not in the format of figures) and marked with numbers, in the order in which they appear in the text. The formulae and equations should be written carefully takinginto account the indices and exponents. Symbols in formulae should be defined in the order they appear, right below the formulae.

FIGURES

- figures should be made so that they are as uniform in size as possible and of appropriate quality for reproduction;
- the dimensions of the figures should correspond to the format of the journal: figures with a width approximately equal to the width of 1 column (± 80 mm width), width of 2 columns (± 170 mm width) or width of 1.5 columns (± 130 mm width);
- figures should be designed so that their size is not disproportionately large in relation to the content;
- the text on the figures should be minimal and the font used should be the same on all figures (Arial, Times New Roman, Symbol);
- figures should be placed next to the appropriate text in the manuscript and marked with numbers in the order in which they appear in the text;
- each figure should have a caption that is placed below the figure - the caption should not be on the figure itself.

In cases of inadequate quality of reproduction, the author should be required to submit figures as separate files. In this case, the figure should be saved in TIFF (or JPG) format with a minimum resolution of 500 dpi.

TABLES

- tables should be in the form of editable text (not in the format of figures);
- tables should be placed next to the appropriate text in the manuscript and marked with numbers in the order in which they appear in the text;
- each table should have a caption that is placed below the table;
- the tables should not show the results that are already presented elsewhere in the manuscript - duplicating the presentation of results should be avoided;
- tables are without vertical lines as boundaries between cells and shading cells.

REFERENCES

Citation in the text

Each reference cited in the text should be in the reference list (and vice versa). It is not recommended to list unpublished results or personal communications in the reference list, but they can be listed in the text. If they are still listed in the reference list, the journal style references are used, with 'Unpublished results' or 'Personal communication' instead of the date of publication. Citing a reference as ‘in press’ means that it is accepted for publication.

Web references

Web references are minimally listed with the full URL and the date when the site was last accessed. These references can be included in the reference list, but can also be given in a separate list after the reference list.

Reference style

In text: References are given in the text by a number in square brackets in the order in which they appear in the text. Authors may also be referred to directly, but the reference number should always be given.

In reference list: References marked with a number in square brackets are sorted by numbers in the list.

Examples

Reference to a journal publication:

[1] V.W.Y. Tam, M. Soomro, A.C.J. Evangelista, A review of recycled aggregate in concrete applications (2000-2017), Constr. Build. Mater. 172 (2018) 272-292. https://doi.org/10.1016/j.conbuildmat.2018.03.240.

Reference to a book:

[3] A.H. Nilson, D. Darwin, C.W. Dolan, Design of Concrete Structures, thirteenth ed., Mc Graw Hill, New York, 2004.

Reference to a chapter in an edited book:

[4] J.R. Jimenez, Recycled aggregates (RAs) for roads, in: F Pacheco-Torgal, V.W.Y. Tam, J.A. Labrincha, Y. Ding, J. de Brito (Eds.), Handbook of recycled concrete and demolition waste, Woodhead Publishing Limited, Cambridge, UK, 2013, pp. 351–377.

Reference to a website:

[5] WBCSD, The Cement Sustainability Initiative, World. Bus. Counc. Sustain. Dev. http://www.wbcsdcement.org.pdf/CSIRecyclingConcrete-FullReport.pdf, 2017 (accessed 7 July 2016).

SUPPLEMENTARY MATERIAL

Supplementary material such as databases, detailed calculations and the like can be published separately to reduce the workload. This material is published 'as received' (Excel or PowerPoint files will appear as such online) and submitted together with the manuscript. Each supplementary file should be given a short descriptive title.

ETHICS IN PUBLISHING

Authors are expected to respect intellectual and scientific integrity in presentation of their work. The journal publishes manuscripts that have not been previously published and are not in the process of being considered for publication elsewhere. All co-authors as well as the institution in which the research was performed should agree to the publication in the journal.
Authors are expected to submit completely original research; if the research of other researchers is used, it should be adequately cited. Authors who wish to include in their manuscript images, tables or parts of text that have already been published somewhere, should obtain permission from the Copyright owner and provide a proof in the process of submitting the manuscript. All material for which there is no such evidence will be considered the original work of the author. To determine the originality of the manuscript, it can be checked using the Crossref Similarity Check service. For more information, please see our Ethics and Malpractice Statement.

The Journal and Publishers imply that all authors, as well as responsible persons of the institute where the research was performed, agreed with the content of the submitted manuscript before submitting it. The Publishers will not be held legally responsible should there be any claims for compensation.

PEER REVIEW

This journal uses a single blind review process, which means that the authors do not know the names of the reviewers, but the reviewers know who the authors are. In the review process, the Editor-in-Chief first assesses whether the contents of the manuscript comply with the scope of the journal. If this is the case, the paper is sent to at least two independent experts in the field, with the aim of assessing its scientific quality and making recommendation regarding publication. If the manuscript needs to be revised, the authors are provided with the reviewers' remarks. The authors are obliged to correct the manuscript in accordance with the remarks, submit the revised manuscript and a special file with the answers to the reviewers within the given deadline. The final decision, whether the paper will be published in journal or not, is made by the Editor-in-Chief.

AFTER ACCEPTANCE

Once accepted for publication, the manuscript is set in the journal format. Complex manuscript is sent to the authors in the form of proof, for proof reading. Then, authors should check for typesetting errors, and whether the text, images, and tables are complete and accurate. Authors are asked to do this carefully, as subsequent corrections will not be considered. In addition, significant changes to the text and authorship at this stage are not allowed without the consent of the Editor-in-Chief. After online publication, changes are only possible in the form of Erratum which will be hyperlinked to manuscript.

COPYRIGHT

Authors retain copyright of the published papers and grant to the publisher the non-exclusive right to publish the article, to be cited as its original publisher in case of reuse, and to distribute it in all forms and media.

The published articles will be distributed under the Creative Commons Attribution ShareAlike 4.0 International license (CC BY-SA). It is allowed to copy and redistribute the material in any medium or format, and remix, transform, and build upon it for any purpose, even commercially, as long as appropriate credit is given to the original author(s), a link to the license is provided, it is indicated if changes were made and the new work is distributed under the same license as the original.

Users are required to provide full bibliographic description of the original publication (authors, article title, journal title, volume, issue, pages), as well as its DOI code. In electronic publishing, users are also required to link the content with both the original article published in *Building Materials and Structures* and the license used.

Authors are able to enter into separate, additional contractual arrangements for the non-exclusive distribution of the journal's published version of the work (e.g., post it to an institutional repository or publish it in a book), with an acknowledgement of its initial publication in this journal.

OPEN ACCESS POLICY

Journal *Building Materials and Structures* is published under an Open Access license. All its content is available free of charge. Users can read, download, copy, distribute, print, search the full text of articles, as well as to establish HTML links to them, without having to seek the consent of the author or publisher.
The right to use content without consent does not release the users from the obligation to give the credit to the journal and its content in a manner described under *Copyright*.

Archiving digital version

In accordance with law, digital copies of all published volumes are archived in the legal deposit library of the National Library of Serbia in the Repository of SCIndeks - The Serbian Citation Index as the primary full text database.

Cost collection to authors

Journal Building Materials and Structures does not charge authors or any third party for publication. Both manuscript submission and processing services, and article publishing services are free of charge. There are no hidden costs whatsoever.

DISCLAIMER

The views expressed in the published works do not express the views of the Editors and the Editorial Staff. The authors take legal and moral responsibility for the ideas expressed in the articles. Publisher shall have no liability in the event of issuance of any claims for damages. The Publisher will not be held legally responsible should there be any claims for compensation.

Financial support

MINISTRY OF EDUCATION, SCIENCE AND TECHNOLOGICAL DEVELOPMENT OF REPUBLIC OF SERBIA

INSTITUTE FOR TESTING OF MATERIALS-IMS INSTITUTE, BELGRADE

SERBIAN CHAMBER OF ENGINEERS

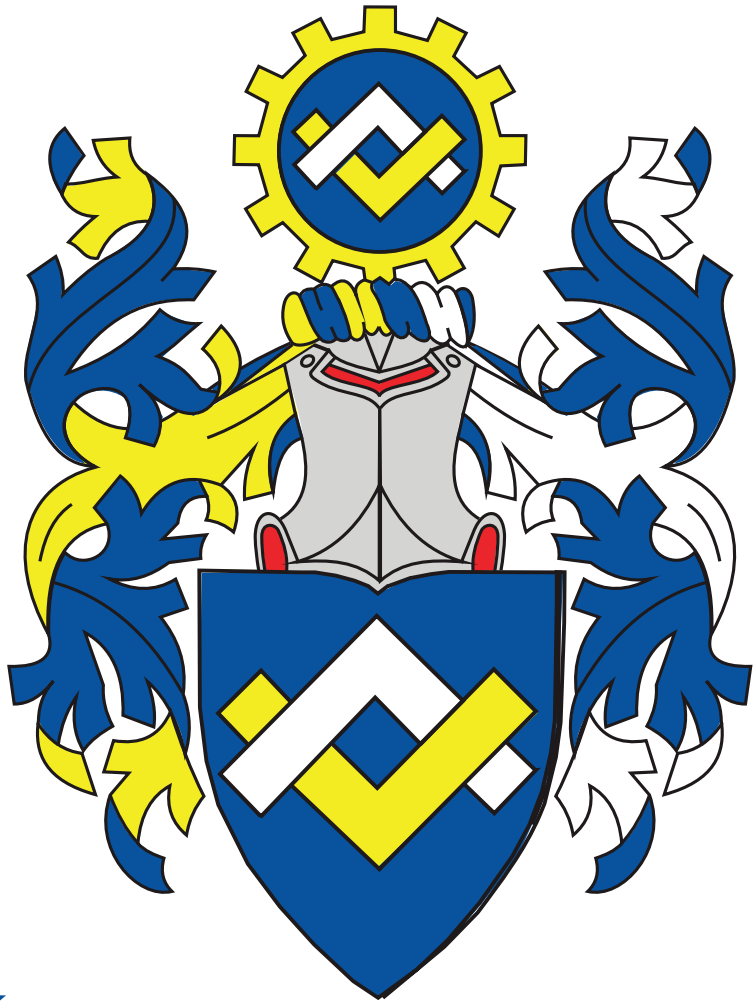

INŽENJERSKA KOMORA SRBIJE

Ringlock

Doka modularni sistem skela.

Bezbedno i efikasno rešenje za skele. Široka oblast primena.

PROVIDING ATPAC COMPLETE SCAFFOLDING SOLUTIONS

Pristupne skele

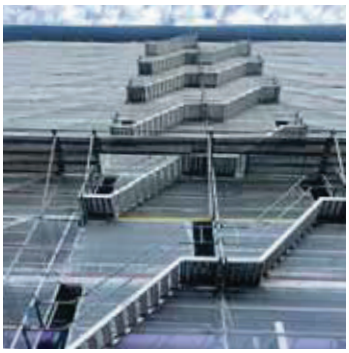

Skele za stambene objekte

Skele za poslovne objekte

Stepenišni toranj

Doka Serb d.o.o. | Svetogorska 4 | 22310 Šimanovci | Srbija | **T** +381 (0)22 400 100 | serb@doka.com | **www.doka.com/rs**

ADING
sastojak svake građevine

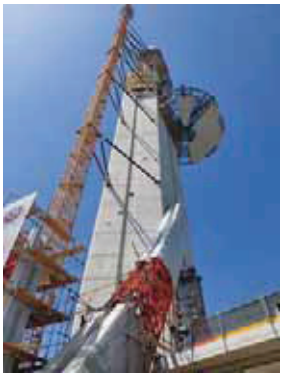

ADITIVI ZA BETONE VISOKIH PERFORMANSI

Adresa: Nehruova 82, 11070 Novi Beograd Tel/Fax: + 381 11 616 05 76 email: ading@ading.rs
www.ading.rs

ACO. The future of drainage.

ACO

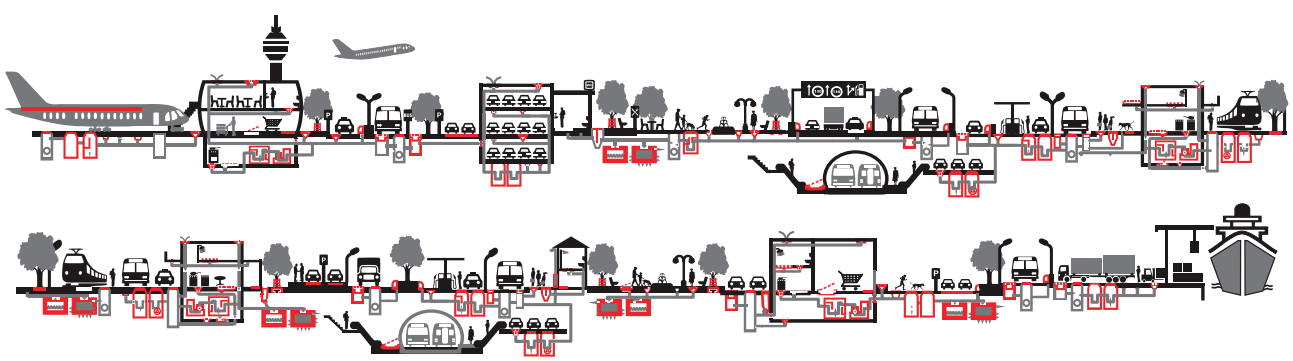

aco.rs

INSTITUT IMS AD
BEOGRAD

CENTAR ZA PUTEVE I GEOTEHNIKU

U okviru centra posluju odeljenja za geotehniku, nadzor i terenska ispitivanja, projektovanje saobraćajnica, laboratorija za puteve i geotehniku. Značajna aktivnost centra usmerena je ka terenskim i laboratorijskim geološko - geotehničkim istraživanjima i ispitivanjima terena za potrebe izrade projekno - tehničke dokumentacije, za različite faze i nivoe projektovanja objekata visokogradnje, niskogradnje, saobraćaja i hidrogradnje, kao i za potrebe prostornog planiranja i zaštite životne sredine. Stručni nadzor, kontrola kvaliteta tokom građenja, rekonstrukcije i sanacije objekata različite namene, izrada studija, ekspertiza, konsultantske usluge, kompletan konsalting u oblasti geotehničkog inženjeringa, neke su od delatnosti centra.

Ispitivanje šipova

- **SLT metoda (Static load test)**
- **DLT metoda (Dynamic load test)**
- **PDA metoda (Pile driving analysis)**
- **PIT (SIT) metoda (Pile (Sonic) integrity testing)**
- **CSL - Crosshole Sonic Logging**

- **Ispitivanje šipova**
  - **Geotehnička istraživanja i ispitivanja – in situ**
    - **Laboratorija za puteve i geotehniku**
      - **Projektovanje puteva i sanacija klizišta**
        - **Nadzor**

Tondach

Krovni sistemi

Najlepši krov u komšiluku

Continental Plus Natura je premium crep u natur segmentu! Dobro poznatog oblika, trajan i veoma otporan, a povrh svega pristupačan, naprosto oduzima dah svima. Čak i vašim komšijama!

Continental Plus Natura crep potražite kod ovlašćenih Tondach partnera.

Wienerberger

PUT INŽENJERING

Put inženjering d.o.o punih 25 godina radi kao specijalizovano preduzeće za izgradnju infrastrukture u niskogradnji i visokogradnji, kao i proizvodnjom kamenog agregata i betona. Preduzeće se bavi i transportom, uslugama građevinske mehanizacije i specijalne opreme.

Za spravljanje betona koristimo drobljeni krečnjački agregat sa našeg kamenoloma, deklarisanih frakcija, kontrolisane vlažnosti. Kompletan proces proizvodnje i kontrole kvaliteta vršimo prema važećim standardima.

Kao generalni izvođač radova, vršimo koordinaciju svih učesnika na projektu, planiranje, praćenje i nabavku materijala, kontrolu kvaliteta izvedenih radova, poštujući zadate vremenske rokove i finansijski okvir investitora.

Obradu armature vršimo brzo, stručno i kvalitetno, sa kompjuterskom preciznošću i dimenzijama po projektu.

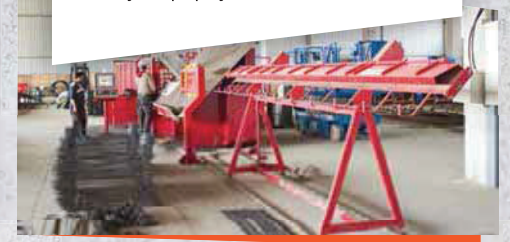

Osnovi princip našeg poslovanja zasniva se na individualnom pristupu svakom klijentu i pronalaženje najoptimalnijeg rešenja za njegove transportne i logističke potrebe.

Koristeći inovativne tehnike i kvalitetan građevinski materijal iz sopstvenih resursa, spremni smo da odgovorimo na mnoge zahteve naših klijenata iz oblasti niskogradnje.

Naša kompanija u oblasti visokogradnje primenjuje sistem prefabrikovnih betonskih elemenata koji u odnosu na klasičnu gradnju ima brojne prednosti.

Usluge građevinskom mehanizacijom vršimo tehnički ispravnim mašinama, sa potrebnim sertifikatima kako za rukovaoce građevinskim mašinama tako i za same mašine.

Osnovna prednost prefabrikovane konstrukcije jeste brzina kojom konstrukcija može biti projektovana, proizvedena, transportovana i namontirana.

Prednapregnute šuplje ploče su konstruktivni elementi visokog kvaliteta, proizvedeni u fabrički kontrolisanim uslovima.

Raspolažemo opremom i mašinama za sve zemljane radove, kipere i dampere za rad u teškim terenskim uslovima, automiksere i pumpe za beton, autodizalice, podizne platforme.

Izvodimo hidrograđevinske radove u izgradnji kanalizacionih mreža za odvođenje atmosferskih, otpadnih i upotrebljenih voda, izvođenjem hidrograđevinskih radova u okviru regulacije rečnih tokova, kao i izvođenjem hidrotehničkih objekata.

Izrađujemo betonske "New Jersey profile" koji se u svetu koriste za preusmeravanje saobraćaja i zaštitu pešaka u toku izgradnje puta, kao i Betonblock sistem betonskih blokova.

Sakupljanje i privremeno skladištenje otpada vršimo našim specijalizovanim vozilima i deponujemo na našu lokaciju sa odgovarajućom dozvolom. Kapacitet mašine je 250 t/h građevinskog neopasnog otpada.

Površinski kop udaljen je 35 km od Niša. Savremene drobilice, postrojenje za separaciju i sejalica efikasno usitnjavaju i razdvajaju kamene agregate po veličinama. Tehnički kapacitet trenutne primarne drobilice je 300 t/h.

Uslugu transporta vršimo automikserima, kapaciteta bubnja od 7 m³ do 10 m³ betonske mase. Za ugradnju betona posedujemo auto-pumpu za beton, radnog učinka 150 m³/h, sa dužinom strele od 36 m.

NIŠ
Knjaževačka bb, 18000 Niš - Srbija
+381 18 215 355
office@putinzenjering.com

BEOGRAD
Jugoslovenska 2a, 11250 Beograd – Železnik
+381 11 25 81 111
beograd@putinzenjering.com

MOBECO

www.putinzenjering.com

Mapei proizvodi i rešenja su izbor onih koji znaju da prepoznaju kvalitet, posvećenost svakom detalju i višedecenijsko iskustvo u građevinskoj industriji.

Zato birajte pažljivo. Birajte kvalitet.

Mapei, svetski lider u proizvodnji građevinskih lepkova, hidroizolacija i masa za fugovanje.

Saznaj više na **www.mapei.rs**

MAPEI®

ŽIVI KVALITETNO

MATEST
YOUR PARTNER IN TESTING

iT TECH

INELAS ERECO d.o.o

MATEST "iT TECH" KONTROLNA JEDINICA

JEDNA TEHNOLOGIJA MNOGO REŠENJA

IT Touch Techlogy je Matestov najnoviji koncept koji ima za cilj da ponudi inovativna i user-friendly tehnologiju za kontrolu i upravljanje najmodernijom opremom u domenu testiranja građevinskih materijala

Ova tehnologija je srž Matestove kontrolne jedinice, software baziran na Windows platformi i touch screen sistem koji je modularan, fleksibilan i obavlja mnoge opcije

iT TECH pokriva

- INOVATIVNOST
- INTERNET KONEKCIJA
- INTERFEJS SA IKONICAMA
- INDUSTRIJALNA TEHNOLOGIJA

SISTEM JEDNOG RAZMIŠLJANJA JEDNOM SHVATIŠ - SVE TESTIRAŠ

NAPREDNA TEHNOLOGIJA ISPITIVANJA ASFALTA

- GYROTRONIC - Gyratory Compactor
- ARC - Electromechanical Asphalt Roller Compactor
- ASC - Asphalt Shear Box Compactor
- SMARTRACKER[tm] - Multiwheels Hamburg Wheel Tracker, DRY + WET test environment
- SOFTMATIC - Automatic Digital Ring & Ball Apparatus
- Ductilometers with data acquisition system

MULTIFUNKCIONALNI RAMOVI ZA TESTIRANJE

- CBR/Marshall digital machines
- Universal multispeed load frames
- UNITRONIC 50kN or 200kN Universal multipurpose compression/flexural and tensile frames

OPREMA ZA GEOMEHANIČKO ISPITIVANJE

- EDOTRONIC - Automatic Consolidation Apparatus
- SHEARLAB - AUTOSHEARLAB - SHEARTRONIC Direct / Residual shear testing systems
- Triaxial Load Frame 50kN

MIXMATIC - Automatic Programmable Mortar Mixer

INELAS ERECO D.O.O
Tošin bunar 274a, 11070 , Novi Beograd tel. +381 11 2284 574 email. info@inelasereco.rs

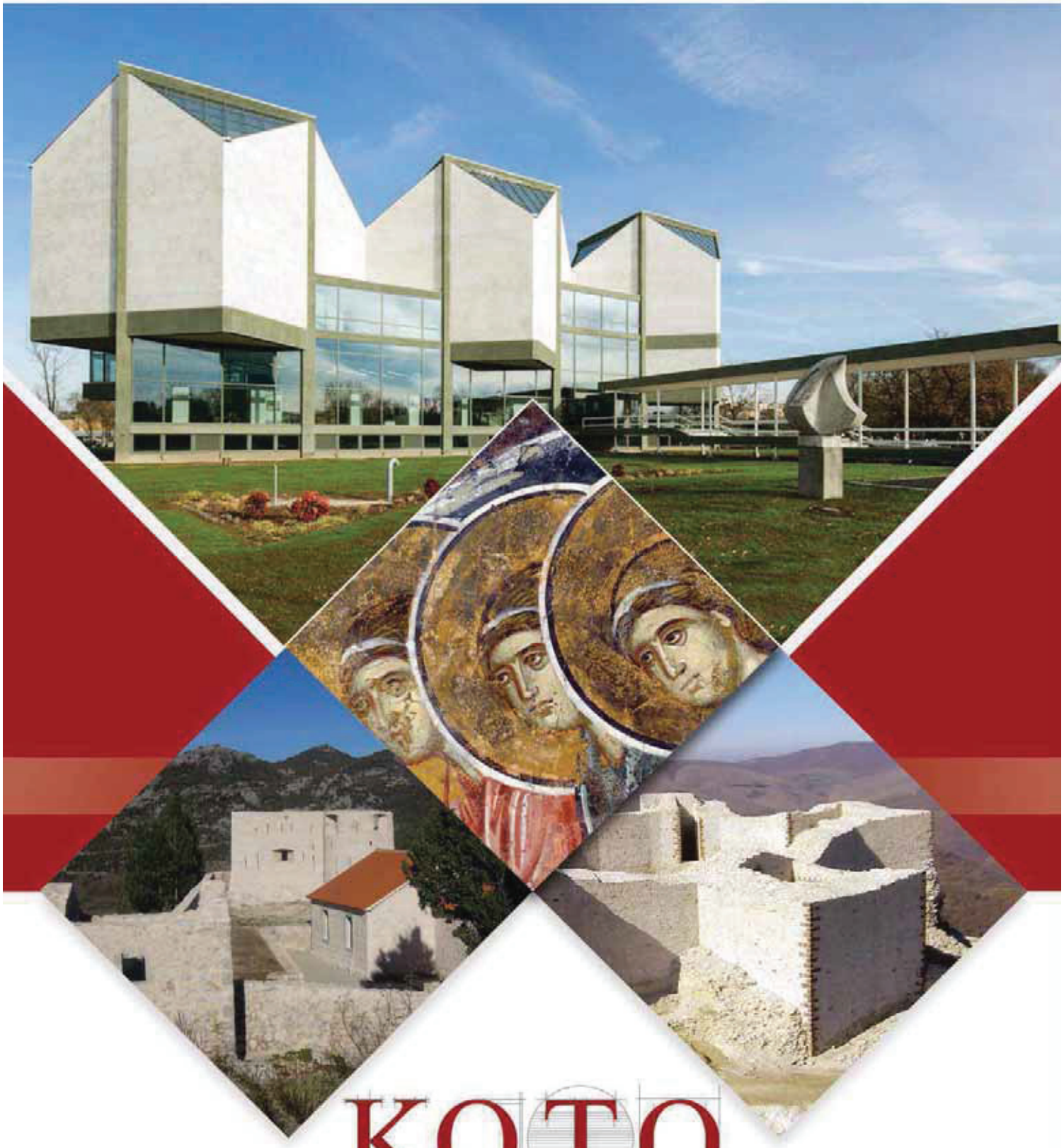

KOTO

www.koto.rs | office@koto.rs | 011 309 7410 | Vojvode Stepe br. 466, Beograd

INNOVATIVE CONSTRUCTION TECHNOLOGIES

NOVKOL

Samarska 6
(bivši Surčinski put 1k),
11077, Novi Beograd, Srbija

+381117129180
+381117129194
+381117129324
+381112607979
+381112607981

Fax:
+381117129183

office@novkol.co.rs
priprema@novkol.co.rs